THE FUNCTIONAL INCORPORATION OF THE MECHANOSENSITIVE CHANNEL OF LARGE CONDUCTANCE WITHIN A TETHERED LIPID BILAYER AND THE FUTURE RECONSTITUTION OF FUTURE DESIGNER CHANNELS

By

DANYELL S. WILSON

A DISSERTATION PRESENTED TO THE GRADUATE SCHOOL
OF THE UNIVERSITY OF FLORIDA IN PARTIAL FULFILLMENT
OF THE REQUIREMENTS FOR THE DEGREE OF
DOCTOR OF PHILOSOPHY

UNIVERSITY OF FLORIDA

2009

© 2009 Danyell Wilson

This document is dedicated to my grandmother, Ms. Addie Martin.

ACKNOWLEDGMENTS

First I would like to thank God for giving me the strength to complete this document. I would also like to thank my committee members, Dr. Randolph Duran, Dr. Paul Blount, Dr. Gail Fanucci, Dr. Joanna Long, Dr. Benjamin Smith, and Dr Tom Lyons, for their advice, guidance, and support. Dr. Blount was a second advisor and a mentor to me; sincere thanks for opening up the Blount's lab to me. Dr. Fanucci and Dr. Lyons special thanks for opening up the biochemistry labs at UF to me as well. These facilities allowed me perform and complete all of the biochemistry techniques I learned while in Dr. Blount's lab. Dr. Duran, Dr. Smith and Dr. Long, a special thanks for encouraging me to continue on to the PhD after my Masters.

I would next like to thank Dr. Martin Andersson, Dr. Irene Iscla, Dr. Li-Min Yang, Senior Scientist (Dr.) Robin Wray, and soon to be Dr. Mandy Blackburn as well as Chenyu Zhu, Jeanette Cervantes, Deneyelle Wilson, and Alan Salgado. I would also like to thank the Duran group members for always being there.

Next, I would love to thank my family and friends. My mother Marjorie Wilson who always, always has my back; I am truly grateful to have such a loving charismatic mother. I would love to thank my father, Danny Wilson; a strong, smart, funny, and a blessing to have as a father and friend. I would like to also thank my sisters Sunceray and Ariel Wilson; I am truly blessed to have both of my sisters in life. Sunceray and Ariel were always just a phone call away and for that I will always be sincerely grateful. I would like to thank my nephew, Jameź Epps, as my inspiration, and the best nephew, ever. I would like to thank all of my friends from childhood, college, graduate school, and church. Without them, I would not have made it through this process. All of their prayers, laughter, consoling, partying, editing, and the staying up late nights with me to ensured I became Dr. Wilson. I would also like to acknowledge my dear friend Dr. Charlee Bennett; we did it! We are Ph officially Done!

Lastly, I would like to thank the people who have financially supported me and helped me find my passion in science: Dr. Anna Donnelly (SEAGEP), Dr. Jonathan Earl and Ms. Margie Williams (FGLAMP), the Office of Graduate Minority Programs (BOE), and both Dr. Blount and Dr. Duran.

TABLE OF CONTENTS

page

ACKNOWLEDGMENTS 4

LIST OF TABLES 9

LIST OF FIGURES 10

LIST OF ABBREVIATIONS 13

ABSTRACT 14

CHAPTER

1 PROJECT OVERVIEW 16

Introduction 16
Biological Membrane 17
Membrane Proteins and Ion Channels 18
Stretch-Activated Channels 24
E. coli's MscL 25
MscL Function and Structure 27
S3-COOH-Bundle 29
Functionality of the S3-Bundle 31
Solid-Supported and Tethered Lipid Bilayers 33
Tethered Lipid Bilayers/Membranes (tBLM) 37
DPTL 39
Surface Binding Region 39
The Polar Tethered/Hydrophilic Region 40
Diphytanyl Tail Regions 40
Diphytanoyl Lipids 41
Summary 42

2 MATERIALS, METHODS, AND EXPERIMENTAL THEORIES 44

Protein Chemistry and Structural Studies 44
Cysteine Mutations in MscL 44
Biochemistry Assays: Disulfide-trapping 47
Western Blotting 49
Experimental Theory and Procedures for Functional Studies 50
Materials 50
Protein Isolation and Purification 51
MscL Isolation and Purification 51
Gramicidin Isolation 52
Proteoliposome Formation 52
DPhPC and DPhPE Vesicle Formation and Protein Reconstitution 54

Single Channel Measurements: Patch Clamping Recording Technique 55
Specialized Patch Clamping Techniques 57
Planar Linear Patching: The Tip-Dip Recording 57
Tethered Lipid Bilayer 58
Experimental Setup.....59
Tip-Dip Recording Experiment.....61
Tethered Devices Experimental Setup 62
The Device 62
Preparation of the Tethered Bilayer 63
Gigaseal 64
Program Analysis for Both Techniques.....65
Analysis of Single Ion Channel Activity 68
Point-Amplitude Histograms.....68
Probability Density Function.....70

3 CYSTEINE SUBSTITUTIONS IN THE S3-BUNDLE OF THE MECHANOSENSITIVE CHANNEL OF LARGE CONDUCTANCE 72

Introduction.....72
Materials and Methods 76
Strains and Cell Growth 76
Phenotype studies.....76
GOF Assays.....76
Loss-of-Function Assays 77
Western Blot Analysis.....79
Electrophysiology.....80
Results.....81
Phenotype Characterization.....81
GOF Studies 82
LOF Assays 83
Biochemical Assays.....84
Discussion.....90
Conclusion 93

4 TESTING THE ELECTRICAL STABLITY OF DIFFERENT LIPID BILAYER COMPOSITIONS OF DPhPC/DPhPE.....95

Introduction.....95
Methods and Materials 97
Results of Lipid Ratios 100
Pure PC Planar Bilayers 100
Pure PE Planar Bilayers.....101
50PC/50PE Planar Bilayers.....102
70PC/30PE and 30PC/70PE Planar Bilayers 103
Single Channel Results of Gramicidin in 70PC/30PE bilayer 105
Discussion.....108
The Effect of Hydration State on the Stability of Bilayers and Electroporation.....108

Tip-dip and Diphytanoyl Lipid System 111
Conclusion 112

5 FUNCTIONAL STUDIES OF GRAMICIDIN AND MSCL WITHIN A TETHERED LIPID BILAYER MEMBRANE 114

Introduction 114
Materials and methods 117
Materials 117
Proteins 117
Device 118
Preparation of the Tethered Bilayer 118
Protein Reconstitution 119
Electrophysiology 120
Results 121
Results of Gramicidin Reconstituted into the tBLM 123
Single Channel Analysis of MscL 126
Ionic Selectivity 127
Lifetime Studies 127
Conductance 127
Discussion 132
Conclusions 135

6 CONCLUSION 137

APPENDIX

A DLS OF THE SIZE DISTRIBUTION OF 70PC/30 PE 142

B STABLE BILAYER TRACE AND I-V CURVES 143

C PROTEIN RECTIFICATION WITHIN THE DEVICE 145

LIST OF REFERENCES 146

BIOGRAPHICAL SKETCH 159

LIST OF TABLES

Table page

1-1 Different types of ion channels. 22

2-1 Oligonucleotide primers with cysteine mutation highlighted in red.....45

5-1 Conductance comparison between the ion channels reconstituted in the tBLM and reported conductance. 133

LIST OF FIGURES

Figure page

1-1 Phospholipids bilayer. And The fluid mosaic model of the cellular membrane. 18

1-2 Equivalent circuit model of the ion channel within the lipid membrane. 20

1-3 Schematic of Gramicidin forming a pore in a synthetic lipid bilayer membrane.....23

1-4 Schematic representation of *E. coli's* MscL amino acid sequence and topology of one monomer. 28

1-5 Helical wheel of the S3-bundle.....30

1-6 Conflicting models of the S3-bundle during gating.....32

1-7 Solid-Confined or supported membrane.....35

1-8 The tethered monolayer component.....38

1-9 1,2-Diphytanoyl-sn-Glycero-3-phosphoethanolamine (DPhPE) and 1,2-Diphytanoyl-sn-Glycero-3-phospho choline (DPhPC) lipid.....41

2-1 Liposome or vesicles formed from phospholipids.....53

2-2 Schematic of the tip-dip recording system.....58

2-3 Experimental Apparatus.....60

2-4 The tip-dip and tethered stage apparatus 61

2-5 Event detection occurring at level zero and level one 67

2-6 The distribution of data points within the histogram are fitted by the maximum likelihood with a continuous Gaussian curve.. 70

3-1 Conflicting models of the S3-bundle during gating.....74

3-2 Amino acid sequence for MscL and a ribbon design of the linker area and S3 bundle of the C-terminal region with the location of the mutations highlighted.....75

3-3 Schematic illustration of gain of function assay. 77

3-4 Loss of Function schematic representation.....78

3-5: Video images obtained during the process of generating and patching giant spheroplasts from *E. coli*.....80

3-6 Growth curves for all of the mutants generated in this study as well as for WT MscL and G26H. 82

3-7 LOF study analyzing the percent survival of the mutants. 83

3-8 Percentage of Dimerization for single mutants A110C, A111C, A112C, and A114C 85

3-9 Disulfide crosslinking in single and double mutants identified using western blotting.. 86

3-10 Monomers of single mutants and WT as a control exposed to reducing agent DTT....86

3-11 Double mutants E119C/V120C, L121C/L122C, L128C/L129C, and AAA exposed to 0.5 M NaCl-LB, water (2nd row), 0.5 M NaCl-LB and 1% H_2O_2 (3rd row), and water with 1% H_2O_2.. 87

3-12 Single channel traces of A110H and A112H when exposed to regular patch clamping buffer, and a patch solution of $ZnCl_2$ 89

3-13 Closed and opened state of MscL with mutations generated in this study highlighted. 93

4-1 A reversible hole in the bilayer formed from electroporation with an applied potential of -138 mV, and a current transition of more then -200 pA. 96

4-2 Mini-electroporation of a 100% DPhPC bilayer at 80 mV. Pores have a uniform current flow of 10 pA. 97

4-3 SEM images of the borosilicate pipette tips. 99

4-4 Electroporation of 100% PC at 120mV with a bilayer lifetime of 56 minutes. 101

4-5 Electroporation of 100% PE planar lipid bilayer with potentials applied from 100mV-180 mV. 102

4-6 Electroporation occurring with a 50PC/50PE bilayer within the 1st 25 sec. 102

4-7 Ramp voltages applied to the 70PC/30PE lipid mixture. 104

4-8 Episodic trace of the current in pA obtained lipid bilayer composed of 70PC/30PE 104

4-9 An 18 minute trace of 70PC/30PE lipid mixture. 105

4-10 Single channel conductance of Gramicidin A is around 67 pS when 60 mV is applied. 106

4-11 Plots of a 1.5 second run at negative 100 mV with and without Gramicidin.. 106

4-12 Plots IV curves for Gramicidin A for various KCl concentrations 107

5-1 Tethered bilayer membrane array. 116

5-2 AFM images of the monolayer deposition and vesicle fusion process.....122

5-4 A stable tethered bilayer form from vesicle fusion of 70PC/30PE LUVs. 123

5-5 Single channel activity of Gramicidin at an applied voltage of 60 mV with a conductance of 60 pS.. 124

5-6 I-V curves of Gramicidin in the tBLM on the device and within the tip-dip system.. 125

5-7 Single channel activity of multiple Gramicidin channels opened within the tethered lipid bilayer. 126

5-8 Single channel activity of WT MscL in the tLBM system: When 300 mV was applied to the membrane MscL opened conducting 266 pS.. 127

5-9 MscL displaying two conducting-states: 128

5-10 MscL with the lysine in the 31 position highlighted.....130

5-10 Single channel recordings of K31E (voltage sensitive mutant of MscL) within the tBLM. 130

5-11 Single channel activity of K31E at 143 mV. ions was 60 pA providing a conductance of 350 pS 131

LIST OF ABBREVIATIONS

DPhPC	1,2-diphytanoyl-*sn*-glycero-3-phosphocholine
DPhPE	1,2-diphytanoyl-*sn*-3-phosphoethanolamine
DPTL	2,3-di-O-phytanoyl-*sn*-glucero-1-tetraethylene glycerol-D,L-α-lipoic acid ester lipid
GOF	Gain of Function
LOF	Loss of Function
MscL	Mechanosensitive Channel of Large Conductance
tBLM	Tethered Bilayer lipid Membrane

Abstract of Dissertation Presented to the Graduate School
of the University of Florida in Partial Fulfillment of the
Requirements for the Degree of Doctor of Philosophy

A PROXIMITY AND FUNCTIONAL STUDY OF THE MECHANOSENSITIVE CHANNEL OF LARGE CONDUCTANCE RECONSTITUTED IN A TETHERED LIPID BILAYER

By

Danyell Simone Wilson

May 2009

Chair: Randolph Duran
Major: Chemistry

When creating a biosensor based on single ion channel activity, the conformational changes within a protein as well as the protein's ability to reconstitute successfully into non-native lipid environment and remain active must be understood. Therefore, the proximity of key residues in the C-terminal region of the Mechanosensitive Channel of Large Conductance (MscL) was quantified via disulfide bridging of cysteine mutations made to conserved hydrophobic residues in the linker and S3-bundle of this region. The biochemical assays utilizing disulfide bridging provided insight into which residues were dynamic and interactive, enabling them to be studied further via patch clamping. The channel's C-terminal region during gating was under debate and our results support the theory of the S3-bundle remaining closed during gating. Results from this study also enabled the generation of two new mutant channels that could coordinate heavy metals and the recognition response was a decrease in conductance, and slowed channel kinetics.

After the correct configuration of the protein was established, the ideal lipid environment for studying single ion channels in a tethered device for biosensor applications was investigated. The tip-dip electrophysiology method was used to determine an electrically stable lipid environment between different diphytanoyl compositions. Diphytanoyl lipids were vital

components of this research due to their increased durability and stability when tethering to solid supports such as the gold surface on the device. Results indicated all of the lipid-ratios suffered from pore formation due to electrical breakdown, both reversible and irreversible. This was the first time that electroporation was reported at such low potentials as 125 mV and 40 mV which may be characteristic of using the tip-dip method with diphtanoyl lipids. The pore formation was random; however distinguishable from single ion channel conductance by configuring I-V curves and evaluating the kinetics of the pores formed in comparison to channel activity. The lipid ratio of 70PC/30PE was chosen as the most stable lipid ratio and was integrated as the synthetic lipid environment for both Gramicidin and MscL on the tBLM device. Results for Gramicidin, indicated that single channel activity within the tBLM were characteristic of the channel. On the other hand, a high applied voltage was required to gate MscL and the conductance response was lower for this channel in comparison to when it is in its natural environment. This lead to the incorporation of a voltage sensitive MscL mutant, K31E, which sensed tension when voltages as low as 85 mV were applied. Preliminary results indicate that this mutant is very active within the tBLM and single channel activity is attainable.

CHAPTER 1
PROJECT OVERVIEW

Introduction

Biosensors are small analytical devices that take advantage and mimics nature's innate ability to sense trace level concentrations of analytes (*1*). Receptor proteins, for example, are classified as a type of affinity-based sensor found within many biological sensory systems (*2*). *Escherichia coli's* mechanosensitive channel of large conductance, MscL is a receptor protein that plays an important role in maintaining osmotic homeostasis of these microbes. This enables it to serve as a prototype for mechanosensory transductions, an excellent pharmacological target, and a candidate for biological nanosensors.

The goal of this project is to characterize the single channel activity of *E. coli's* MscL within a tethered bilayer lipid membrane (tBLM). The lipid bilayer environment provides both the hydrophobic and hydrophilic requirements of this membrane protein. Tethering the bilayer to a solid support and observing the single channel activity of wildtype (WT) MscL is the first step in creating a biological nanosensor. Results from this research can provide insight about the standard characteristics of WT MscL within the tBLM system. Once such standards are configured, future research projects can incorporate heavy metal, toxin-specific mutants of MscL, or we could generate mutants that alter the single channel activity. For instance, if the large conductance of this channel needs to be decreased to prevent overwhelming the microelectronic device, as part of this study we have molecularly engineered a lower conductance MscL. Combining this mutant and the tBLM system can lead to an array of stochastic nanosensors utilizing mechanosensitive channels (*3, 4*). Target environments might include biomedical systems such as blood or other biological fluids, and/or contaminated water samples (*2*).

In the following sections, a brief introduction of biological membranes and membrane proteins are presented. Ion channels, and pore forming peptides such as Gramicidin, are also reviewed. The latter will give a historical perspective and an in depth analysis of the advantages and disadvantages of studying bacterial mechanosensitive channels, in particular *E. coli's* MscL. Concluding this chapter will be details as to why planar lipid bilayers and tethered bilayer systems provide the best environment for this research.

Biological Membrane

The plasma membrane for both eukaryotes and prokaryotes serves as a semi-porous barrier encapsulating the cellular constituents (*5*). Phospholipids make up most of the lipids present in the plasma membrane (*5*). The structures of these oily substances include a hydrophilic phosphate head group, and a glycerol backbone connecting a hydrophobic tail region. As shown in Figure 1A, these compounds easily self-organize such that the hydrophobic tails are oriented inwards forming two integrated layers, known as a bilayer (*5*). The hydrophilic heads face the inside of the cell (establishing the intracellular face) and the outside (establishing the extracellular face) of the membrane. Since 1970, this system has been described as a fluid mosaic model of lipids and proteins.

Isolated and synthetic phospholipid bilayers can closely resemble the cell membrane and are excellent model systems for investigating specific biological processes that occur at the cellular level (*6-9*). Membrane proteins can be reconstituted into phospholipid bilayers, permitting the study of both *in vitro* functional analysis and protein-lipid interactions (*10, 11*). The amphipathic bilayer remains in a fluidic state allowing membrane proteins to diffuse through the double layer to serve as transporters, receptors and facilitators; enabling the cell to communicate with its environment as shown in Figure 1B.

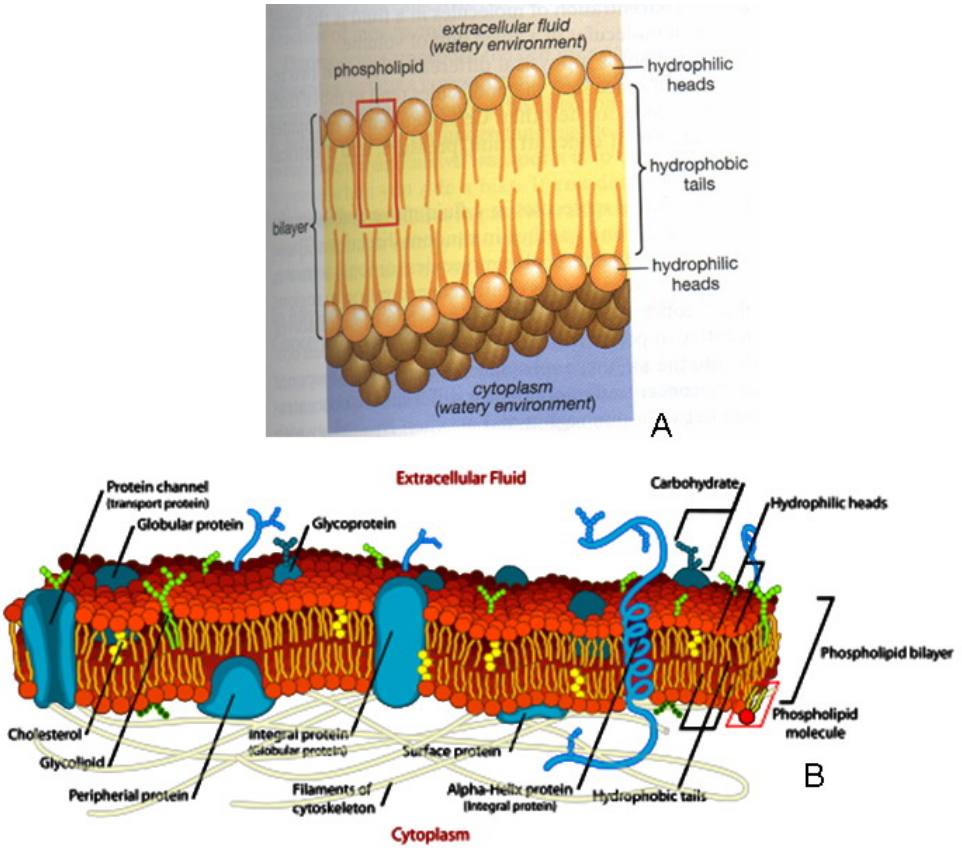

Figure 1-1. A) Phospholipids bilayer. B) The fluid mosaic model of the cellular membrane. Image obtained from Mariana Ruiz Villarreal with permission.

Membrane Proteins and Ion Channels

Membrane proteins are either attached to or associated with the membrane of a cell (*12, 13*). They exist in two main categories: peripheral membrane proteins and integral membrane proteins. Peripheral membrane proteins attach to the lipid bilayer or temporarily to an integral protein by a combination of hydrophobic, electrostrostatic, or other non-covalent interactions (*13*). Integral membrane proteins, on the other hand, are permanently attached to the membrane. They can be further classified according to their relationship with the bilayer as integral monotopic proteins or transmembrane proteins. Integral monotopic proteins are permanently attached to the membrane from either the extracellular or intracellular side (*13*). Transmembrane

proteins, the second form of integral membrane proteins, are usually amphipathic and span the entire membrane. One particular type of transmembane proteins are ion channels.

Ion channels are found within the membranes of all living cells. They lower the energy barrier for ions to permeate through the cell membrane. (*14*). An unequal distribution of ions including Na^+, K^+, Cl^- and Ca^{2+} between the intracellular and extracellular domain creates an energy barrier (dielectric barrier) termed the membrane potential. This potential which appears across the lipid membranes of all cells can be quantified in several manners. One estimate is given by the Goldman-Hodgkin-Katz Equation derived from the Nernst equation:

$$V_{\text{rest}} = \frac{RT}{F} \ln \frac{P_{Na}[Na+]_e + P_K[K+]_e + P_{Cl}[Cl-]_i}{P_{Na}[Na+]_i + P_K[K+]_i + P_{Cl}[Cl-]_e} \tag{1.1}$$

where R is the gas constant, T is temperature, F is the Faraday constant, P_x is the permeability and $[X]_I$ and $[X]_e$ are the internal and external concentrations of the respective ions (*15*). The equilibrium (resting potential) of a cellular membrane occurs when the intracellular and extracellular ionic concentrations are equal. According to the Goldman-Hodgkin-Katz equation, ion permeability depends on the ion's size, mobility and concentration. Therefore at different membrane potentials, certain ion channels will translocate specific ions to reach equilibrium.

The cellular membrane can be viewed as an RC circuit (refer to Figure 1-2). According to Ohms law the resistance R is equal to the current I, times the voltage V, as seen in equation 1.2:

$$R = IV \tag{1.2}$$

The conductance also according to Ohms law is the inverse of the resistance. Ion channels are like conductors G or gi for specific ions I, across the cell's membrane. The electromotive force (Ei) (refer to Figure 1-6) fueling ions to translocate through the channel is the difference of the total potential (potential across the membrane, and the potential of the pore):

$$Ii = gi\ (E-E_0) \quad (1.3)$$

$$G = 1/R \quad (1.4)$$

The capacitor would represent the membrane separating the salt solutions (internal and external ionic solution).

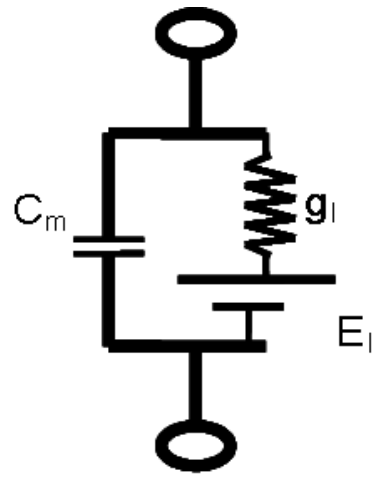

Figure 1-2. Equivalent circuit model of the ion channel within the lipid membrane. The ion channel g_i, for ion i, the membrane capacitance and the electromotive force of the pore are C_m and E_i respectively.

This capacitance contributes to defining the number of ions needed to transmit an electrical charge as exemplified in the following equation (*15*):

$$C = Q/E \quad (1.5)$$

C is the capacitance that measures the amount of charge Q, which is required to set up a given potential difference, E across the conductors (the membrane and eventually ion channels). The change of potential due to current flow I_m through the ion channels in the membrane and by small ions that are able to diffuse through microscopic opening in the membrane is expressed as:

$$dE/dt = I_m/C \quad (1.6)$$

For a given membrane environment, the capacitance is relatively constant. When characterizing membrane properties, the capacitance of the lipid bilayer is described by:

$$C=K\varepsilon_0 A/d \quad (1.7)$$

Where K is the dielectric constant of the given lipid, ε_0 is the vacuum permittivity of the system, A is the surface area of the lipid layers and d is the thickness of the bilayer (*15*).

The membrane capacitance adds resistance to the flow of ions at a given time τ, making the previous equation:

$$dE/dt = Im/C = -E/RC = E/\tau \quad (1.8)$$

Where R is the resistance; we next take into account the initial potential E_0, and derive the equation as follows:

$$E = E_0 \exp(-t/RC) = E_0 \exp(-t/\tau) \quad (1.9)$$

From this we see that the resistance of the membrane and the time constant τ when ions are transfusing during rest varies from membrane to membrane which is important when considering the results from Chapters 4 and 5.

Ion channels are very selective towards specific ions; and certain entities may play a major role with the functioning of a channel. For instance, all ion channels have two functional units: 1) a gate that is triggered to open or close via a ligand, a voltage, or changes in the surrounding bilayer 2) a selectivity filter that determines the ions that may pass. Listed in Table 1 are the triggers that are responsible for initiating either a change in conformation of the ion channel or an opening of a gate/plug within the channel. The opening of an ion channel either allows an influx of specific ions from the extracellular region or an outflow of specific ions from the intracellular region. This exchange of ions is known as translocation.

The selectivity filters for individual ion channels consist of specific transmembrane amino acids within a certain "signature sequence" near the N or C terminus and/or a limitation of the translocating pore size (*16*). Dr. MacKinnon, the 2003 Nobel Prize winner in chemistry,

discovered conserved signature sequences of amino acids near the N or C terminus with potassium channels from bacteria to eukaryotic cells (*16*).

Table 1-1. Different types of ion channels.

Ion Channels	Conformational Triggers
Voltage-gated channels	Open or close, depending on the membrane potential
Ligand-gated channels	The channel is usually embedded in a larger molecule that has a binding site for a specific ligand on the surface above the membrane. The binding actives opening of the ion channel
Cyclic nucleotide-gated channels	Internal solutes mediate cellular responses to secondary messengers, along with Ca^{2+} activate opening of these channels
Stretch-activated channels	Activated open and closure response from local stretching or compression of the surrounding membrane
G-protein-gated channels	G-protein attaching to the receptor triggers opening
Inward-rectifier K	Only allows for the influx of K^+ into the cell only
Light-gated channels	Directly opened by light
Resting channels	Constantly open

Channel forming Pores

Some ion channels are formed from single peptides that span the membrane, allowing the translocation of ions. These channels do not require a particular stimulus to control the opening and closing of the channel. In nature these channels are usually released from certain organisms as a poisonous defense mechanism or as an antibody. Some of these single peptides include neutral carriers like Valinonycin and Nonactin, while other transmembrane spanning pores are Nystain, Amphotericin, Tyrocidin and Gramicidin A (*17, 18*). One of the most studied channel-forming-pores is Gramicidin. This hydrophobic peptide antibiotic is produced by *Bacillus brevis* through an enzymatic synthesis at the onset of sporulation (*17*). Five different types of Gramicidin exist: Gram-A, B, C, D, and S. Gramicidin A, B, C, and D all form linear structures while Gramicidin S forms a cyclic peptide. Gramicidin D is a combination of Gramicidin A, B, and C (*17-19*). The difference between Gramicidin A, B, and C exist within the amino acid sequence. The trptophan in position 11 for Gramicidin A is replaced by a l-phenylalanine for

Gram-B, and l-tyrosine for Gram-C (*17-20*). The duration of this paper will focus on Gramicidin A which will be termed Gramicidin.

Gramicidin forms a transmembrane pore when two of the 26Å long monomers connect at their N-termini. Six H-bonds at the dimer junction stabilizes the pore in this conformation as shown in Figure 1-3. Solid-state NMR, 2-dimensional NMR, circular dichroism and single channel analysis were all used to determine the structure of Gramicidin as a right-handed (RH), single stranded β-helical membrane-spanning dimer (*18*). This structure only occurs when the protein is in a bilayer, and/or micellar environment. In organic solvents, Gramicidin's structure is either an unfolded (random coil) monomer or several intertwined double-stranded (DS) dimer β-helixes (*18*). The folding of the Gramicidin within the bilayer depends on the length of the acryl chains. Bilayers with a chain length of at least eight carbons tend to provide a sufficient environment for the proper folding of Gramicidin (*18*). The pore diameter is roughly 4 Å wide and the channel is selective to monovalent cations (K^+) and some small anions like Cl^- (*18*).

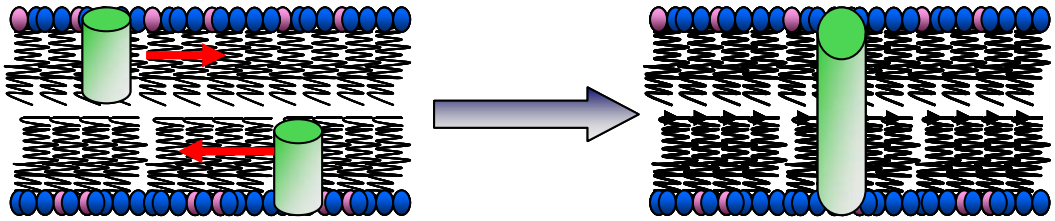

Figure 1-3. Schematic of Gramicidin forming a pore in a synthetic lipid bilayer membrane.

As a model system a number of biophysical characteristics have been determined and compared for Gramicidin. Some of them include: effects of the surrounding membrane thickness, the salt concentration in the surrounding solution, the membrane potential and temperature have been assayed for different lipid membrane environments. The short 15 amino acid sequence of alternating L-and D- configurations, enables it to serve as a model system for understanding basic characteristics of ion channels in synthetic lipid bilayer membranes. In

addition, Gramicidin has also served as a model for studying ion permeations, both local and long range protein-lipid interactions as well as structure-function relationships (*19*).

In this study, Gramicidin is used to evaluate the tBLM approach as a suitable environment for incorporation of ion channels before introducing the mechanosensitive channel into the system.

Stretch-Activated Channels

Stretch-activated or mechanosensitive (MS) channels participate in many important physiological processes including pain sensation, micturition (discharge of urine), hearing, salt and fluid balance, and turgor (pressure control of the cell) changes (*21*). They react to mechanical stimuli triggering a shift in equilibrium from a closed to open conformation of the protein (*10*). MS channels have been discovered in all the fundamental branches of the phylogenic tree including Bacteria, Archaea, and Eukarya (*22*).

In eukaryotes MS channels subsist in the degenerins and epithelial sodium (DEG/ENaC) family, the transient receptor potential (TRP) family, and the mammalian two-pore K^+ family. They sense mechanical stimuli in auditory cells, as stretch receptors; and they are located in muscle spindles, in vascular endothelium and in neurosensory tissues (*23*). Most of the information obtained concerning the functionality of these channels is inferred from genetic data, both cellular/tissue localization of the proteins or functional manifestations in mutant or knockout animals (*22*). Theses channels usually form multi-component protein complexes, and their actual gating mechanisms are largely unknown. For these reasons, it is difficult for eukaryote MS channels to serve as model MS channels.

Bacterial MS channels have largely served as the model system for mechanosensory transductions for several reasons (*24, 25*). 1) Their genetic sequence was the first to be cloned and the small gene size allowed for random mutagenesis generating massive libraries of mutant

MS channels (*22, 26-29*). 2) Conserved sequences were discovered from different bacteria, permitting the identification of conserved regions in 35 MS homologs, providing information relevant to similar regions within these channels (*22*). 3) Bacterial MS channels gate by sensing tension in the membrane independent of other proteins or artifacts allowing them to serve as a "simple", easy-to-gate molecular model for functional studies. 4) To add to the plethora of information obtained from genetic modeling, both structural and functional evidence of MS channels in eukaryotes and prokaryotes were obtained from studying bacterial mechanosensitive channels. For instance, *Escherichia coli's* MS channel of large conductance (MscL) is the most functionally studied MS channel.

***E. coli's* MscL**

To give a historical perspective about the discovery of this protein, there were two incidents that contributed in the early 1990s: the advancements in the patch clamp technique and the unveiling of E. coli's genomic sequence. The patch clamp recording technique at that time measured electrical current from small patches of eukaryotic cellular membranes, allowing the isolation of ion channels (*30*). Modifications to the preparation of bacterium by Kung *et al.* which will be discussed in detail in Chapter 3, allowed the patching of these once inaccessible single cell organisms (*31*). The application of suction to the patch clamp electrodes containing the membrane, led to the discovery of channels that responded to the changes in mechanical characteristics of the bilayer (*32*). These channels were novel at the time and identified as mechanosensitive channels. When different variations in pressure were applied to the electrode causing changes in tension in the membrane, different conductance states were observed, indicating the existence of multiple mechanosensitive channels.

Remaining mindful of the Gram negative classification of *E. coli*, a series of experiments were conducted to examine the actual location of these channels within the inner membrane of

the cell (*33*). This modification took place in 1989, and it was not until 1993 that Kung *et al.* discovered the genetic sequence of the mechanosensitive channel of large conductance (MscL).

The biochemical assay employed to identify the gene responsible for MscL was achieved by a series of membrane fractions being solubilized using columns that separated the protein according to their biochemical properties (*34*). This was followed by reconstitution of each fraction into azolectin lipids that were assayed by patch clamping for channel activity. Gel electrophoresis was then used to assay fractions containing a significant number of channels followed by a second separation using an independent column (*34*). This process was performed repeatedly, until results from electrophoresis provided one single protein band indicating the channel was generated from a single gene product. The band was 17kD (*34*). Consequently, the 37 amino acids that were identified at the N-terminal matched a sequence that was generated unintentionally by a group studying the gene for *trkA* (*35*). Hamann *et al.* over sequenced the gene predicting the first 38 residues of the next gene which was a perfect match for the putative MscL sequence. These key experiments provided the genetic information enabling the cloning and sequencing of the proposed *mscL* gene encoding a 136 amino acid protein in length with two transmembrane domains by Sukharev *et al.* (*34*).

It was at this point, that the team leading the discovery of *E. coli's* MscL, which included Drs. Sergi Sukharev, Paul Blount, Boris Martinac, Frederick Blattner, and Ching Kung, realized the larger protein band obtained from electrophoresis and a non-denaturing gel filtration column suggested the overall structure had to be a homo-multimer. Unsure of the actual structure and mechanisms driving the functionality of this protein, the authors began an intensive investigation to determine if the gene sequenced was responsible for the activity of MscL. They generated *mscL*-null (deletion of the gene encoding for MscL) mutants using insertional disruption and

assayed for channel activity by patch clamp; the lack of activity was consistent with MscL playing a role. They also conducted biochemical studies that correlated with the electrophysiology studies. The final experiment involved translating the gene that encoded the 136 amino acids with a cell-free system, followed by reconstitution of the resulting protein into liposomes and utilizing patch clamping as the electrophysiological assay to observe the single channel activity of MscL (*36*).

MscL Function and Structure

The proposed function of MscL as a biological "emergency release valve" for bacteria under hypo-osmotic stress came with the identification of smaller mechanosensitive channels with a redundancy in function (*26, 32, 37*). When the bacteria cell is placed in hypo-osmotic conditions, MscL senses the tension in the membrane causing it to open a conducting pore releasing osmolytes (*38-41*). MscL has a conductance of ~3 nS. When there was no distinct phenotype characteristic for null MscL, MscS and MscM (mechanosensitive channel of small and mini conductance) open saving the cell by suppressing the phenotype. These two channels also sensed tension in the bilayer and are characterized according to their conductance. The two smaller conducting MS channels are the mechanosensitive channel of small conductance, MscS (~ 1 nS), and the MS channel of mini conductance, MscM (0.3 nS). This report does not serve as a review for all of the MS channels in *E.coli*. The remainder of this report will focus on MscL from *E. coli* because it is the most functionally studied and the basis of this research. If the reader is interested in the other MS channels, reference (*42*) provides a very good introduction.

Topology studies of the MscL revealed the location of both the N- and C-termini within the cytoplasm and supported the idea of the protein consisting of two transmembrane domains (*43*). As with most topology studies that lack crystal structures, discrepancies can lead to misinterpretations that in this case suggested the protein was a hexamer instead of a pentamer

(*43*). Theses studies did however; lay the foundation for structural studies of this protein. It was not until 1998, when Douglas Rees's group obtained the crystal structure of the MS channel from *M. tuberculosis* using X-ray crystallography data with a resolution of 3.5 Å, that MscL was confirmed to be a pentamer (*10, 21, 44-48*). The identification of both the N and C terminal in the cytoplasmic region of the cell was also confirmed. The identification of two transmembrane domains (TM1 and TM2) joined by a periplasmic loop, as shown in Figure 1-4 was confirmed as well. The TM1 from each peptide forms the 30-40 Å pore in response to tension in the membrane bilayer, releasing ions and other solutes from the cytoplasm while the TM2 domain faces the lipid membrane (*49*).

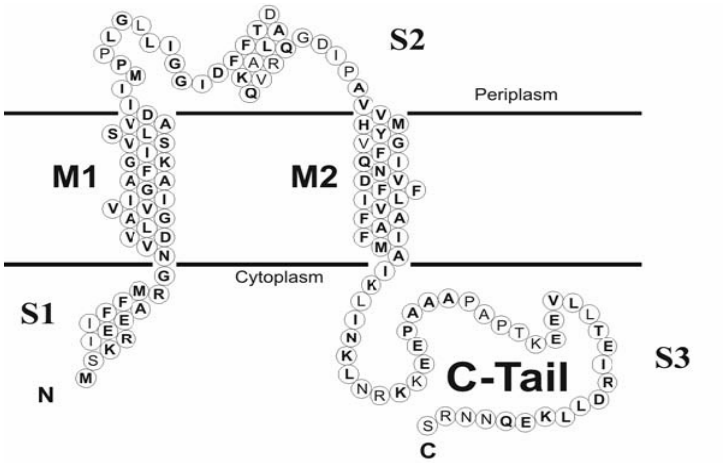

Figure 1-4. Schematic representation of *E. coli's* MscL amino acid sequence and topology of one monomer. Each peptide of the homo pentamer has a S1 region that begins with the N-terminal, two transmembrane regions TM1 (forms the pore) and TM2 which interacts with the lipid bilayer. They each have a perplasmic loop, and S3 region that ends with C-terminal. Images adopted from reference with permission from Dr. Blount (*43*).

Mutagenesis studies have indicated the periplasmic loop plays the role of a torsional spring, inhibiting the channel from gating under non-osmotic conditions (*50*). The role and conformation during gating of the two cytoplasmic domains, the N-terminal and the C-terminal,

however, is unclear. What is known about the C-terminal region is that it consists of a linker area starting just after TM2 and the α-helical bundle termed S3-bundle.

S3-COOH-Bundle

A detailed evaluation of the S3-α-helical bundle obtained from the crystal structure of *M. tuberculosis* revealed a conformation in which the hydrophobic side-chains were exposed outside the S3 helix with the hydrophilic and charged side-chains packed inside the bundle as shown in Figure 1-5A (*51*). This conformation was originally predicted to be an artifact of the acidic conditions used in the crystallization process, for such a conformation is not predicted to be stable at physiological pH (*52*). In 2001, Sukharev *et al.* proposed a molecular model of *E. coli's* MscL. Given that the C-terminal structure was in dispute, this group predicted its structure under physiological conditions and changed the orientation of the helices.

In 2003, Sukharev proposed a similar model for the S3-bundle based on an apparent structural homologue, the COMP protein (*51*). COMP is an extracellular protein that mediates the assembly of the cartilage. It has an extracellular matrix with a five-fold coiled-coil N-terminal stabilized by polar interaction in a bundle (*51*). The C-terminal of *E. coli's* MscL computationally generated from the COMP model has a "refined" structure with a stabilized left-handed coiled-coil S-3 bundle as shown in Figure 1-5B. Indeed, a recent reanalysis of the raw X-ray density map has led to a revised model of the *M. tuberculosis* crystal structure, which is now within the Protein Data Bank (http://www.rcsb.org 20AR) where one of the more significant changes is that the S3 helical bundle more closely resembles Sukharev and Guy's model.

Note, however, that the models described above dealt only with the structure of this domain while the channel is in the closed conformation. Given that there are large structural changes that occur upon channel gating, an obvious question was whether the S3-bundle

remained intact upon channel gating. If so, the linkers between S3 and TM2 behave as "sieves" allowing the passage of only smaller intercellular components (see Figure 1-6).

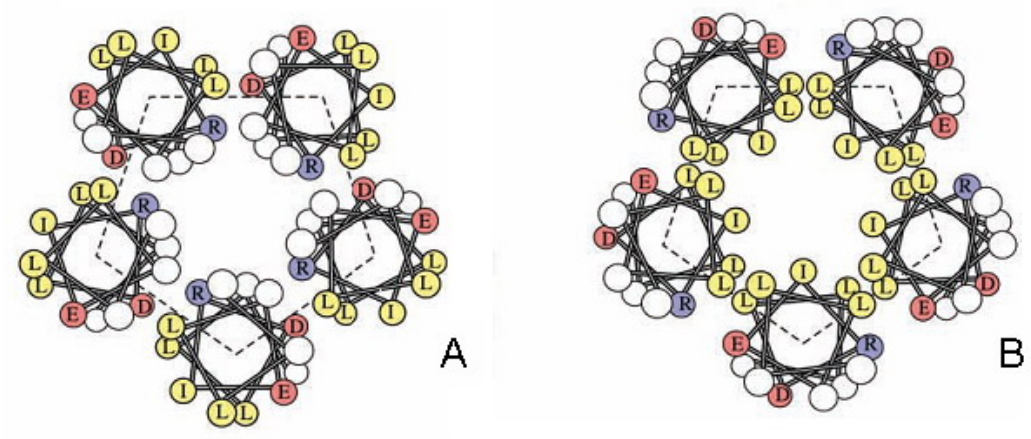

Figure 1-5. Helical wheel of the S3-bundle adapted from A) *M. tuberculosis* and B) the COMP protein. A) The hydrophobic residues, leucine and isoleucine are facing the cytoplasmic region while the hydrophilic arginine is buried inside the bundle. B) The correct orientation at physiological pH of the S3-bundle modeled by Sukharev and Guy, with the hydrophobic residues inside the bundle. Image borrowed from reference *(12)* with permission from Sukharev.

To test this model, disulfide bridging of mutated cysteines within the helical bundle was assayed subsequent to French pressing the cells and following protein purification. These data were compared to patch clamp data. Since disulfide bridging was observed in the biochemical assay, it was assumed the S3-bundle remained intact during gating and these results were representative and comparable to the patch clamping of sheroplast (giant bacterial cells). However, biochemical studies using disruption buffer, French pressing and/or ambient oxidative conditions may influence oxidation either before, after or even during gating. Many factors including the degassing of the buffer prior to usage with ambient oxidative conditions and French pressing which destroys the membrane by using extremely high pressure may cause changes in the oxidative conditions of the protein. Therefore, one can not assume disulfide bridging occurring with these biochemical conditions is comparable to bridging occurring *in vivo* with sheroplast using the patch clamp. This leads us to examine the functionality of the S3-

bundle for possible clues to its conformation during gating. There is a possibility that mutating this region can decrease the channel conductance.

Functionality of the S3-Bundle

In the proposal where MscL S3 domain is modeled after COMP, the actual function of this region is believed to limit the size of small inorganic molecules that can pass during osmotic shock (Figure 1.6) (*51, 53*). However, in 1997, Cruickshank *et al.* conducted molecular sieving studies that suggested the pore must be at least 30-40 Å (*49*). The cytoplasmic proteins released by osmotic shock includes the fairly large thioredoxin, the elongation factor Tu, and the molecular chaperone DnaK (*54*). The mechanism release for these molecules was up for debate until recently. The discrepancy between these two studies was resolved by a subtle difference in experimental approach, indicating these proteins are actually released through MscL (*54, 55*). These studies however support the possibility of the S3-bundle opening and folding into the bilayer, accommodating the sizes of the proteins being release (*55*).

Regardless of which of the models shown in Figure 1-6 are correct, it seems likely that the C-terminus can be manipulated to decrease the conductance of MscL. If the S3-bundle dissembles during gating as shown on the left in Figure 1-6, then locking this area together using cysteine bridging should decrease the conductance. If the other model (on the right) is correct and the S3-bundle remains stable allowing the linker region to stretch and filter the osmolytes, then creating disulfide bridging in this region and immobilizing the linkers should decrease MscL's conductance. Decreasing the conductance of MscL may enable it to be reincorporated within the tBLM on a microelectronic device with other ion channels and its conductance will not over shadow the other lower conducting channels. In addition, decreasing the conductance would also be a preventive measure in assuring MscL's large conductance does not over-whelm the small microelectronic devices due to the large amplification of the signal. Understanding the

possible conformational changes in this region may also assist with the reconstitution this protein into the tBLM. If the S3-bundle does remain stable and does not affect the functionality of MscL, then cleaving it may yield greater protein expression and reconstitution.

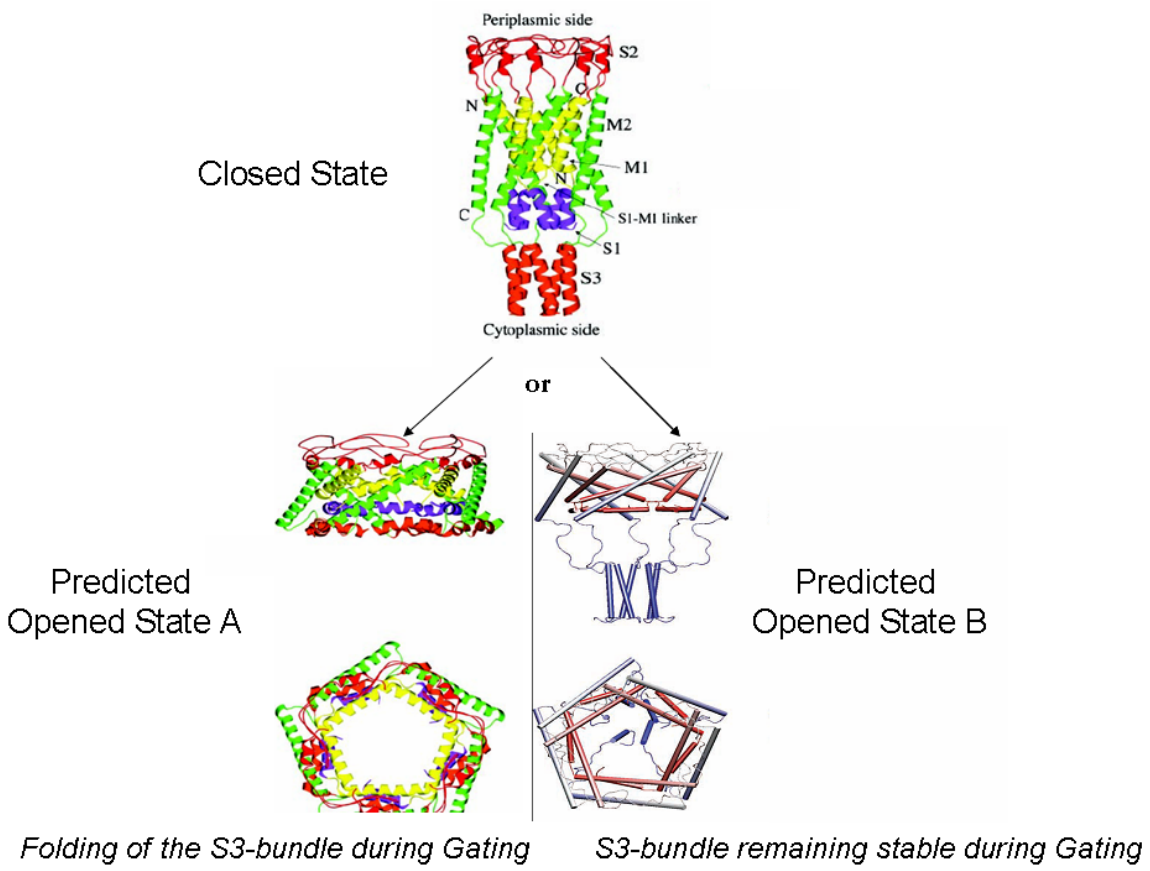

Figure 1-6. Conflicting models of the S3-bundle during gating. The top schematic is the closed state of MscL according the pdb structure (OAR). On the right there is a side and top view of the opened state with the S3-bundle separated and folded into the bilayer. On the left is a side and top view of the open state of MscL with the S3-bundle closed during gating and the linker region expanded. Images adopted with permission from references: (*51, 56*)

In collaboration with Dr. Paul Blount's laboratory at the University of Texas's Southwestern Medical Center we utilized disulfide trapping to examine the dynamics of the S3-bundle and the TM2-S3 linker region. Specifically, we performed disulfide-trapping experiments *in vivo* to assay the proximity and mobility of key residues in C-terminal region. We chose to mutate amino acids that may be either in close proximity (hydrophobic residues

located inside the S3-bundle) or that may interact over time (residues in the linker region) to cysteines and assessed the multimerization via disulfide bonds using an immune blotting technique. Then, we used the inside-out patch-clamping method to characterize the function of the mutations that yielded the most intense disulfide bridging. These mutants were assayed under oxidizing conditions using 0.5% H_2O_2 to determine if disulfide bridging between amino acids in the C-terminal domain affected the functionality of the protein. We predicted that a decrease in conductance under these conditions would verify bridge formation and a successful alteration of the conformation during gating. By performing this set of experiments, we determined whether the S3-bundle remains shut allowing the C-terminal region to behave as a sieve regulating the release of cytoplasmic solutes. We then took it one step further and attempted to lock the sieve region and looked at the overall single channel activity using inside out patch clamping. Finally, we characterized WT MscL within a tethered lipid bilayer as the first step to creating an MscL-based biosensor. Incorporating *E. coli's* MscL into the tethered lipid bilayer, which was done in this study, has added to the overall fundamental knowledge of MS channels in different environments.

Solid-Supported and Tethered Lipid Bilayers

Modifying solid-substrates with lipid bilayers provides mechanical mobility, functional stability and a non-denaturing environment for membrane proteins (*57*). Solid-supports or substrates range from glass, silicon and mica to metals such as platinum and gold (*11*). Several technical approaches have been employed to create solid-supported lipid bilayers as shown in Figure 1-7. These bio-mimetic supports include solid-supported lipid bilayer (ssBLM) (*7, 11, 58, 59*), polymer-cushioned lipid bilayer (*60, 61*), hybrid bilayer (*62, 63*), tethered lipid bilayer membrane (tBLM) (*64-68*), freely suspended lipid bilayer (*69, 70*), and a supported vesicular layer (*71, 72*). It can be quite confusing when such systems are generally referred to as solid-

supported lipid bilayers (ssBLM), which is a specific type of solid substrate and bio-mimetic technique. Therefore, for the duration of this manuscript, the actual technique will be referred to as either solid-supported lipid bilayer or ssBLM, and the category or membrane model will be termed solid substrate or solid supported systems.

In 1985, Tamm and McConnell conducted one of the first solid supported lipid bilayer studies (*73*). They studied the lateral diffusion of a mixture of lipids sequentially transferred from two monolayers at the air-water interface under an oxidized silicon wafer by extreme pressures (*73*). Utilizing fluorescence recovery after pattern photobleaching, they concluded from lateral diffusion measurements that the lipids alignment and movement on the solid supports was similar to conventional multilayer systems (*73*).

The early experiments by Tamm and McConnell have enabled others to further explore the field by attaching polymers to solid substrates, allowing them to serve as cushions, supporting the bilayer and enabling the reconstitution of membrane proteins. Some researchers have also taken advantage of redox reactions that enable thiol-lipids to bind to oxidized metal substrates and form monolayers that can tether planar bilayers. Today an abundance of both analytical and physical techniques such as electrical impedance spectroscopy (ESI) and atomic force microscopy (AFM), which are used for analyzing globular proteins and require a solid surface, can now be employed for characterization of membrane proteins when reconstituting them into solid-supported bilayers.

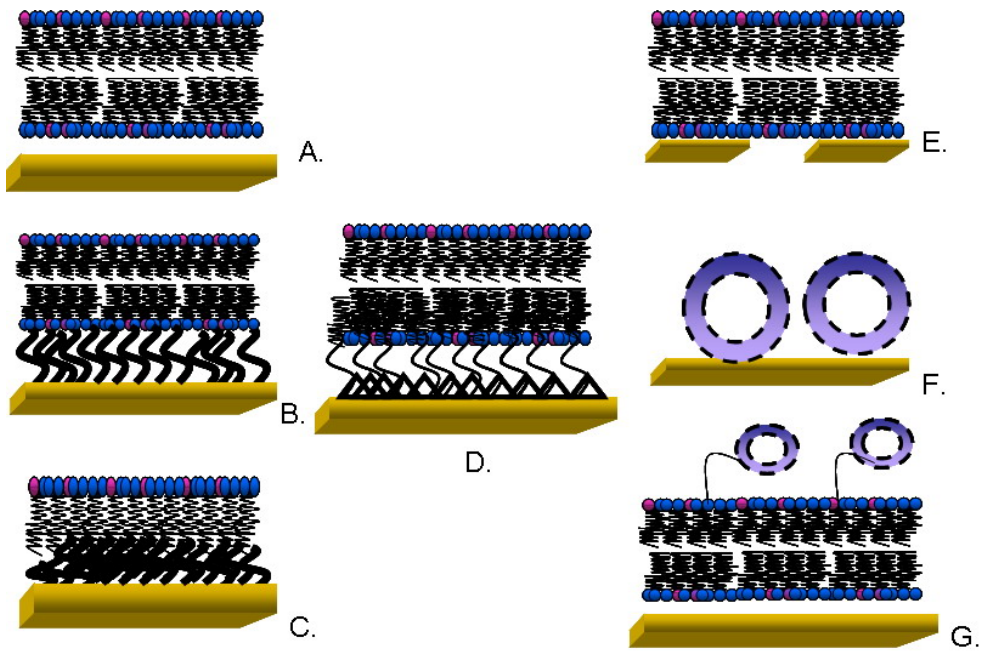

Figure 1-7. Solid-Confined or supported membrane. A) Solid-supported lipid bilayer. B) polymer-cushioned lipid bilayer. C) Hybrid bilayer. D) Tethered lipid bilayer. E) Freely suspended lipid bilayer. F-G) supported vesicular layer.

Relevant to this work, these previous studies have confirmed several key features of solid-supported systems: 1) It is possible to fabricate solid substrates that can interact with lipid bilayers. The substrates can either become charged by oxidizing the surface, or hydrophobic from which a thin aqueous layer between the lipid and the solid surface exist (*73*). 2) Van-der-Waals, electrostatic, hydration and steric forces control the interactions between the oxidized supports and the planar bilayer. 3) The physiochemical behavior of planar bilayers, including a solvent-free environment is still required for solid-supported bilayers (*11*). 4) Rehydration of the bilayer is required in order to ensure the lamellar phase of the lipids. 5) Lastly, bilayers can be formed from either two monolayer transfers or via vesicle fusion (*63*). The goal of this research project, which is to establish a stable, fully fluidic, electrically insulating and robust planar lipid bilayer, is made possible due to the previous research accomplished in this interdisciplinary field.

Bilayer requirements for this research include having a conducting solid support, a planar bilayer and a substantial aqueous layer between the metal's surface and the bilayer. Therefore, four out of the seven solid-supported techniques were considered for possible membrane systems: the solid-supported BLM, polymer-cushioned lipid bilayers, hybrid bilayers, freely suspended bilayers and tethered bilayers. Solid-supported lipid bilayers as shown in Figure 1-7A, are usually formed on a hydrophilic support (glass or oxidized silicon wafer) by vesicle fusion or by the sequential transfer of two monolayers from the air-water interface (*68*). Even though this was the first solid-supported system, there were a number of shortcomings that exist within this device, including the small aqueous layer between the bilayer and the solid support. Some researchers hypothesize that this configuration would negatively affect the function of the proteins and their lateral mobility, particularly for proteins containing large domains outside of the membrane (*73*). Another concern associated with the ultra thin aqueous layer between the support's surface and the bilayer is the lack of support for total reconstitution of membrane proteins with cytoplasmic regions, as in the case for MscL (*65, 67, 68, 74-77*).

Polymer-cushioned and hybrid bilayers would both offer long-term stability of the bilayer in this research project. Polymer-substrates form by creating a double tethering of the polymer to the substrate's surface and to the bilayer. This interface enhances the robustness of the system (*61*). However, when studying the polymer-cushioned system, Neumann *et al.* concluded that lateral diffusion within the polymer-cushioned bilayer is highly restricted (*61*). Lateral diffusion is an important parameter for this study due to the necessity of reconstituting MscL into the bilayer. When researching the hybrid bilayer system, Anne Plant *et al.* noted the lack of electrical resistance that occurs when the synthetic monolayer that forms the hybrid bilayer

combines with the natural phospholipid's upper leaflet. High electrical resistance enables proper measurement of single ion channel studies(*63*).

Freely suspended lipid bilayers as shown in Figure 1-6E, resemble the classical planar/black lipid bilayers. The difference between the two systems is the formation of the bilayer over an aqueous pore. Planar lipid bilayers formation occurs over an aperture of 0.1-1 mm. Whereas freely suspended lipid bilayers are formed over a 25-75 nm hole (*69*). Nonetheless, the membrane's resistance within both the freely suspended and planar lipid bilayer is low, which allows for an increase in background noise from leakage through the bilayer (*58, 69, 78*).

Tethered lipid bilayers provide an ideal system for the development of the biosensor studies occurring in this research. They possess a large hydrophilic ionic reservoir for ion mobility and incorporation of the cystoplasmic-terminal region of MscL. Bilayer formation via vesicle fusion in this technique, provides a bilayer with high electrical resistance and one that is fluidic in nature, allowing lateral diffusion of different sized proteins (*61, 65-68*).

Tethered Lipid Bilayers/Membranes (tBLM)

Tethered lipid bilayers are prepared in a two-step process. First, a monolayer is self-assembled using a small percentage or lipids which are covalently attached to the substrate. Then lipid vesicles fuse to the monolayer, tethering the bilayer to the system (*79*). Membrane proteins such as ion channels are either incorporated into the vesicles before they fuse to the bilayer or proteins can be added to the bilayer once it has self assembled on the monolayer substrate. Cornell *et al*. first developed the tethered bilayer system in an effort to create a biosensor based on ion-channel switches in 1997 (*57, 80*). In 2003, Knoll *et al.* introduced a stable thiolipid system, 2,3-di-O-phytanoyl-sn-glucero-1-tetraethylene glycerol-D,L-α-lipoic acid

ester lipid (DPTL), that now serves as the monolayer forming component for tethered bilayers developed on gold surfaces (*9, 81*).

This monolayer system consists of a thiol anchor group that covalently attaches to the solid gold surface, a hydrophilic region that forms an aqueous reservoir, and an isoprenoid chain tail region that interfaces in the bilayer formed from vesicle fusion as illustrated in Figure 1-8 (*81*). Each component of the thiolipid system plays a key role in the overall stability of the tethered bilayer.

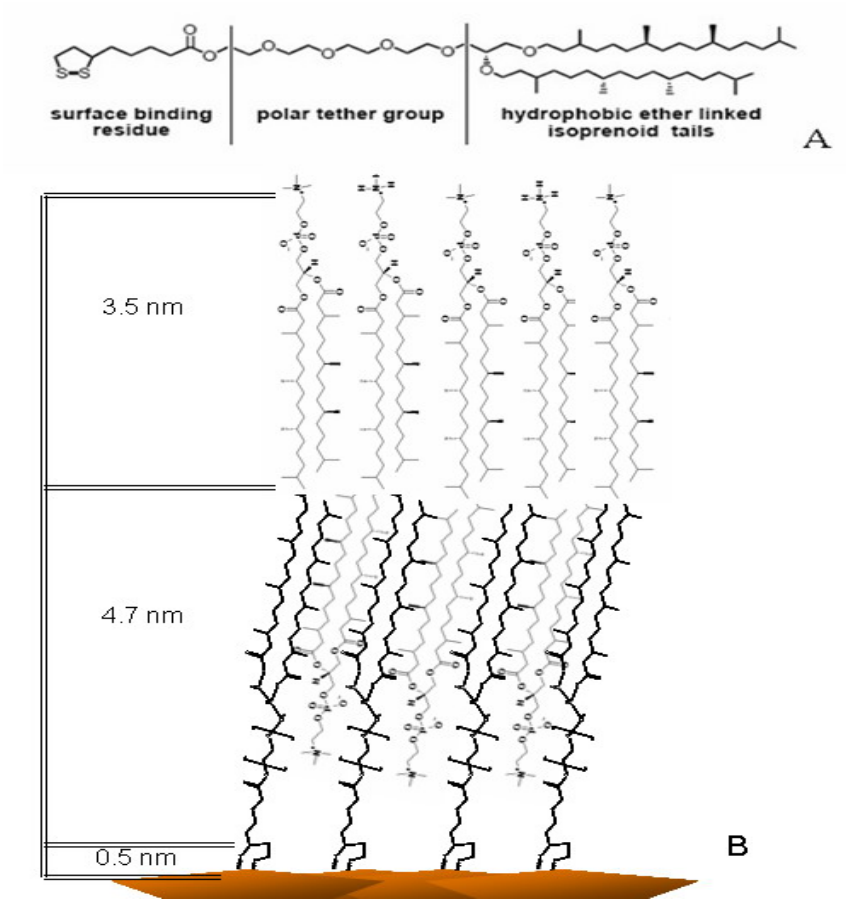

Figure 1-8. The tethered monolayer component. A) The structure of 2, 3-di-O-phyl-sn-glucero-1-tetraethylene glycerol-D, L-α-lipoic acid ester lipid (DPTL). B) The length of DPTL attached to a gold surface and the tethered bilayer.

DPTL

Surface Binding Region

The surface binding region of the tBLM creates the foundation of the system, stabilizing the lipid matrix to the solid support. A gold surface is utilized in this research as the solid support. The thiol (R-SH) group from DPTL forms covalent bonds with the oxidized gold surface via a self-assembling monolayer (SAM) process that offers a number of advantages including (*82*):

- Ease of preparation
- Tunability of surface properties via modification of the molecular structure
- Enhancement of lateral structuring on the nanometer scale

SAMs spontaneously form, creating complex hierarchical structures from random molecular assemblies (*61, 82*). Thiols (R-SH) on gold surfaces are identified as both a traditional and model SAM system where the bond becomes a thiolate (RS-Au) because of sulphur's affinity to first adsorb to the gold (*82*). The next step in this chemisorptions process includes the diffusion of DPTL on the gold's surface. One of the major benefits of using DPTL is the dithiol (sulphur bond) which covers 5% of the gold's surface. This allows for maximum insertion of membrane proteins with intracellular components as well as an increase in the aqueous reservoir under the bilayer. Another benefit of having the dithiol bonds is it ideally decreases the ability of the sulphur to move on the gold's surface. The sulphur is known to be mobile on the gold surface, sometimes moving with one or more gold atoms bound to it (*82*). By creating a dithiols, we believe the affinity for movement will be decreased, allowing the development of a stable monolayer. One of the most important requirements in developing a thiol-gold SAM, is an extremely clean and ultra smooth surface, which leads to better insulating properties of the tBLM, better self-assembly, and overall heterogeneity of the monolayer (*9, 65, 82*).

The Polar Tethered/Hydrophilic Region

The tetraethylene-glycol region of DPTL provides a hydrophilic ionic reservoir between the gold's surface and the membrane. This area is structured similar to that of the cytosol/cytoskeleton found in natural systems (*80, 81*). It spans roughly 1.4-4.7 nm and ion flow is driven by an externally applied potential between the gold surface and a reference electrode in a bulk solution above the bilayer (*76, 83*). An increased length of the ethylene glycol chain affects the stability and viscosity of the ionic reservoir. Adding more ethylene glycols causes the oligimer to adopt motifs slightly distorted in a helical conformation, which hinders the formation of a monolayer on the surface (*9, 68*). DPTL takes on a 7/2-folded-chain-crystal (FCC) helical conformation (lamellar phase) that is stable and allows the disulfides to adsorb perfectly to the gold's surface (*79*). A decrease in ethylene glycol chains will also decrease the depth of the ionic reservoir and the mobility of ions in this region. Therefore, tetraethylene glycol provides a stable structure suitable for the experiments taking place in this study.

Diphytanyl Tail Regions

The isoprenoid chains that carry four isoprene units of diphytanyl form the hydrophobic tail of DPTL. This region assists with forming the lower leaflet of the tethered bilayer (*66, 79, 81, 84*). Serving as the protective membrane surrounding extremeophiles and archaea, 2,3-di-O-phytanyl-sn-glycerol units are known to form stable biomembranes under extreme living conditions (*81*). They have low phase-transition temperatures enabling them to remain in a fluidic structure at room temperature (*66, 81, 85*). Two diphytanyl chains also add to the stability and fluidity of the monolayer compared to a single phytanyl unit, which was used in earlier studies (*80, 81*). As a key component in forming the lower leaflet of the bilayer, the lipids of choice for this research also have a phytanoyl (ester instead of ether connection to the fatty

acid chains) tail region. Diphytanyl lipids are utilized to create the tethered bilayer and also to prevent the development of a hybrid bilayer.

Diphytanoyl Lipids

1-palmitoyl-2-oleoyl-sn-glycero-3-phospho-ethanolamine (POPE) and 1-palmitoyl-2-oleoyl-sn-glycero-3-phosphocholine (POPC) have served as the most commonly investigated membrane supporting environment for reconstituted membrane proteins (*86-89*). Diphytanoyl-based lipids were chosen for this research because of their enhanced chemical stability throughout a wide temperature range even though they have an ester bond. This bond has a better interaction with the protein then the ether bond present on the DPTL. Diphytanoyl lipids also tether easily to solid surfaces such as gold substrates which were used for the development of our microelectrode arrays. They function as a more rigid bilayer in comparison to natural lipids. This may be related to the methyl groups present on the fatty acid chains (refer to Figure 1-8) (*76*). Diphytanoyl lipids are not unsaturated like their natural counterparts. The branched chain fatty acid section of the lipid is extremely disordered, resulting in highly fluidic membrane structures (*90*). They are also able to fully mix well with many amphiphiles including cholesterol. Such characteristics enable diphytanoyl lipids to act as a supportive environment for ion channels.

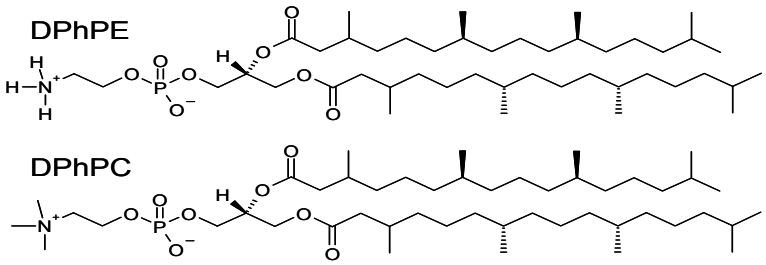

Figure 1-9. 1,2-Diphytanoyl-sn-Glycero-3-phosphoethanolamine (DPhPE) and 1,2-Diphytanoyl-sn-Glycero-3-phospho choline (DPhPC) lipid

The last step in forming the tethered bilayer system occurs via vesicle fusion. Liposomes or vesicles spontaneously form when heterogeneous mixtures of phospholipids are suspended in aqueous solutions (*9, 68*). They take on a vesicular structure whereby the bilayer forms a series of concentric shells encapsulating an aqueous core. Vesicles of lipids DPhPC and DPhPE, 1,2-diphytanoyl-*sn*-glycero-3-phosphoethanolamine as shown in Figure 1-9 are utilized in this research. Phosphatidylcholine and Phosphatidylethanolamine head structures make up 64 and 17 percent of the mammalian plasma membranes, respectively (*12*). Therefore, vesicle mixtures of these two lipids will be developed and allowed to fuse to the DPTL monolayer creating the tBLM.

This fusion process is facilitated by Van der Wals, hydrophobic and hydrophilic interactions whereby the vesicles open and the hydrophobic tail regions align with the tail region of DPTL. Some of the lipids integrated with the DPTL and form the lower leaflet in a manner where the headgroups enter the reservoir and the tails align side by side with the 2,3-di-O-phtanyl-sn-glycerol units. The remaining lipids form the upper leaflet of the bilayer with the headgroup facing the bulk solution above the bilayer as shown in Figure 1-8B. Vesicle fusion is also a self assembling process were the rate of formation is temperature dependent.

Summary

In summary, the three main goals of this research were: 1) Determine the proximity and mobility of like residues in the C-terminal of MscL to understand if this region changes conformation during gating, to decrease the overall conductance of the protein with disulfide bridging. 2) Determine the most stable lipid ratio between DPhPC/DPhPE lipids for use in the tBLM device. This was done by reconstituting a model channel, Gramicidin, into a stable planar lipid bilayer and analyzing the single channel activity of this protein using the tip-dip method. 3) Incorporate both Gramicidin and MscL independently into the tBLM and measure their single

ion channel activity as the first step in creating a stochastic biosensor. The chapter to follow will discuss the isolation and purification of MscL as well as the development of the tethered bilayer system. Chapter 2 will also examine the variations of the classical patch clamp technique that was used in this study for analysis of planar linear bilayers. Chapter 3 will examine the results from creating the cysteine mutations while Chapter 4 will examine the most stable lipid ratio using a classical planar lipid bilayer technique. Concluding this dissertation will be an assessment of both Gramicidin and MscL, reconstituted in the tethered bilayer while utilizing a modified patch clamp technique to analyze the single channel activity.

CHAPTER 2
MATERIALS, METHODS, AND EXPERIMENTAL THEORIES

Protein Chemistry and Structural Studies

Cysteine Mutations in MscL

Mutations, cloning, expression, and biochemistry assays were done by Robin Wray and me at the University of Texas Southwestern Medical Center in Dr. Paul Blount's laboratory. Oligonucleotide primers with cysteine mutations at positions A110, A111, A112, A114, E119, V120, L121, L122, L128, and L129 were generated with 15 to 17 base-pair flanking sequences on each side (refer to table 2-1). The Quick-Change kit (Stratagene La Jolla, CA) and a modified MegaPrimer PCR technique were used to extend and amplify the target DNA. The Quick-Change kit was used for mutants A110C and A111C and the MegaPrimer technique was used for the rest of the mutants.

Quick-Change amplifies DNA using *PfuTurbo*, a cloned version of both *PFU* DNA Polymerase and ArchaeMaxx-polymerase (*91*). ArchaeMaxx-enhancing factor functions as a dUTPase converting dUTP (caused by dCTP deamination) to dUMP which improves the total yield of PCR product (*91*). Quickchange reagents included: 5 µl of Reaction buffer (100 mM KCl, 100mM $(NH_4)_2SO_4$, 200mM Tris(HCl) (pH 8.8), 20mM $MgSO_4$, 1% Triton X-100, 1 mg/ml BSA), 1 µl of dsDNA template (62.5 mg/ µl), 1.25 µl of oligonucleotide prime 1 (1 µg/µl), 1 µl of dNTP (10 µM), 39.50 µl of ddH_2O, and 1 µl of Pfu Turbo DNA polymerase (2.5 U/µl). The 1st temperature cycle used to denature and unwind the DNA was 95°C for 30 seconds. The second temperature cycle included 18 rounds of denaturing the plasmid at 95°C for an additional 30 seconds, annealing the oligonucleotide primers with the cysteine mutation to the plasmid at 55°C for one minute, and both extending and incorporating the mutagenic primer with nicked circular DNA strands was done at 68°C for twelve minutes (2 minutes per kb of the

plasmid length). 1 µl *Dpn I* endonuclease was incorporated following the temperature cycling to digest the paternal DNA template. The sample was gently mixed with *Dpn I* followed by a quick spin. The solution was incubated at 37°C for 1 hour and15 minutes in a water bath to digest the parental DNA.

Table 2-1: Oligonucleotide primers with cysteine mutation highlighted in red

Mutation Primers	Sequences
A110C	5'-CGG AAA AAA GAA GAA CCA TGC GCC GCA CCT GCA CCA AC-3'
A110C COMP	3'-GT TGG TGC AGG TGC GGC GCA TGG TTC TTC TTT TTT CCG-5'
A111C	5'-GGA AAA AAA GAA GAA CCA GCA TGC GCA CCT GCA CCA AC-3'
A111C COMP	3'-GT TGG TGC AGG TGC GCA TGC TGG TTC TTC TTT TTT CC-5'
A112C	5'-GAA GAA CCA GCA GCC TGC CCT GCA CCA ACT AAA GAA G-3'
A112C COMP	3'-C TTC CTT TAG TTG GTGCGG GCA GGC TGC TGG TTC TTC-5'
A114C	5'-G AAC CAG CAG CCG CAR CCT TGC CCA ACT AAA GAA GAA G-3'
A114C COMP	3'-C TTC TTC TTT AGT TGG GCA AGG TGC GGC TGC TGG TTC-5'
E119C/V120C	5'-C ACC TGC CCA ACT AAA GAA TGC TGC TTA CTG ACA GAA ATT CGT G-3'
E119C/V120C COMP	3'-C ACG AAT TTC TGT CAG TAA GCA GCA TTC TTA GTT GGT GCA GGT G-5'
L121C/L122C	5'-C ACC AAC TAA AGA AGA AGT TGC TGC ACA GAA ATT CGT GAT TGC-3'
L121C/L122C COMP	3'-G CAA ATC ACG AAT TTC TGT GCA GCA TAC TTC TTC TTA GTT GGT G-5'
L128C/L129C	5'-C TGA CAG AAA ATT CGT GAT TGC TGC AAA GAG CAG AAT AAC CGC TC-3'
L128C/L129C COMP	3'-GA GCG GTT ATT CTG CTC TTT GCA GCA ATC ACG AAT TTC TGT AG-5'
A110C/A111C/A112C	5'-GG AAA AAA GAA GAA CCA TGC TGC TGC CCT GCA CCA ACT AAA GAA G-3'
A110C/A111C/A112C COMP	3'-C TTC TTT AGT TGG TGC AGG GCA GCA GCA TGG TTC TTC TTT TTT CC-3'
Quickchange primer #1	5'-CCA TGA TTA CGC CAA GCG CGC AAT TAA CCC TCA C-3'
Quickchange primer #2	5'-GTG AGG GTT AAT TGC GCG CTT GGC GTA ATC ATG G-3'

The MegaPrimer procedure was done in a two PCR step process, where the product of the first PCR step was used as the primer for the second PCR step. The first primer was the

mutation codon flanked by 12 codons at each side. The Megaprimer reagents for the 1st PCR included: 34.5 µl of ddH_2O, 10 µl of 10X turbo Pfu polymerase buffer, 1.5 µl of DMSO, 1 µl of dNTPs (200 uM), 2.5 µl of 5'long primer (0.5 µM), 0.29 µl of 3' primer with the cysteine mutations (0.5 µM), 1 µl of DNA template, and 0.5 µl of Phusion DNA polymerase (0.02U/ µl). The cycles used with this technique were similar to those of Quickchange with the exception of the extension cycle. The temperature used to extend the PCR product was 72°C. The product obtain from this PCR was assayed on an agrose gel to check for specificity and the correct size. If the proper band was obtained the second PCR step was done for the reverse primer. All of the PCR ingredients remained the same except for the 0.5 µl of the product from first PCR was added for extension by the 3' long reverse primer (0.5 µM) for pB10b. Restriction enzymes Xho/Xba were used to cut the plasmid expression vector and T4-DNA ligase was used to ligate the mutated DNA product to the pB10b vector.

Plasmid constructs were transformed, via electroporation, into DH10β bacteria to yield DNA for sequencing. DH10β cells and the pB10b construct were mixed and allowed to incubate for 10 minutes on ice before being exposed to a pulse of 1.8 kV. After transformation, 500 µl of SOC (super optimal broth with concentrated magnesium chloride or glucose) media was added to the cells. Next, cells were placed at 37°C while shaking at 250 cycles per minute before plating them overnight on Luria-Bertani Broth (LB) plates. Single colonies were selected from each plate and added to 4 ml of liquid LB. Colonies were grown overnight at 37°C while shaking at 250 cycles per minute. Mutated DNA was isolated from DH10β cells using QIAprep 8 Turbo Miniprep plasmid DNA isolation and purification kit (Qiagen Valencia, CA). This miniprep kit uses alkaline lysis in the presence of high denaturants to isolate DNA. The denaturants assist with the inactivation of exogenous and endogenous nucleases which degrade

DNA. Both the lipids and proteins are denatured by strong alkali and detergents. The detergents are precipitated out with a neutralizing salt. The pB10b plasmid constructs remain stable in the presence of alkali. Centrifugation was done to separate the plasmid solution from the cellular debris. The solution was then forced though the apparatus with vacuum in the presence of silica glass beads. The DNA attached to the cationic silica glass was washed and eluted with distilled water and stored at -80°C.

After purification, the pB10b constructs were analyzed by restriction digestion using Xba and Xho and separated using 1% agarose gel electrophoresis. The target MscL DNA sequence was identified and the mutations in the DNA were confirmed by automated sequencing at the UTSW McDermott Center for Human Genetics. After the MscL mutated sequence was confirmed, it was transformed to *E.coli* strain PB104 (*null* MscL) (*26, 27, 43, 92*). Biochemistry assays were performed *in vivo* using PB104 strains.

Biochemistry Assays: Disulfide-trapping

Disulfide-trapping is a classical fragment scanning method which was used to determine the proximity of selective residues in the C-terminal region. Disulfide-trapping uses the oxidation of cysteines, either native or introduced, to stabilize the proteins in specific conformations by generating S-S bridges within or between the subunits. This technique has been used by Dr. Blount and coworkers to identify key residues in the TM1 and the N-terminal domains of MscL (*93, 94*). Disulfide trapping of MscL *in vivo* can be enhanced by "shocking" the cells. Shocking the cell occurs when *E. coli* cells are first grown in high osmolarity media containing high salt concentrations. At a certain point when the cells are healthy and protein expression is high, the cells are subsequently diluted into a low osmotic environment with little to no salt. This rapid change in environments is termed osmotic downshock, coined by McClure and Britten in their 1962 review (*95*). The tugor pressure in the membrane created by the

downshock conditions triggers the opening of MscL as a release valve, saving the cell. The key component in this reaction that enhances the intensity of disulfide bridging is the release of the reducing agents usually found in the cytoplasm. With these biochemicals missing, the cysteine residues in close proximity (3.6-6.8 Å) are able to crosslink.

In these experiments, single colonies were grown in LB containing 1M NaCl while shaking in an incubator at 37°C and rotating at 250 cycles per minute. Culture growth was measured to an optical density $(OD)_{600}$ at 30 minute intervals. At an early log phase, an OD of 0.2-0.3, protein expression was induced by the addition of 1 mM Isopropyl β-D-1-thiogalactopyranoside, IPTG (Fisher Scientific, Pittsburgh, PA). IPTG is a reagent that binds and inhibits the *Lac* 1 repressor, inducing the transcription of the protein. At an OD of 0.3-0.4, cultures were diluted 20-fold in either 37°C water thereby shocking the cells or in 500 mM NaCl LB media which serves as a control for the experiments. Cultures were then allowed to incubate at 37°C while rotating at 250 cycles per minute for 20 minutes. Another control was done to ensure crosslinking, whereby cells were diluted 20 fold in LB containing 1% of oxidizing agent H_2O_2.

Subsequently, cells were pelleted by centrifugation at 4000 rpm for 20 minutes and resuspended in non-reducing Lammi buffer (62.5 mM Tris pH 6.8, 25% v/v glycerol, 2% w/v sodium dodecyl sulfate (SDS), 0.01% w/v bromophenol blue (Sigma, St. Louis MO)) to a final volume which was normalized based on the OD_{600} before dilution. In order to study the reversibility of disulfide bridging, reducing agent, ß-mercaptoethanol (5%), was added to the sample buffer for half of the samples. All samples were heated at 70°C for 4 minutes to ensure protein denaturation followed by centrifugation for 3 minutes at 12000 rpm. Samples then underwent SDS-Page analysis in a 4-20% gradient Tris-HCl polyacrylamide gel (Bio-Rad

Hercules, CA). Briefly, SDS-PAGE (sodium dodecyl sulfate polyacrlylamide) gel electrophoresis uses polyacrlylamide gel to separate protein strands using two electrodes. The SDS coats the proteins giving them a negative charge which ideally enables them to travel vertically to the anode. Smaller proteins travel faster through the pores of the gel while larger proteins move slower. Ladders with known protein molecular weights are used to identify the MW of target proteins. MscL's molecular weight is around 17 kDa. Therefore when two cysteines form a disulfide bond linking two monomers of MscL to form dimers, the molecular weight, doubles to 34 kD. When three protein subunits crosslink and form trimers, the MW increases to 57 kD. Four different subunits crosslinking would be represented by a band 77 kD and be called a tetramer.

Western Blotting

Once the proteins were fractionated, western blot was conducted to visualize the protein and to determine if the cysteines were able to crosslink. This immunological technique attaches antibodies to the target protein in a given sample for identification and quantization. First, the proteins fractionated by SDS PAGE are transferred to a membrane sheet. Primary antibodies are next added to the membrane sheet to bind the specific proteins. This is followed with enzyme-tagged antibodies that attach to the primary-antibodies. Binding a substrate to the enzyme allows visualization of the selected protein by either colorimetric or fluorimetric detection.

MscL was electro-transferred to Immobilon Polyinylidene Fluoride (PVDF) membranes (Millipore Corporation, MA) at 105mV for 70 minutes. Blots were blocked in 2% milk/TBS for an hour at room temperature. Western Blot analysis was performed using one of the following: primary-antibodies against the MscL C-terminus, penta-His-tag antibody or HRP-His-Probe (Thermo Fisher Sic. Pierce Protein Research, Rockford, IL). The 2nd antibody used for MscL was Goat-anti-Rabbit HRP (BioRad). The primary-MscL antibody poorly recognized the double

mutants L121C/L122C and L128C/L129C due to the close proximity of the mutation sites to the epitope requiring us to use antibodies which recognized the His-tag epitope. When protein expression was too low for recognition with the penta-His-antibody, we used the HRP-His-Probe (HRP-His-Probe was used for the majority of the study). The HRP-His-probe uses a Ni-chelating group that binds to the 6His-tag present on the protein. The HRP-His-probe reacts with the substrate. This reaction gives off a chemiluminescent signal that was quantified using X-ray sensitive film (Kodak). The film was developed using the dipping method whereby the film was submerged in each of the following for 90 second intervals: developer, water, and fixer (Developer and Fixer purchased from Kodak). The film was then rinsed under running water for 2 minutes and quantification was done by measuring the density of the bands using Scion Image Software (NIH).

Experimental Theory and Procedures for Functional Studies

Materials

Different molar ratios of the archaea phospholipids, 1, 2-diphytanoyl-sn-glycero-3-phosphocholine (DPhPC) and 1,2-diphytanoyl-sn-glycero-3-phosphoethanolamine (DPhPE), (>99% pure purchased from Avanti Polar Lipids Inc) were used to form the bilayers in both the planar linear and the tethered bilayer studies. 2,3-di-O-phytanoyl-sn-glucero-1-tetraethylene glycerol-D-L-α-lipoic acid ester lipid, DPTL was used to form the monolayer region of the tethered lipid bilayer. The buffer, Morpholinopropanesulfonic acid (MOPS), >99.5% ultra grade was purchased from Fluka. Potassium chloride (certified ACS grade), calcium chloride (certified ACS grade) and potassium hydroxide (certified ACS grade) were purchased from Fisher Scientific and utilized upon receipt.

Protein Isolation and Purification

Recombinant protein isolation and purification is a process that requires first the known location of the protein in the cell and a means to identify the protein once it is separated from its natural environment. This is achieved by adding a tag to the protein and designing the experiments around locating that tag. Common protein tags include Histadines, and Strepadvin. Since MscL is a known membrane protein, the focus of protein purification will be strictly on membrane protein techniques. The first step in this process is to solubilize the cell membrane with either an ionic or nonionic detergent. Knowing the critical micelle concentration (CMC) of the detergent is important for removal of the detergent soon after the membrane has been disrupted. Another technique that enhances the disruption of the cellular membrane using mechanical forces is the French Pressing method. This techniques works by applying an extreme pressure to the cells that causes them to burst. Once the cell membrane is disrupted, a chromatography technique is required to separate the protein from the cellular debris. These techniques range from affinity chromatography, which binds a certain part of the protein to the beads in the column, to ion exchange chromatography. In the latter method, charged materials within the column attract ionic groups on the protein (either cationic or anionic depending on the specificity of the column). As a stronger ion enters the column and reacts with the binding agent, the protein is concentrated and eluted in a concentrated form.

MscL Isolation and Purification

In order to isolate and purify MscL, the protein is first generated with a C- terminal 6His-tag and expressed in the MscL-null strain PB104 using the pET21a expression vector. The pET vector is able to mass-produce proteins due to its T7-promoter site that binds T7 RNA polymerase and promotes transcription of the target protein. Secondly, cells were grown to an OD of about 0.6 and induced with 1mM IPTG for 1 hour at 37°C. The cells were then

centrifuged at 4000 rpm and the pellets were re-suspended in 40 ml of base buffer (10 mM NaPi and 300 mM pH 8.0) and 100 µl of protease inhibitor cocktail (His-tag Protease Inhibitor from Sigma) was added to prevent the denaturing of the proteins. A few crystals of DNase and lysozyme was added and allowed to mix for 45 minutes. The samples were then disrupted by French pressing at 16K PSI at 4°C and membrane fractions were separated and resuspended in extraction buffer (50 mM Na_2HPO_4/Nah2PO_4, pH 8.0, 300 mM NaCl, 20 mM imidazole plus 2% (v/v) Triton X-100) (*96*). The resulting suspension was incubated with 500 µl of pre-equilibrated extraction buffer containing Ni-NTA agarose (Qiagen) for 30 min at room temp to bind the proteins.

To prepare for the protein purification by affinity chromatography, the NTA-agarose matrix was loaded into a 10 cm column with the protein bound. The column was washed with 10 ml of extraction buffer in the presence of 50mM of imidazole and 1% Triton X-100. Proteins were then eluted in 1.5 ml extraction buffer with 200mM imidazole and 0.2% Triton X-100. They were lastly analyzed by SDS-Page gel for purity and stored at -80°C.

Gramicidin Isolation

Gramicidin A was purchased from Sigma and stored in methanol at -20°C. This protein did not require an isolation or purification and was used as received.

Proteoliposome Formation

Purified membrane proteins reconstituted into phospholipids vesicles are proteoliposomes. This technique allows for *in vitro* functional studies of membrane proteins reconstituted into either native lipids, a mixture of different lipids, or synthetic lipids (*97*). This process occurs by first developing the liposomes or vesicles of choice.

Liposomes (or vesicles) as shown in Figure 2-1 spontaneously form when heterogeneous mixtures of phospholipids are submerged in aqueous solutions at high temperatures (*9, 68*).

They take on a vesicular structure whereby the bilayer forms a series of concentric shells encapsulating an aqueous core. Different preparation techniques, including extrusion, sonication, and increasing the pH, can create unilamellar vesicles of certain sizes. Both small unilamellar vesicles (SUVs) and large unilamellar vesicles (LUVs) are formed with the additional steps of either sonication, freeze-thawing, or extrusion through different size membranes (*98*).

To create proteoliposomes, the liposome must first be disrupted in order to accommodate the insertion of the purified membrane proteins. Because most membrane proteins once purified are stored in mix solutions of native lipids and detergent, detergents are used to solubilize the vesicles. The purified proteins are then introduced into the mixed detergent-lipid solution and allowed to self assemble or reconstitute into the lipids. Removal of the detergent is vital to ensuring the complete reconstitution of the protein. This is done by either dialysis in the presence of lipids or by adding polystyrene bio beads that absorb the detergents.

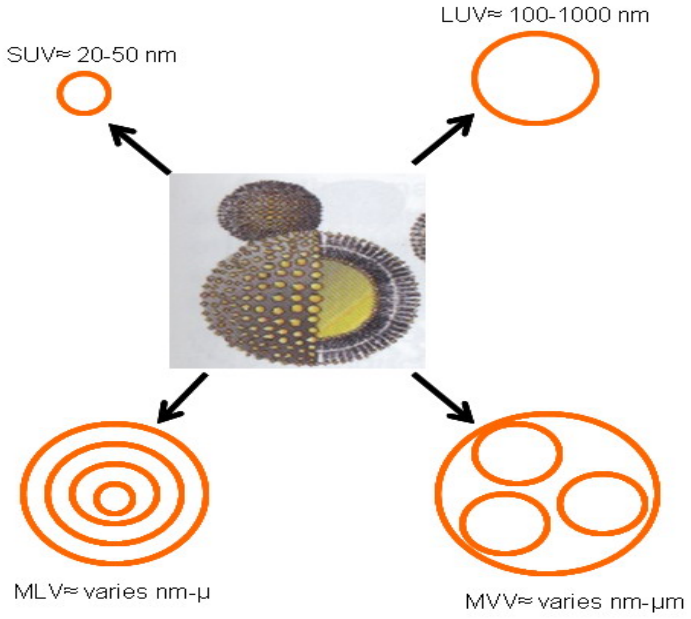

Figure 2-1 Liposome or vesicles formed from phospholipids.

DPhPC and DPhPE Vesicle Formation and Protein Reconstitution

DPhPC and DPhPE lipids were mixed in a 7:3 molar ratio and the solvent was evaporated in a vacuumed rotor vapor for 2 hours. For proteoliposomes containing Gramicidin (0.2 mg/ml), 4 µl of the protein was added at this step in a ratio of 1:1000 proteins to lipid. Once a thin film of the lipids was observed, indicating the evaporation of the chloroform, 1 mL MOPS buffer (5 mM MOPS, 25 mM KCl, 0.5 mM $CaCl_2$) was added to rehydrate the lipids. They were next heated while stirring for 2 hours at 50°C to form vesicles. The vesicles were cooled to room temperature and sonicated for 5 minutes creating a cloudy solution. The homogenizer or extruder along with the 100 nm membrane and filters were hydrated for 5 minutes. Vesicles were then extruded 17 times at room temperature to ensure homology of the LUVs. Vesicle solutions were then placed at 4°C until one of the following occurred: they were prep for an experiment, size verification was done using Dynamic Light Scattering (DLS), or proteoliposomes with MscL were made.

There were two different techniques used to create proteoliposomes of MscL once it was purified. In one of the methods, a 5 ml HiTrap Desalting column (GE healthcare life sciences) packed with cross-linked dextran was used for the removal of salts from the purified protein extracts by gel filtration. This chromatography technique separates molecules according to their size as they pass through a gel filtration packed column. The column used in this study has a size exclusion limit of MW 5000. The column was first equilibrated with 25 ml or 5 column volumes of degassed buffer (20 mM Tris, 500 mM KCl, 0.1 mM CaCl2, pH 7.4) at a flow rate of 1ml/min. The void volume of the column was 1.5 ml, therefore, 1 ml of the protein fraction was loaded onto the column, at a flow rate of 1 ml/min, 0.5 ml of buffer is allowed to elute from the column and discarded, and a total of 2 ml of the desalted sample is collected from the column. MscL was then mixed with the lipid vesicles in a ratio of 1:1000, proteins to lipid.

In the other MscL proteoliposome technique that was used in this study, purified MscL (0.9 mg/ml) was slowly added in a 1:120 protein to lipid mixture after vesicles were extruded and disrupted by the addition of 1% Triton-X 100. The protein-lipid-detergent matrix was then heated in the water bath at 60°C for 30 minutes. While the sample was heating, Biobeads (Bio-Rad) were washed 3X with the MOPs buffer used to create the vesicles. The proteoliposome solution was added to the bio-beads and incubated with light rotation for either 4 hours at room temperature or overnight at 4°C. The proteoliposome solution was lastly removed from the bio-beads and stored at 4°C.

Single Channel Measurements: Patch Clamping Recording Technique

In 1967, Dr. Erwin Neher and Dr. Bert Sakmann, two cell physiologists, designed the patch clamp technique which measures ion channel activity. The most common technique at the time was voltage clamping. Patch clamp offered the advantage of measuring electrical current in the picoamperes (pA) range from single ion channels within the cell's membrane (*99*). Information obtained from patch clamp recordings includes the conductance, voltage dependence, selectivity, open probability, dwell times, resistance of the membrane, and pharmacological profile of the ion channels (*99*). This method can also record channel activity from the interior and exterior of the cell membrane as well as from ion channels in synthetic membranes. In 1991, both physiologist were awarded the Nobel Prize in Medicine for their discoveries in the field of electrophysiology (*99*).

The basis of all patch clamp recordings began with the "cell attached" method. In this method, a glass micropipette tip containing the reference electrode and electrolyte solution is micromanipulated into the cell's surface, isolating a "patch" of the membrane. Suction is next applied to create a seal. This seal indicates a significant amount of electrical resistance was obtained between the patch containing the ion channels and the tip. This electrical resistance is

needed to measure ion channel currents free of background noise. The current flow is reflective of all the ion channels within this patch and measured with a specific patch clamp amplifier. The amplified current transitions are then recorded and analyzed with a data acquisition program. Each channel exhibits a unique amplitude threshold, lifetime profile, and conductance parameters which relates to the single channel activity of the ion channel and can be obtained using patch clamp techniques.

One biological process measured using the patch clamp is the action potential. Action potential is the opening and closing of specific ion channels in an effort to balance the ionic concentration over the interior and exterior of the cell (*100*). This macroscopic process usually occurs with the exchange of Na^+ ions from the exterior for K^+ ions in the interior (*100*). Once a cell reaches its resting potential (70-80mV) the ion channel activity decreases and the cellular membrane is theoretically at equilibrium. Whole cell patch clamp configurations are capable of measuring this process.

Recording systems that evolved from the "cell-attached" configuration include: whole cell, inside-out, and outside-out recording of excised patches. Whole cell configurations are similar to the attached cell configuration; however whole cell measurements reflect the electrical current of the entire cell. Inside-out and outside-out methods record activity with the patch detached from the cell when suction is applied. Even then, the resistance is still high enough to reduce background noise. These configurations allow for measurements of ion channels on the internal and external sides of the membrane respectively. More recently developed are specialized recording techniques that take advantage of synthetic planar bilayers.

Different types of ion channels have been discovered and characterized by the above patch electrophysiology techniques including voltage-gated ion channels, ligand gated channels, and

second messenger-activated channels (*78, 99*). *In vivo* studies of MscL using the patch clamp technique requires an increase in *E coli* cell size to enable patching. It also requires a decrease in the peptidoglycen layer to access the inner membrane. In 1987, Dr. Kung and coworkers adopted a technique to generate giant sphereoplast from the J. Adler group. They were able to harvest patchable bacterial spheroplasts by adding chemical reagents: cephalexin, lysozyme, and ethylenediaminetetraacetic acid (EDTA). Cephalexin inhibits cell division but not growth; leading to long filamentous syncitia termed "snakes" that collapses to into giant spheres, between 5-10 µm; which is acceptable for patching (*38, 101*). Digestion at room temperature with the addition of lysozyme and (EDTA) will hydrolyze the peptidoglycan layer weakening the cell wall causing the *E.coli* spheroplasts to swell (*31, 38, 39*). $MgCl_2$ and sucrose will be incorporated lastly to stabilize and complete the spheroplast for proper patching.

Specialized Patch Clamping Techniques

Planar Linear Patching: The Tip-Dip Recording

Specialized patch clamp techniques have been developed to simplify the recording methods in which blockers and other analytes are only used for pharmacology studies. The tip-dip bilayer recording method is a planar lipid bilayer technique that enables the investigation of ion channels reconstituted in synthetic lipid environments as shown in Figure 2-2 (*99*). This configuration also allows one to investigate the electrical stability of the bilayer, which was achieved in this study.

In this technique, the ion channel/lipid solution is added to the surface of an aqueous solution in order to form a monolayer at the air-water interface. A ground electrode is placed in the aqueous bath solution. The micropipette tip containing the reference electrode, is next micromanipulated onto the surface of the monolayer. Upon retracting the tip from the solution, the hydrophilic lipid head groups align the surface of the glass tip forming a monolayer. The tip

is then carefully micromanipulated down again just to touch the monolayer's surface. At this point a seal and a bilayer are formed from the two lipid layers mergering. The seal is a measurement of the resistance created between the two electrodes by the bilayer. If the ion channel Gramicidin was present, then single channel activity would be measured. If an ion channel was not present then the electrical properties of the bilayer were studied over time.

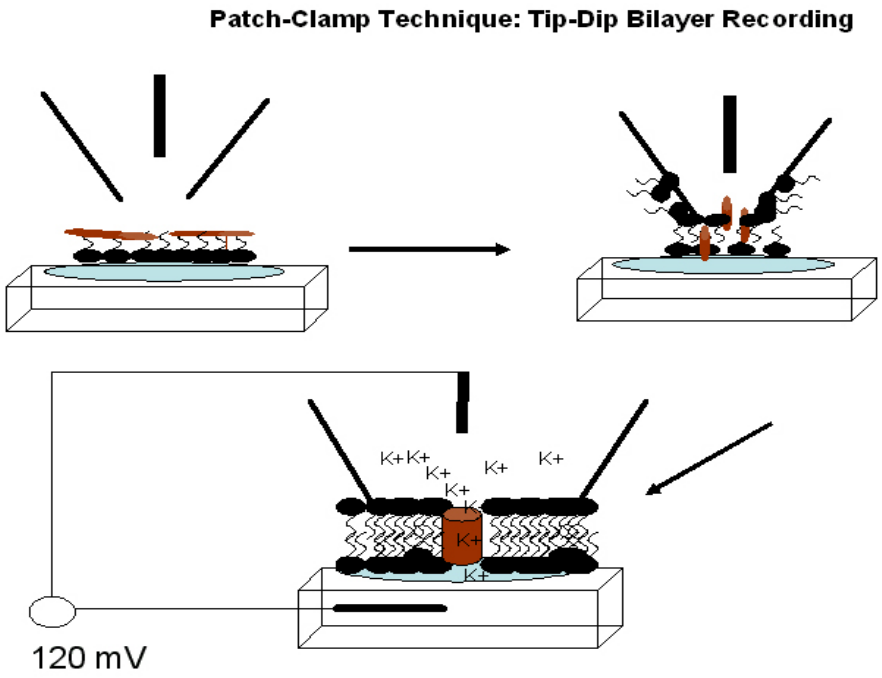

Figure 2-2. Schematic of the tip-dip recording system. First the pipette tip is inserted into the monolayer at the air-water interface. When the tip is removed form the surface, the hydrophilic groups align the surface of the glass micropipette. The tip is carefully brought back in contact with the monolayer and the hydrophobic and hydrophilic interactions between the lipids develop a bilayer and the protein or peptides within the bilayer self assemble into an ion channel. Potentials are applied and the electrical current transitions are recorded. (Figure borrowed from previous work)

Tethered Lipid Bilayer

Solid supported lipid systems as explained in Chapter 1 are fairly new methods of incorporating phospholipid bilayers on solid substrates. One of the most successful techniques and the one currently used in this research is the tethered bilayer lipid membrane system, tBLM. This system is composed of a gold substrate that connects to a probe pad where the ground

electrode is placed, a monolayer that is covalently linked to the gold surface and a bilayer that is formed via vesicle fusion. A number of both optical and electrical methods have been employed to study membrane proteins within this environment (*75, 77, 79, 81, 83, 102-104*). In this study, the functional activity of MscL and Gramicidin were analyzed independently for the first time in this system.

In this technique, a bilayer is self assembled via vesicle fusion on top of a monolayer covalently bonded to a gold sensor pad. This bilayer is either pure lipids or proteoliposomes containing Gramicidin or MscL. The sensor pad is attached to a probe pad where the ground electrode was placed. In order to maintain a level of hydration for the bilayer, a droplet of buffer or water is added to the sensor pad. A microelectrode filled with the same buffer solution was then micromanipulated into the bilayer solution and a 3 mV pulse was passed to measure the electrical resistance (bilayer covering the gold surface) of the system. If the resistance was in the giga-ohm range then higher voltages were applied and the change in current was measured for the bilayer or the ion channels.

Experimental Setup

The experimental setup for both the tip-dip and the tethered bilayer methods consisted of a patch-clamp amplifier, a micromanipulator, two electrodes, a data recording system, an anti-vibration table, and a Faraday cage with a dust cover (refer to Figure 2-3). A noise and dust free environment for the recording systems was established with an anti-vibration or vibration isolation table surrounded by a Faraday cage. To limit surrounding vibrations that may disturb the results, a stack of cinderblocks served as the base of the apparatus. In addition, the apparatus was stationed in the corner of the room where vibrations are at a minimum. A wooden plank with inner-tube air cushions was placed on top of the base to separate a sand filled container. The air cushions suspended the apparatus a little under an inch above the wooden plank in the

center of the cinderblocks as shown in Figure 2-3. The vibration isolation table was placed on top of the sand box followed by a piezoelectric anti-vibration table which provided the stage for patch clamp recording. To reduce the amount of electrical noise a copper mesh Faraday cage with aluminum corner connectors was placed around the stage. In principle, all outside electrical signals are shielded and unable to enter the cage due to the copper mesh serving as a conductor and blocking noise. Finally, in order to reduce dust and debris from entering the sample stage a plastic covering was placed over the Faraday cage.

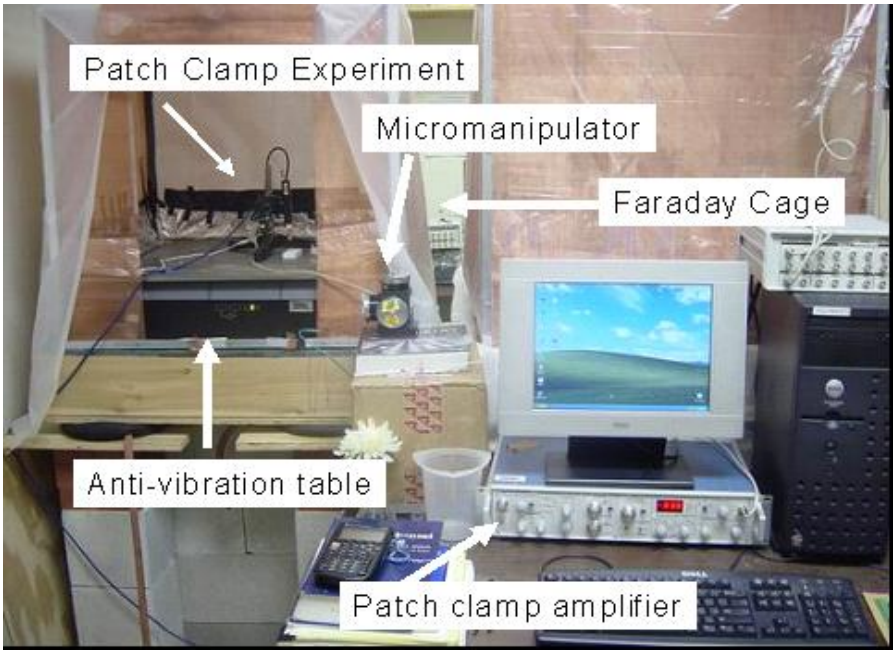

Figure 2-3. Experimental Apparatus. The experimental setup for both the tip-dip method and the tethered device consists of a patch-clamp amplifier, a micromanipulator, two electrodes, a data recording system, an anti-vibration table, and a Faraday cage.

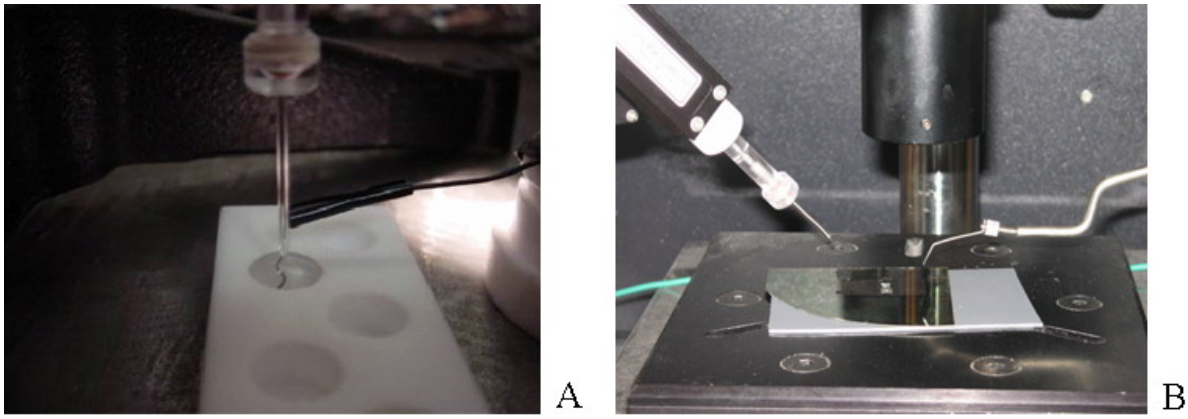

Figure 2-4. The tip-dip and tethered stage apparatus. A) The patch clamp headstage containing the reference electrode which is also attached to the micro-manipulator. There is also a Teflon-well-plate containing six wells 25 by 25 cm wide where the ground electrode is embedded in the electrolyte solution. B) The electronic components for the tethered bilayer experiment include a microscope that allows visualizing the tungsten ground electrode on the probe pad, a micro-manipulator that lowers the tungsten electrode and a patch clamp headstage containing the reference electrode which is also attached to another micro-manipulator.

Once we established a noise and dust free environment the head stage of the patch-clamp amplifier was locked to the base plate and attached to the micro-manipulator. (refer to Figure 2.4a) All metallic and electrical objects within the cage were then grounded. The amplifier (Axopatch 200B patch clamp amplifier from Molecular Devices formerly Axon Instruments), data acquisition and digitizer (Digidata 1322A from Molecular Devices formerly Axon Instruments), manipulator controls, and computer were stationed on a desk next to the cage see Figure 2-3.

Tip-Dip Recording Experiment

When performing a tip-dip recording we first coat a silver wire in a commercial bleach solution for 30 minutes to create a silver/silver chloride Ag/Ag/Cl electrode. This reference electrode was chosen because it is cost efficient, stable, robust, and compatible with our KCl 250 mM, $CaCl_2$ 1 mM, and Morpholinopropanesulfonic acid (MOPS) 5mM filling solutions. Both KCl, and $CaCl_2$ were purchased from Fischer Inc., and MOPS was purchased from Fluka. A

Teflon well plate was sanitized, first by rinsing with distilled water from a MilliQ pH 7.4 and with ethanol (ethanol purchased from Fischer). After The buffer solution (MOPS 5 mM/KCL 250 mM/CaCl2 1mM pH 7.4) was added to the Teflon well and the ground electrode was inserted as shown in Figure 2-6a.

The micropipette tip was prepared by a Flamming/Brown Micropipette Puller (Model 97, Sutter Instruments Co.) with a heated filament separating a single borosilicate capillary tube. Borosilicate capillaries purchased from Warner Instruments Inc., were 7.5 cm long and 1.5 mm wide. One capillary created two 1 μm^2 cross tip diameter because the filament heated the glass vertically in the center resulting in two 3.25 cm long micropipette tips. SEM scanning electron microscope (Hitachi S-4000 FE-SEM) images of the tip were taken to ensure the tip diameter was 1 μm across. Once the electrode and buffer were inserted into the tip, and we initiated the aforementioned tip-dip recording.

Tethered Devices Experimental Setup

The Device

The fabrication of the gold device was done in the Microelectronics Research Center at the University of Texas Austin in Dr. Ananth Dodabalapur laboratory by Dr. Daniel Fine. The core element of the tethered lipid bilayer which is based on planar lipids attached to a solid support is a microelectrode device. The microelectrode arrays used contained 66 pixels per wafer, with each sensor pad formed by evaporation of 3nm of Ti followed by 500 nm of a 60% Au / 40% Pd alloy on the silicon substrate. A 200 nm gold layer was deposited on top of the alloy and a polyimide resist was photolithographically applied to define the pad size as well as to electrically isolate the pads from each other. The device was cleaned with hexane, acetone, ethanol, water, and treated with UV/ozone for 10 min.

Preparation of the Tethered Bilayer

The device was submersed into a DPTL-ethanol solution, (0.3 mg/ml) and left over night in a saturated ethanol environment and the DPTL-ethanol solution was placed in a closed container and stored in a desiccator. The device was then rinsed with ethanol. A chloroform solution (2 mg/ml) containing 70PC/30PE mol% was mixed and the solvents were evaporated under vacuum. The vesicle film was rehydrated with 1 ml of water or buffer as explained earlier. They were heated at 50 ^{o}C until a clear solution was obtained (ca 1 hour). After cooling to room temperature the suspension was sonicated for 5 min, followed by filtration through a 0.45 µm filter. The vesicle size was determined by Dynamic Light scattering (DLS) (Precision Detectors). DLS also know as Photon Correlation Spectroscopy correlates information obtained from small particles scattering light from a monochromatic light beam such as a laser. The measurements were performed using a 683 nm laser source and a 90 degrees scattering angle, at 20° C. When needed, additional dilutions were performed until the count rate was between the recommended 200 000 and 400 000 counts per second. CONTIN analysis was used for the size determinations. These small spherical vesicles move in Brownian motion within solutions causing a Doppler shift in the presence of this light beam. A size distribution is correlated from this Doppler shift over a short period of time.

Typically, vesicle diameters of 150 ± 50 nm were found. A drop of the vesicle solution was deposited on the gold DPTL treated sensor pad and left for >5 hours at 4°C or for 2 hours at room temperature with constant rehydration allowing for the vesicle to fuse, i.e., form the tethered bilayer. Prior to the electrophysiology examinations a drop (5 µl) of buffer solution (5.0 mM MOPS, 250.0 mM KCl and 0.1 mM $CaCl_2$, titrated to pH=7.4 using KOH) was applied to the treated sensor pads. Fabrication of the microelectrode tip was done in a similar manner to the tip-dip method stated above. The microelectrode tip was then placed in the headstage and micro-

manipulated into the tBLM solution. We used a CCD camera to visualize micro-manipulation of the gold plated tungsten ground electrode on to the surface of the probe pad.

Gigaseal

Every patch clamp technique including both the tip-dip method and the tethered bilayer requires high resistances. The seal resistance between both the reference and ground electrode must be at least 1 GΩ in order to observe single ion channel activity and ideally create an electrical stable bilayer (*15, 78*). A high resistance enables the complete electrical isolation of the membrane patch, and reduces the current noise (*78*). Experiments were not done if the resistance was not in the giga-ohm range because reduced noise increases resolution, consequently increasing accuracy in detecting transitions in current levels. The discrepancy of the current noise is related to Johnson voltage noise S_i:

$$S_i^2 = 4kTf_c/R \tag{2.1}$$

Where k is the Boltzmann's constant, T is temperature (in Kelvins), f_c is the low pass filter (Hz) (*78*), and R is the resistance. The Johnson noise for a 1 GΩ resistance at 298 K, with a 1 kHz filter is 0.1 pA, and a 10 GΩ resistance results in current noise of 0.04 pA. Now if the resistance is 100 MΩ under the same conditions as the first seal, the noise becomes 0.4 pA. Therefore the higher the seal resistance, the less noise observed. This resistance in electrophysiology is termed the gigaseal.

A strong gigaseal depends on the pipette material used, the size of the tip, and a sample area free of microscopic debris. Both soft (thin wall CEE BEE glass) and hard glass pipettes may be used for patch clamp measurements (*78*). However, hard glass like borosilicate can establish greater resistance because it has thicker walls. The diameter of the tip depends on the pulling technique and can range form 0.5 to 5 μm (*78, 105*). For instance, in a tip dip recording the tip should roughly be 1 μm across in order to establish a proper gigaseal with the planar

bilayer (*78*). The first dip into the monolayer establishes the pipette's resistance. When using borosilicate pipettes, the resistance of the first dip should be 6 MΩ (*99*). The second dip reflects the resistance of both the pipette's tip and the bilayer and must be within the giga-ohmic range. There is no limitation within the giga-range because the process of establishing the seal is a "hit or miss" situation.

The resistance's readout obtained from a gigaseal with the tethered-bilayer is quite different from previous patch clamp techniques described including the tip dip method. In the tethered-bilayer method the microelectrode does not actually submerge into the bilayer. The microelectrode is inserted into the bulk buffer solution above the bilayer. The tethered bilayer is formed on the gold surface of the sensor pad, creating barriers between the two electrodes. The resistance measured is the ability of the bilayer to completely cover the sensor pad.

Overall, having a gigaseal eliminates or decreases the noise from the systems, other background noises are controlled through the experimental setup, and both of these techniques offer a number of advantages to measuring single channel activity including the following:

- These methods are capable of obtaining high resistance seals
- The channel activity can be recorded in a timely manner
- Recording reflects activity of one type of ion channel which reduces the need for blockers
- The lipid compositions can be exactly defined

Program Analysis for Both Techniques

Software used during experiments included Axon Instrument's Clampex 8.0 or 9.0 for data collection and Clampfit 9.0 for data analysis. "Episodic" and "gap-free" were the two main software protocols involved in characterizing the bilayer and the single channel activity. The Episodic protocol was used to determine the conductance of the bilayer. During these

experiments automated potentials from negative 200 mV to positive 200 mV were applied to the system for several seconds. From these studies, we determined the stability of the bilayer system. The gap free protocol gave us a chance to observe the ion channel's activity over a long period of time with different potentials. With the gap free protocol, we controlled the change in potential manually. Therefore a number of experiments were conducted using the gap-free protocol. The recording filter was 5 kHz low pass 8-pole Bessel.

Event Detection

Data analysis was done using the event detection for single channel statistics within the Clampfit program. From the event detection, we obtained statistics on the channel's average current during open and closed states, dwell time (average time spent at one level during the duration), and current transitions. We also determined the probability to which the channel was in an open and closed state. In order to conduct this analysis, signals were first filtered at 1 kHz by an 8-pole low-pass Bessel filter to reduce the high frequency noise during recording. Once the signal was filtered, the baseline was manually adjusted to zero, for the closed state and event detection was performed.

The event detection for single channel analysis goes through a single trace and counts the number of events at different amplitude levels as in Figure 2-5. An event is a continuous section of the trace at one level. In the event viewer, we manually set the different levels that are detected. Level zero accounts for when the channel is closed or not conducting and level one, or two correspond to the open states of the channel. This opening is called a threshold. Each change in amplitude to a different level must meet a maximum threshold in order to be counted as an event. The maximum amplitude $A_{max}/A_{0,}$ threshold depends on the error function erf, the frequency of the filter recording system, and the duration of the event w.

$A_{max}/A_0 = \text{erf}\,(2.668\ f_c w)$ (2.2)

Because this value varies, we set a 10% level contribution within the software in which the changes in amplitude contributing to a new event have to be within 10% of that level's amplitude. For instance, if the existing level is open at 5 pA and a new event begins at 5.5 pA, the 10% contribution setting will reduce the transition in current to 5.05 pA.

$(0.9 \times 5.0\ \text{pA}) + (0.1 \times 5.5) = 5.05\text{pA}$ (2.3)

Rapid deviations of the trace that are not within the range of the current level were ignored. Due to possibility of the channel being open or closed upon entering the event detection, the first and last events were also excluded from the statistics. Once a count of all the different events at both the open and closed levels was obtained, single channel (*15*) analysis of the Gramicidin and MscL ion channels was performed.

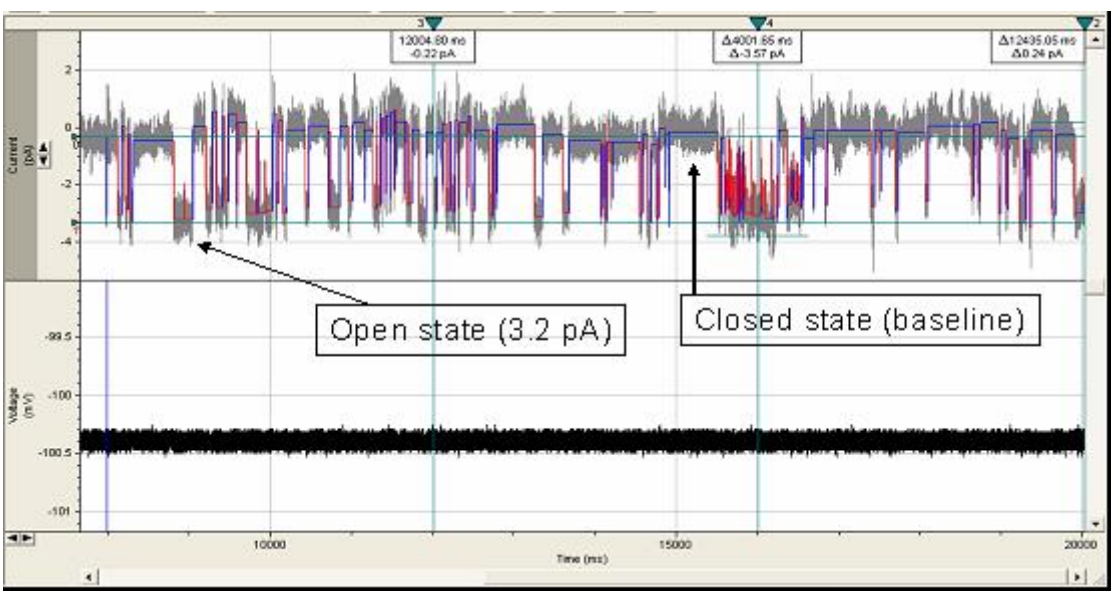

Figure 2-5. Event detection occurring at level zero and level one. Level zero indicates the closed state of the channel or the non-conducting level and it is adjusted to fit the baseline. Level one is roughly at -3.0-3.3 pA. Events are highlighted in red and accounts for the open state of the channel. The duration of this experiment was roughly 12 seconds with an applied potential of -100.5 mV. Events ranged from 54.5 ms to 200ms at level one.

Analysis of Single Ion Channel Activity

Single ion channels exhibit stochastic activity. Theoretically the durations of events and the order in which they occur are random variables (*99, 100*). The channel has no memory system of opening or closing at a given time, and behaves independently of specific potentials, and lipid environment. Therefore, parameters representative of single channel activity, and the information contained in each event are measured from statistical distributions (*78, 100*). Unlike most ion channels, MscL does not have an ion preference. There exist two specific aims when analyzing single ion channel activity of this channel: 1) amplitude studies to understand ion permeation through open channels at different ionic compositions, and different membrane potentials, 2) the duration of open and shut times or the dwell time for lifetime and kinetic studies (*100*).

Point-Amplitude Histograms

The conductance of biological ion channels is restricted by the channel's topology including its maximum pore expansion, length and structure in the lipid bilayer membrane (*15, 106*). Because of this restriction, there is a specific range in which channels will conduct. For instance, the conductance of Gramicidin is between 20-90 pS. The conductance for MscL is roughly 3 nS; this pore is very large and non-selective due to the nature of the channel. The large range is also due in part to the calculation of conductance and the method used for recording single channel activity. Conductance can be calculated by stationary fluctuation using voltage clamp measurements on large ensembles of channels or measurements of unitary current analysis using patch clamp (*15*).

Variance calculations are used for stationary fluctuations to calculate N, the number of the independent and identical channels open and contributing to macroscopic current I from single channel conductance i:

$$\sigma_I^2 = iI\text{-}I^2/N \quad (2.4)$$

Where σ_I^2 is the variance from each channel (*15*). Patch clamp techniques require a gigaseal which allows the isolation of single ion channels resulting in direct measurements of unitary current (*50*). The conductance is calculated from the slope of current-voltage curves derived from Ohm's law. Unitary conductance is calculated from point amplitude histograms at given potentials.

All digitized current can be plotted as a histogram with a peak for each closed and open level. The area under the peak is proportional to the time spent at that level as shown in Figure 2-6. Point-amplitude histograms for each experiment at a known potential were plotted from information obtained from the single channel event detection. A statistical frequency count with a minimum bin width of 0.05 mm was performed and fitted by the maximum likelihood with a continuous Gaussian curve using Origin software as in Figure 2-9. The open P_{open} /close P_{close} probability and the unitary conductance γ, are calculated from this distribution. Both probabilities were estimated as a fraction of the time the channel remained in the respective state, divided by the overall time of the recording. Unitary conductance is calculated by dividing the average amplitude from the amplitude histograms by the applied potential.

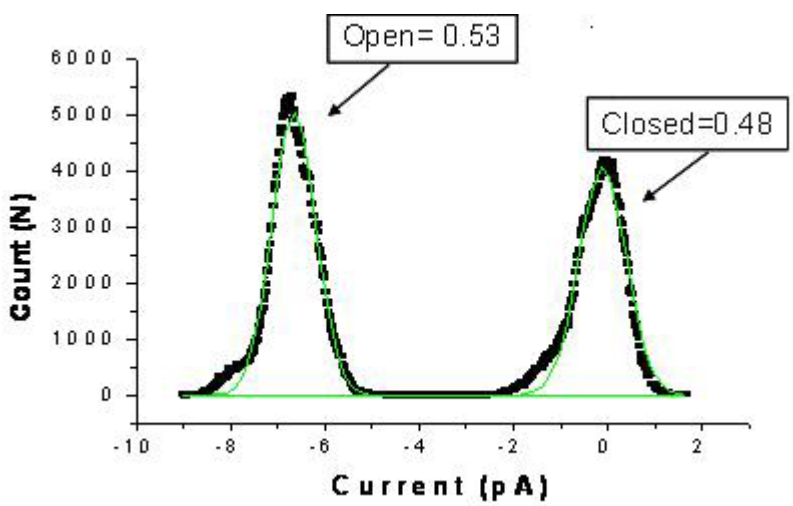

Figure 2-6. The distribution of data points within the histogram are fitted by the maximum likelihood with a continuous Gaussian curve. Closed and open events of an ion channel at a potential of -60 mV. The maximum open amplitude is -7 pA and the open probability is 0.53 and the closed at level zero is 0.48.

Understanding the conductance of biological ion channels indicate that the channels are aqueous pores. In 1959, Mullin combined theories of the past and postulated the modern pore theory in relation to ion channels. Past theories assumed ions with their hydration shells are spherical, and that an electrical force lines the walls of a cylindrical pore (ion channel) determining which would permeate (*15*). Mullin's theory examines the ion's ability to shed all but the innermost layer of water molecules and travel through the pore by solvation obtained from the pore's wall (*15*). He also stated that the channel's length and inner diameter served as a selectivity filter allowing a maximum amount of ions at a certain size to translocate the pore (*15*). This theory is accepted today, and the root of the actual mechanistic knowledge is dependent upon ionic flux measurements (*15*). Therefore, pore forming proteins like Gramicidin and reconstituted ion channels such as MscL must reproducibly conduct in a specific range to be considered as ion channels. Kinetic calculations of lifetime are determined by using a probability density function (pdf).

Probability Density Function

As mentioned throughout this chapter, single channel activity exists in at least two states: the open and closed state. Considering the simplest model of just two states the transition mechanism from one state to the other is denoted by:

$$\text{closed} \underset{k_{12}}{\overset{k_{21}}{\leftrightarrow}} \text{Open}$$

State: 1 2

Where k_{21} is the transition from closed to the open state, and k_{12} is the transition from open to the closed state. This unimolecular transition reaction involves conformational changes of the

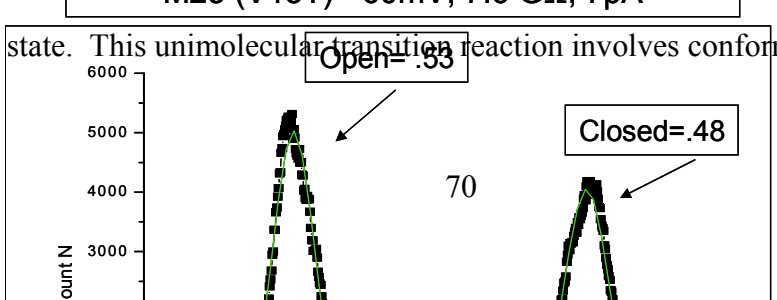

ion channel from one state to the other (*107-109*). Random thermal movement allows the bonds of the protein to vibrate, bend, and stretch in the correct rapid transition on the picosecond scale. This unsystematic motion leads to the randomness in the lifetime of the open and closed state (*78*). The probability p that the channel will overcome the energy barrier holding the channel open and fail to close is (1-p)p. The probability that it will succeed in the next attempt r is independent of the first attempt:

$$P(r) = (1-p)^{r-1}p, \quad r = 1, 2, 3, \infty \tag{2.5}$$

The lifetime is therefore a probability distribution and is expressed by a probability density function (pdf) where the area under the curve represents the probability that the lifetime is less than the specified time t (*15, 78*). The exponential density of a time interval with mean of $\tau = 1/\lambda$, and equals:

$$f(t) = \tau_i^{-1} e^{-t/\tau} \qquad t>0 \tag{2.6}$$

The area under the curve for any pdf must equal unity. Therefore an ensemble of ion channels will lead to a corresponding number of exponential distributions *a*, and the total area of the *i*th component, will also have to equal unity when τ_i is mean (*15*).

$$f(t) = \Sigma\, a_i \tau_i^{-1} e^{-t/\tau} \tag{2.7}$$

Data obtained from pdf are displayed in muti-component histograms where they are usually characterized by three different time values. These time values are representative of the different open and closed levels exhibited by the ion channel.

CHAPTER 3
CYSTEINE SUBSTITUTIONS IN THE S3-BUNDLE OF THE MECHANOSENSITIVE CHANNEL OF LARGE CONDUCTANCE

Introduction

Mechanosensitive (MS) channels in bacteria regulate the osmotic homeostasis of the cell and are currently the most functional and structural studied mechanosensitive channels. Incorporating *E. coli's* mechanosensitive channel of large conductance, MscL within microelectronic devices will provide a new environment for channel analysis. More importantly, this combination of supported lipid bilayers and MscL holds promise for many types of biosensory applications. For instance, within a device MscL can serve as the actual biosensor, or it can serve simply as a release valve. The stimulus required to gate MscL has been extensively researched and is now reflected by the creation of "Designer Mutated MscL Channels". These channels have been engineered and manipulated to respond to changes in pH, redox reagents, sulfhydryl reagents and toxic heavy metals (*4, 42, 110, 111*) thus producing an analyte sensing property of the protein.

Although utilizing MscL presents many advantages for such studies, there are also some likely systematic limitations with incorporating this channel within a microelectronic device. Although the large conductance of MscL should yield a large signal to noise ratio, it may also be overwhelming in some cases. Just a handful of MscL channels opening at a high voltage potential could overwhelm a normal amplifier. In the future, one may wish to combine MscL with other sensors within the same chip. MscL, even with its condensed conductance within a microchip (see Chapter 5) still shows a conductance an order of magnitude greater than most high-conducting channels reconstituted into the device (*64, 77, 112*). Hence, it would be advantageous to decrease the conductance of the channel.

The structure of the C-terminal of the protein suggests one possible approach for designing an MscL channel with decreased conductance. The C-terminal area consists of a linker region that begins directly after the TM2 region at approximately residue K96 and ends before the alpha helical S3-bundle. The S3-bundle consists of five identical α-helices, one provided from each subunit, and the bundle in one model is considered to began at residue V120 (*113*). The C-terminal's function is thought to be that of a size exclusion filter. Osmolytes pass through one of the two parts of this region before transversing the pore of the channel. A debate exists to whether the S3-bundle remains stable during gating of the channel, or if it opens and folds into the bilayer as shown in Figure 3-1. Since the crystal structure of *M. tuberculosis* was resolved in the closed state, at a low pH 3.5 and in the presence of detergents, the amino acids were arranged in a conformation that is predicted to be physiologically probable. Molecular models have been designed to correct the structure and placed the amino acids in the correct orientation (*51*). Disulfide-trapping experiments, with cysteine substitutions to residues located near the end of the S3-bundle, were also done *in vitro* after French Pressing to analysis the possible conformation of this region during gating (*51*). These experiments also termed cysteine bridging, enable sulfur groups to disulfide bind with neighboring cysteines when placed in an oxidative environment, and they provided insight concerning the proximity of specific amino acids. Surkharev *et al.* found that cysteine bridging occurred under both oxidative and ambient conditions, concluding that this region remains in the cytoplasm during gating. Surkharev *et al.* then formulated a newer model based off of the COMP (as seen on the right of Figure 3-1) that placed the amino acids in the ideal positions during physiological pH (*51*). A recent re-evaluation of the *M. tuberculosis* structure was more consistent with this latter model and uploaded in the pdb-20AR (*114*).

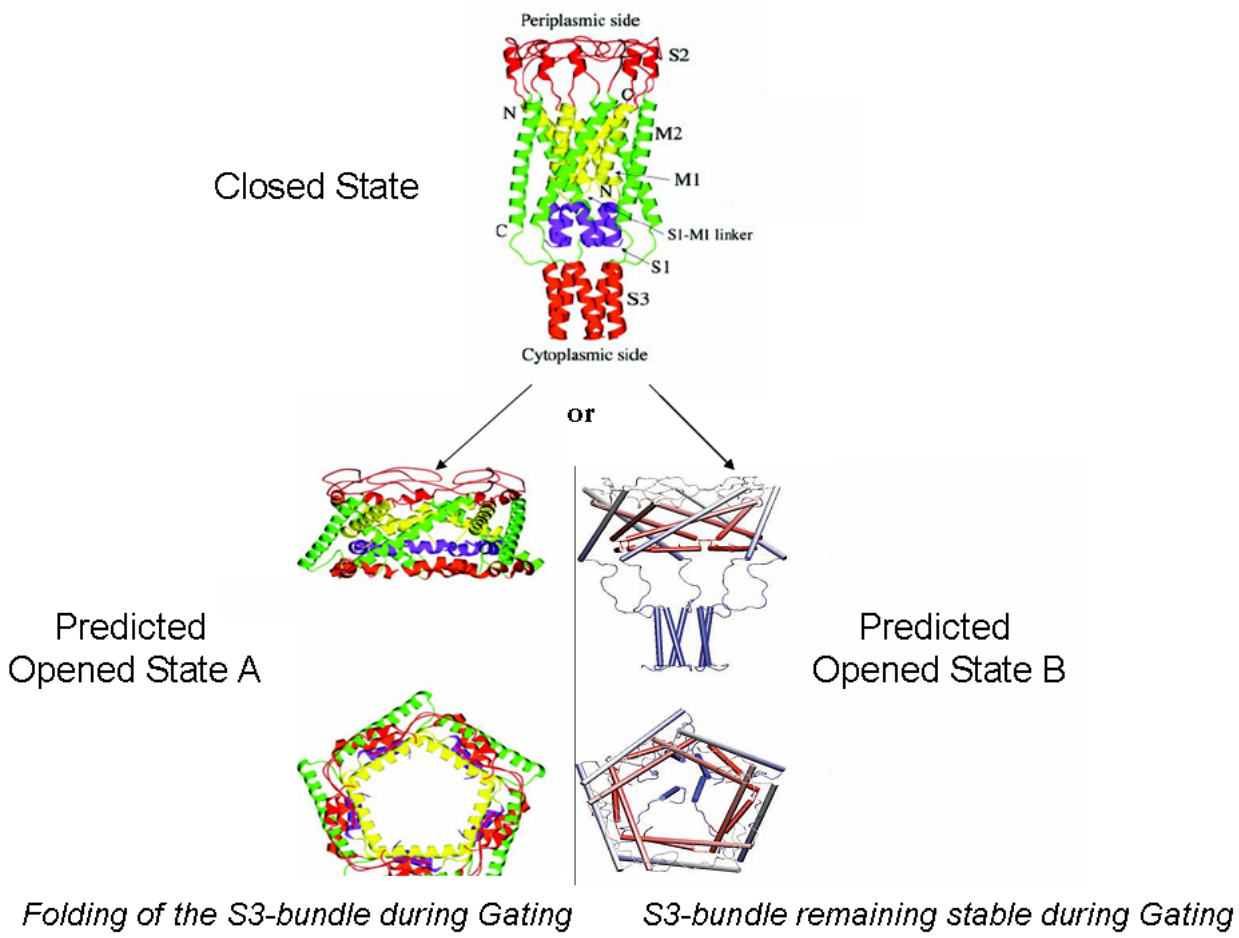

Figure 3-1. Conflicting models of the S3-bundle during gating. The top schematic is the closed state of MscL according the pdb structure (OAR). On the right there is a side and top view of the opened state with the S3-bundle separated and folded into the bilayer. On the left is a side and top view of the open state of MscL with the S3-bundle closed during gating and the linker region expanded. Images adopted with permission from references: (*51, 56*)

In this study, we used cysteine substitutions to restrain movement of portions of this C-terminal region in order to investigate key areas that will enable future modulation of conductance. The disulfide bridging resulting from the cysteine crosslinking between neighboring subunits will occur if specific residues are consistently in close proximity or if they come into contact with one another (due to mobility or dynamics of the region). If the S3-bundle does actually disassemble upon gating, then cysteine mutations made to residues E119, V120, L121, L122, L128, and L129 would constrain its movements and should decrease the

conductance by locking the S3-bundle together. On the other hand, if the S3-bundle remains in a stable confirmation during gating, then cysteine mutations to residues A110, A111, A112 and A114 in the linker region between the second transmembrane domain and S3 should decrease the conductance of the channel as shown Figure 3-2. These above disulfide-trapping experiments were explored *in vivo* and the results were quantified using the western blot technique.

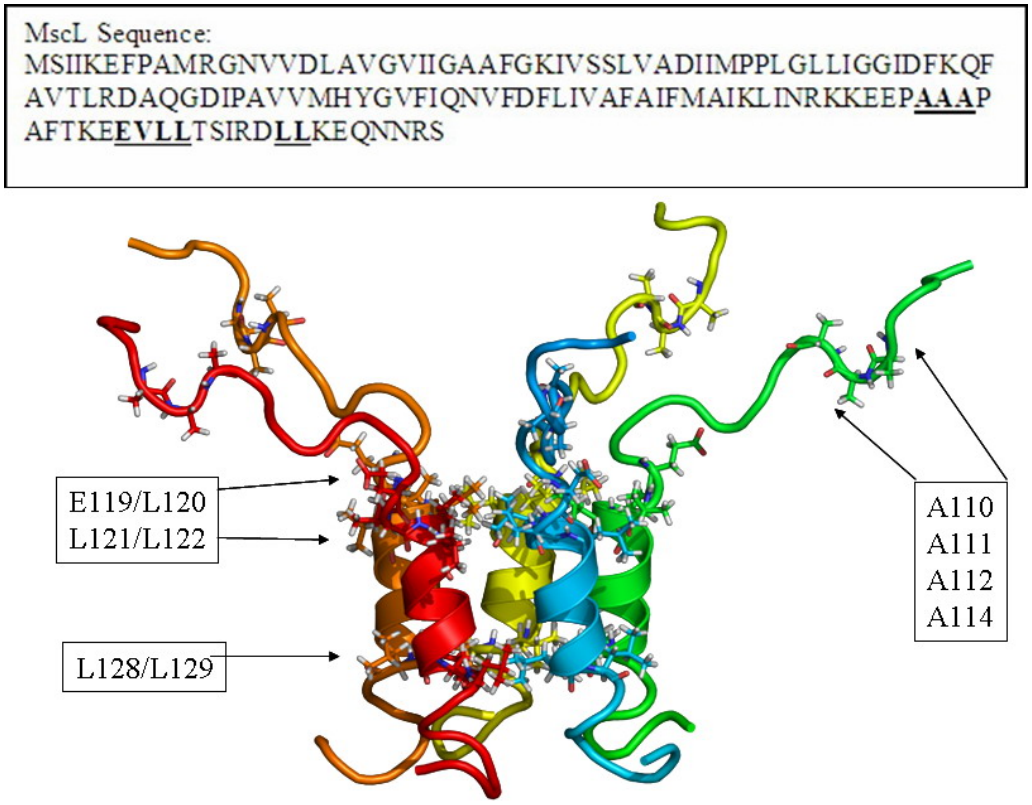

Figure 3-2. Amino acid sequence for MscL and a ribbon design of the linker area and S3 bundle of the C-terminal region with the location of the mutations highlighted. Molecular model was configured according the MscL crystal structure of *M. tuberculosis* in the pdb-20AR.

Mutants A110, A111, A112, L121 and L122 displayed a high level of crosslinking and were assayed with patch clamping for functional analysis under ambient, reduced and/or oxidized conditions. The information obtained from this research has provided insight into the

interaction of key residues in the C-terminal region and its dynamics during gating, as well as suggested possible ways of controlling the conductance of the channel.

Materials and Methods

Strains and Cell Growth

Cysteine mutations, A110C, A111C, A112C, A114C, E119C/V120C, L121C/L122C, L128C/L129C, and A110C/A111C/A112C (AAA), were made using the QuickChange site-directed mutagenesis kit (Stratagene Corporation). This kit provides amplification of double-stranded DNA using the *PfuTurbo* Polymerase Chain Reaction (PCR) technique.

pB10D plasmid constructs were then transformed to DH10β bacteria to yield more DNA for sequencing. Qualitative analysis of the mutation and wildtype genetic sequences were performed using Agarose Gel electrophoresis, and the genetic modifications were verified using automated sequencing. Once the mutated sequence was confirmed, the constructs were transformed into *E.coli* strain PB104 (*null* MscL), then used for GOF assays and disulfide trapping experiments and MJ455 for LOF studies.

Phenotype studies

Before performing the actual biochemical assays and electrophysiology, the affect of the cysteine mutation on the survival of the cell was examined. Two extreme phenotypes can occur when mutating MscL: Gain of Function (GOF) or Loss of Function (LOF) mutations.

GOF Assays

GOF mutants show a slowed- or no-growth phenotype not normally observed. Electrophysiological characterization of these mutants have shown that the MscL channel require less tension for gating. Thus, the interpretation is that these channels are “leaky”, and *in vivo,* open spontaneously making the cell sick, or even killing it as shown in Figure 3-3.

For these assays overnight cultures of mutants, WT (negative control) and G26H (positive control) were diluted until an early lag phase in LB with 100µg/ml ampicillin at 37°C while shaking at 250 cycles per minute. The optical density, OD_{600}, was taken every 20 minutes. At an OD of 0.2, the samples were split and Isopropyl-β-D-thiogalactopyranoside, IPTG (2mM) was added to induce half of the samples. The OD was measured every 20 mins for the next 5 hours and again the next morning. Growth curves for each mutant were generated and compared to WT and G26H.

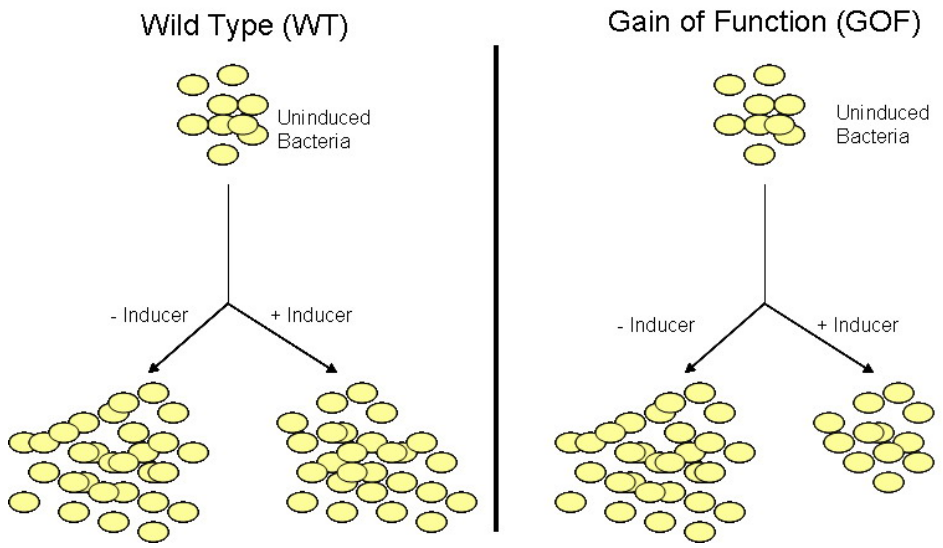

Figure 3-3. Schematic illustration of gain of function assay. These mutants tend to grow slower because of the leaky channels that compromise the membrane's integrity. Therefore, growing the bacteria in liquid media and recording the optical density in intervals will allow proper screening of GOF. Inducing the cells, which promotes protein expression essentially reveals the GOF.

Loss-of-Function Assays

LOF are quite the opposite of GOF; these channels only respond to extremely higher membrane tension as shown in Figure 3-4. In order to assay for LOF mutants, expression must take place in bacterial strains lacking both MscL and MscS (Mechanosenitive channel of small conductance explained in Chapter 1) since MscS has a redundancy of function with MscL (*114-*

116). As a result, an inducible plasmid containing MscL's gene is transformed into MJ455 cells which lack the genes for both MS channels.

To test for LOF mutants, MJF455 cultures were grown for 8 hours at 37°C at a pH 7.0 in Citrate/Phosphate-minimal-media. Cultures were next diluted with 0.5 M NaCl and at an OD_{600} of 0.25 at 37°C they were induced with ITPG for 30 minutes. After induction, cells were divided and diluted 1:20 in either water (which shocked the cells) or in LB containing 0.5 NaCl (served as a control) for 20 minutes. Colonies were next diluted into 96-well plates followed by further dilution of 20 µl of the cultures into 180 µl of media. Lastly, 5 µl were added to the LB plus ampicillin plates and grown overnight. After 24 hours, the colonies were counted and Colony-forming units (CFU) per volume were calculated. Quantification was achieved by determining the relative survival rate of the different mutants versus cells expressing wild type MscL (negative control) and vectorless cells (positive controls) (*3, 46*).

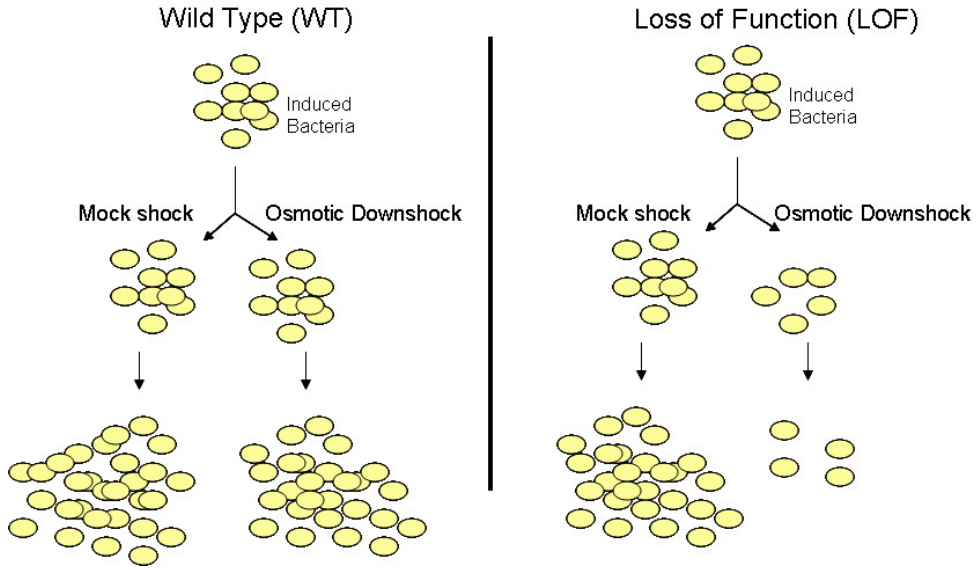

Figure 3-4. Loss of Function schematic representation. A LOF mutation causes a decreased in survival of bacteria cells due the delayed responds of MscL sensing an increase in tension. These mutants are identified upon osmotic shock where the mutation inhibits the release of osmolytes causing cell lyses.

Western Blot Analysis

For a detailed description of this procedure see Chapter 2. Briefly, single colonies were grown in LB in the presence of 1 M NaCl while shaking in an incubator at 37°C rotating at 250 cycles per minute. Culture growth was measured at 30 min intervals. At an early log phase, an OD of 0.2-0.3, protein expression was induced by adding 1 mM IPTG. At an optical density of 0.3-0.4, cultures were diluted in either pre-warmed (37°C) destilled water, shocking the cells or in LB with 500 mM NaCl as a control. To insure crosslinking, another control was prepared using LB containing 1% of oxidizing agent H_2O_2. To study the reversibility of disulfide bridging, reducing agent mercaptoethanol was added to the sample buffer for SDS-PAGE analysis. All samples were then heated at 70°C for 4 minutes followed by centrifugation for 3 minutes at 12000x g before resolution in a 4-20% gradient Tris-HCl polyacrylamide gel. Proteins were electro-transferred to Immobilon Polyinylidene Fluoride (PVDF) membranes at 105 mV for 70 minutes for proper visualization of the protein.

Western Blot analysis was performed using one of the following: primary antibodies against the MscL C-terminus, penta-His- antibody or HRP-His-Probe. The secondary antibody for MscL was goat-anti-rabbit HRP Bio-rad). The primary MscL antibody poorly recognized the double mutants L121C/L122C and L128C/L129C due to the close proximity of the mutation sites to the epitope. When protein expression was too low for recognition with the penta-His-antibody, we used the HRP-His-Probe (which was used for the majority of the study). The HRP-His-probe uses a Ni-chelating group that binds to the 6His-tag present on the protein. The HRP-His- probe reacts with the substrate giving off a chemiluminescent signal that was quantified using X-ray sensitive film (Kodak) and the dipping method. Quantification was completed by measuring the density of the bands using the Scion Image Software.

Electrophysiology

Electrophysiology studies of MscL require an increase in *E. coli* cell size to enable patching. It also requires a decrease in the peptidoglycen layer in order to access the inner membrane. In 1987, Dr. Kung and coworkers adopted a technique to generate giant sphereoplast from the J. Adler group. Patchable bacterial spheroplasts were obtained by the addition chemical reagents: cephalexin 10 mg/ml, lysozyme 5 mg/ml, ethylenediaminetetraacetic acid (EDTA) 125 mM, and DNAase 5mg/ml. Cephalexin inhibits cell division but not growth: leading to long filamentous syncitia termed "snakes" that collapse into giant spheres, between 5-10 µm, which is acceptable for patching (*38, 101*).

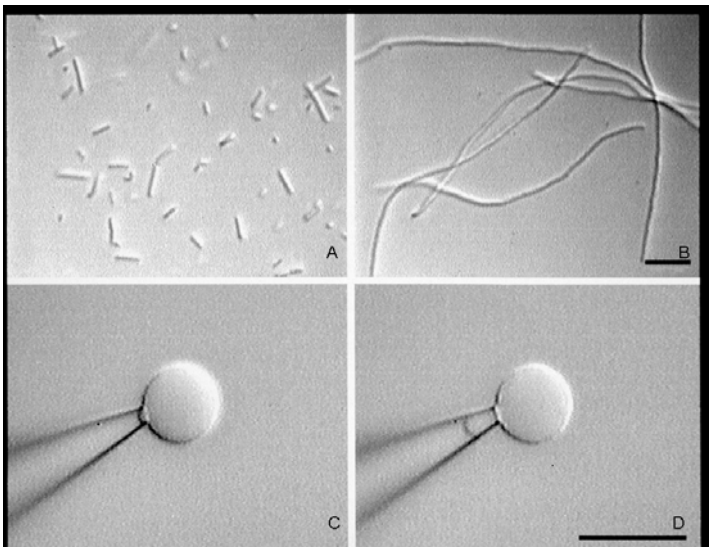

Figure 3-5: Video images obtained during the process of generating and patching giant spheroplasts from *E. coli.* Image A) rapidly growing *E. coli* cells. Image B) large filamentous cells also known as "snakes" generated from treatment with cephalexin. Image C) a giant spheroplast created from collapsed "snakes." Image D) the patch is established between the pipette tip and the giant spheroplast and upon suction a giga-ohm seal was formed. Image donated from Dr. Blount and ref: (*39*)

Digestion at room temperature with the addition of lysozyme and (EDTA) leads to hydroxylation of the peptidoglycan layer, weakening the cell wall causing the *E.coli* spheroplasts to swell (*31,*

38, 39). Lastly, $MgCl_2$ and sucrose was incorporated to stabilize and complete the spheroplast shown in Figure 3-5 for proper patching.

An inside-out patch clamp configuration that accounts for pressure applied to the membrane was exploited for single channel analysis of the mutants. Negative pressure was applied and monitored using a piezoelectric pressure transducer at room temperature. Once a gigaohm resistance was obtained between the micro-pipette tip and the patch, gentle suction and micro-manipulating of the tip away from the spheroplast disassociated the patch. This inside-out patch technique allows exposure of MscL's cytoplasmic region to the bath/buffer solution (200 mM KCl, 90 mM $MgCl_2$, 10 mM $CaCl_2$, and 5 mM HEPES adjusted to a pH of 6). Because the pressure required to gate MscL differs from patch to patch (due to the different sizes and geometry of the patched membrane; see ref Moe et al 1995), the pressure required to gate MscL is normalized to that of the MscS. MscL constantly opens at 1.4 times the pressure required to open MscS (*27*).

Results

To test the proximity and the dynamics of the C-terminal region during gating, we generated cysteine substitutions at a number of positions and assayed their ability to disulfide bridge. We individually mutated residues A110C, A111C, A112C, and A114C; while double mutants were made near the end of the C-terminal at positions E119C/V120C, L121C/L122C, and L128C/L129C as shown in Figure 3-2. We also examined a triple mutant A110C/A111C/A112 (AAA). These residues were chosen because they are highly conserved and are of three different regions of the proposed linker/S3 bundle.

Phenotype Characterization

Conserved residues can play an important role within the protein and their mutation can sometimes indirectly harm the bacterial cell. Therefore, to give a rapid glimpse of possible

functional changes in channel activity, we decided to conduct two *in vivo* phenotype studies to understand the effect of the mutated protein on the survival of the host.

GOF Studies

Growth curves were generated for all of the mutants used in this study. WT was used as a negative control and G26H (a known GOF mutant) as a positive control to assay for the GOF mutants. Results suggest that none of the mutations from this study were GOF as shown in the growth curves in Figure 3-6. This may be due to the location of the mutations in the C-terminal which would be in agreement with a deletion study where residues deleted from position 110-136 mildly increased the sensitivity to tension and sub conducting states. Therefore, the mutations within the C-terminal region did not increase the sensitivity of the protein to the tension of the bilayer.

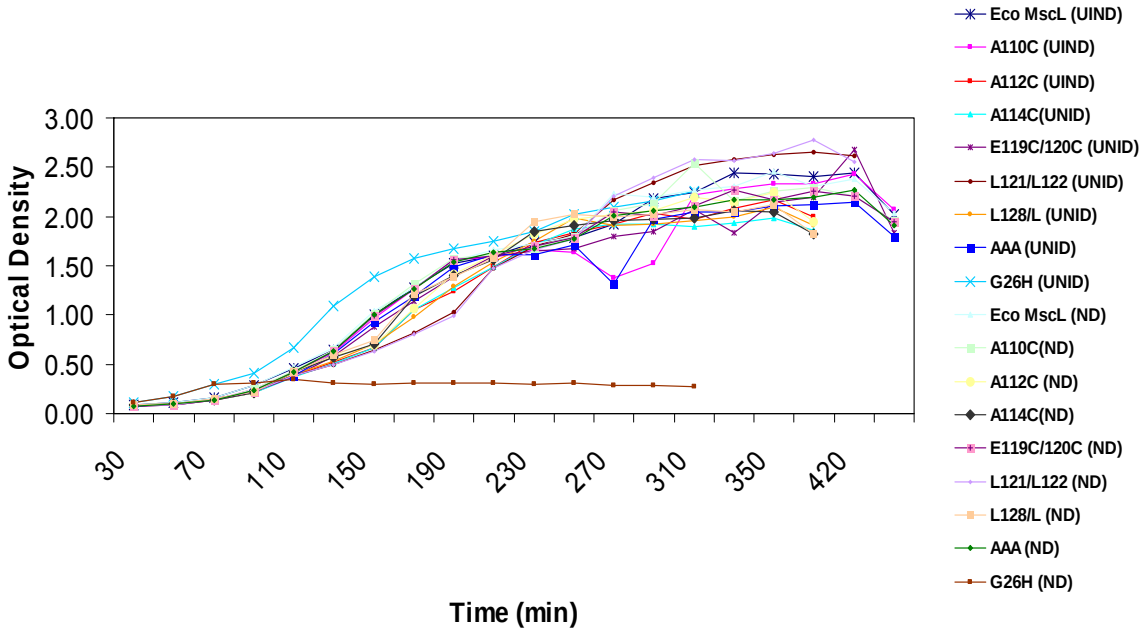

Figure 3-6. Growth curves for all of the mutants generated in this study as well as for WT MscL and G26H: UNID-Uninduced and ND-induced (n=3).

LOF Assays

Single colonies were counted after a series of dilutions following osmotic downshock and the relative survival rate was calculated for each mutation to determine if they complemented the LOF phenotype. As shown in Figure 3-7 only one mutant in this study has demonstrated the characteristics of a partial LOF phenotype, L121C/L122C. A full LOF, as determined using an empty plasmid as a positive control, is consistently less than 10% survival.

This result is not fully understood, however it does suggest that these residues may play some role in channel gating. As shown in Figure 3-4 residues 121 and 122 are located directly at the beginning of the S3-bundle. Bridging these residues together may decrease the conductance of the channel by either locking the S3-bundle together, or by decreasing the expansion of the linker region. Either of these actions may increase the sensitivity to tension required to open MscL. Nonetheless, actual functional studies are required to determine if this partial LOF affects the conductance of the channel. It may just affect the single channel kinetics.

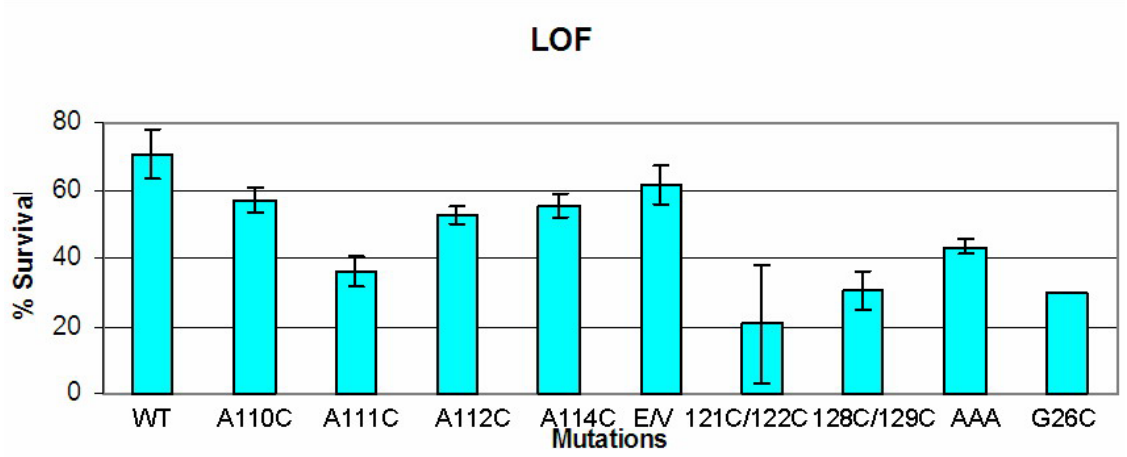

Figure 3-7. LOF study analyzing the percent survival of the mutants (n=3). G26C was used as a control.

Biochemical Assays

Disulfide-trapping can utilize the oxidation of cysteines, either native or mutated, to stabilize a protein in specific conformations by generating S-S bridges within or between subunits. Disulfide trapping of MscL *in vivo* is enhanced by osmotic shock, as shown in Figure 3-8 where the average dimer formation of single mutants A110C-A114C display a 20 fold increase in intensity upon osmotic shock. Since the cytoplasm contains many reducing pathways using thioredoxin and glutathione/glutaredoxin to maintain reduced thiols, preserving a disulfide bridge in this region is a challenge (*117, 118*). In every case measured thus far, it appears that the amount of disulfide bridging increases subsequent to osmotic shock (*94*). Presumably during the osmotic shock some of the reducing agents including thioredoxin are released through MscL (*54, 55, 94*). Therefore, osmotic shock intensifies the dimer formation signal indicating an interaction of residues either by them dynamically passing each other or by them remaining in close enough proximity to bridge during one of the conformational states.

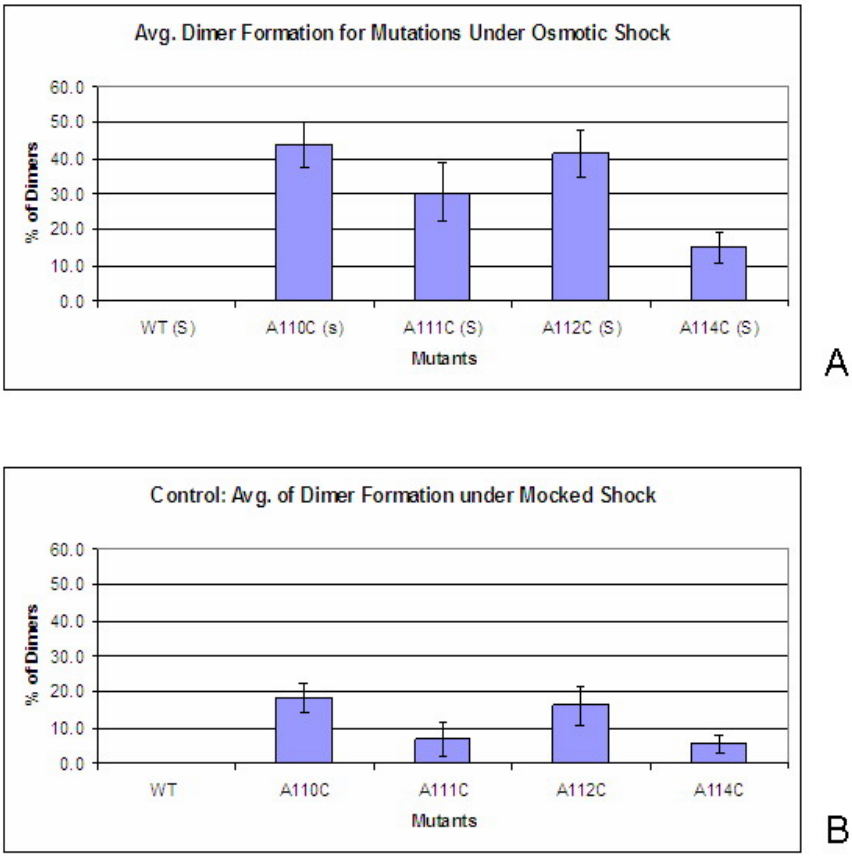

Figure 3-8. Percentage of Dimerization for single mutants A110C, A111C, A112C, and A114C (n=12). A) Avg. Dimer formation under osmotic shock. B) Avg. Dimer formation under normal conditions.

According to our biochemical assays, all cysteines in this study crosslinked at some level. Single mutants formed dimers while double mutants formed dimers, trimers, tetramers, and even some pentamers as shown in Figure 3-9. Monomer bands were observed with all of the mutants indicating not all of the cysteines crosslinked. This was true for both shocked and non-shocked mutants.

Reversibility of the disulfide bridging was also conducted to ensure that the visualized bands were a direct result of cysteine crosslinking. Dimerization was reversed when 5% of reducing agent ß-mercaptoethanol was added to the sample buffer as shown in Figure 3-10;

where only monomer bands were observed. To increase crosslinking or enhance the probability of disulfide bridge formation, the cells were also exposed to an oxidizing agent.

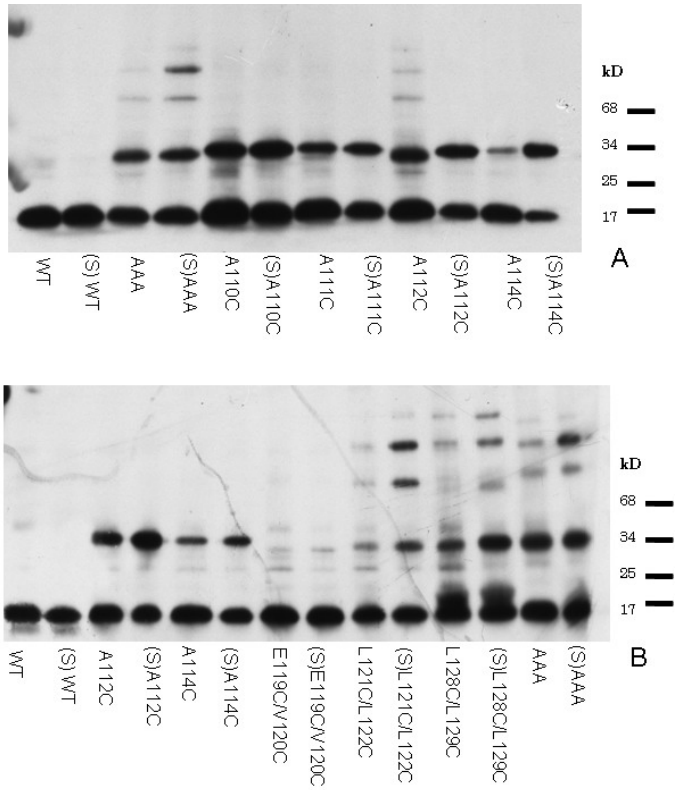

Figure 3-9. Disulfide crosslinking in single and double mutants identified using western blotting. A) Single cysteine substitution forming disulfide bridges under both mock shock and osmotic shock (S) conditions. B) Double cysteine substitutions forming crosslinking between multiple cysteines. One monomer is about 17 kD.

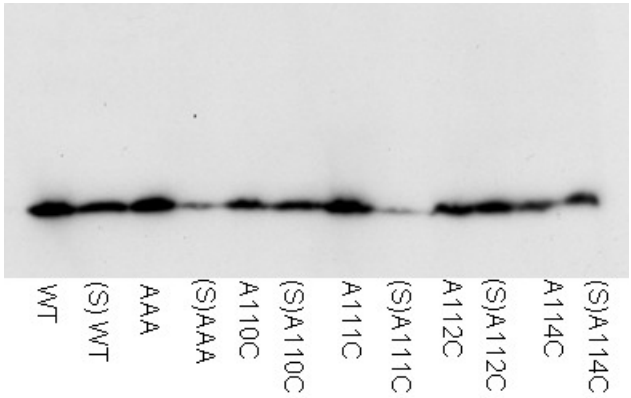

Figure 3-10: Monomers of single mutants and WT as a control exposed to reducing agent DTT. Both Shocked (S) and Nonshocked identified using western blotting

Both shocked and nonshock liquid media containing 1% H_2O_2 reared bands with higher intensity than without the oxidizing agents as shown in Figure 3-11. Dimerization *in vivo* for all of the double mutants exposed 1% H_2O_2 yielded higher intensity than under ambient conditions. They both form tetramers and pentamers under both ambient and oxidative conditions suggesting their existence within 3.6-6.8Å of their analogues in the α-helical bundle. While this supports the idea that these residues are in close proximity, it tells little of any movement or changes that occur in this area upon channel gating.

The results from the triple mutant A110C, A111C, and A112C, and double mutant L121C/L122C, under both shocked and oxidized conditions displayed greater crosslinking, making these mutant candidates for the electrophysiology studies. Therefore, inside-out patching was performed with these mutants under ambient, oxidative, or reduced conditions.

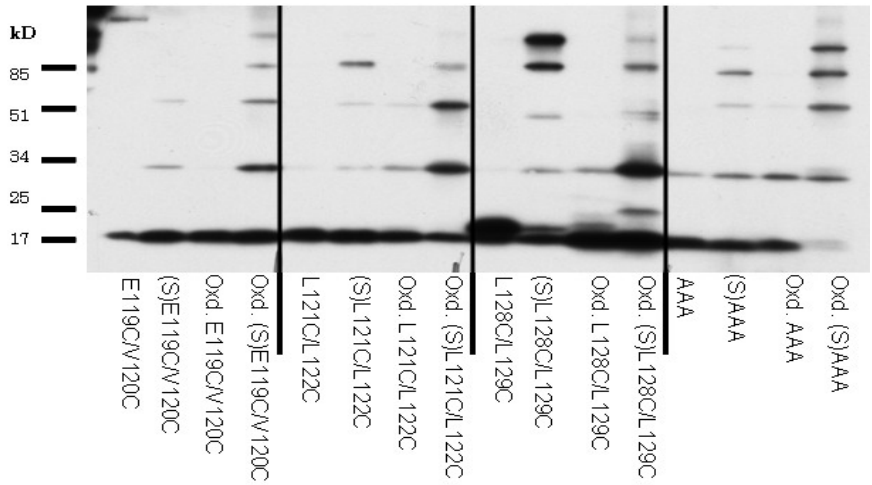

Figure 3-11: Double mutants E119C/V120C, L121C/L122C, L128C/L129C, and AAA exposed to 0.5 M NaCl-LB (1st row), water (2nd row), 0.5 M NaCl-LB and 1% H_2O_2 (3rd row), and water with 1% H_2O_2. Quantified using western blotting.

Electrophysiology was preformed in Dr. Blount's laboratory by Drs. Irene Iscla and Li-Min Yang. A tetra-mutant of L121C/L122C and L128C/L129C was generated and inside-out patch clamped in PB104 cells. During these saturation experiments, the change in channel

activity and conductance were examined in the present of both oxidized and reduced conditions. Results from this study indicated there was not a change in the number of active channels or their conductance when the tetra-mutant was placed in either oxidative or reduced conditions (results not shown). This suggests that these residues are buried inside the S3-bundle and that they are unlikely to move upon gating.

Electrophysiology of the AAA-MscL included exposing this mutation to buffer solutions containing reducing agent 1 mM dithiothreitol (DTT) or oxidizing agent H_2O_2. In these studies, the single channel activity of this mutant changes in consistent ways when exposed to both the reducing and oxidizing agents (results not shown). Briefly, oxidizing reagents decreased the conductance of the channel, while reducing agents increased it. However, the triple mutant enables disulfide bridging at multiple positions within the complex and in numerous possible combinations. Therefore, we were unable to determine which sets of cysteinses were crosslinking therein any given functional channel. Thus, we next attempted to decrease the conductance of the channel by generating Histidine mutations, which can coordinate metal ions.

Both A110C and A112C showed a 20 fold increase in dimerization upon osmotic downshock, therefore these two mutants were converted to A110H and A112H using Quick-change site-directed mutation, and sphereoplasts were generated in the same manner as stated above. By mutating them individually to Histidine, and coordinating heavy metals, we should be able to constrain the movement of this proposed 'filtering' domain and thus the amount of osmotolytes translocating the pore of the channel, thereby decreasing the channel's conductance. Previous studies with wild type MscL have shown no functional changes upon heavy metal treatment (*110*). In contrast, when 1-2 mM of $ZnCl_2$ was added to the bath solution of native

bacterial membranes expressing A110H or A112H, a decrease in conductance and a change in the single channel kinetics were observed, as shown in Figure 3-12.

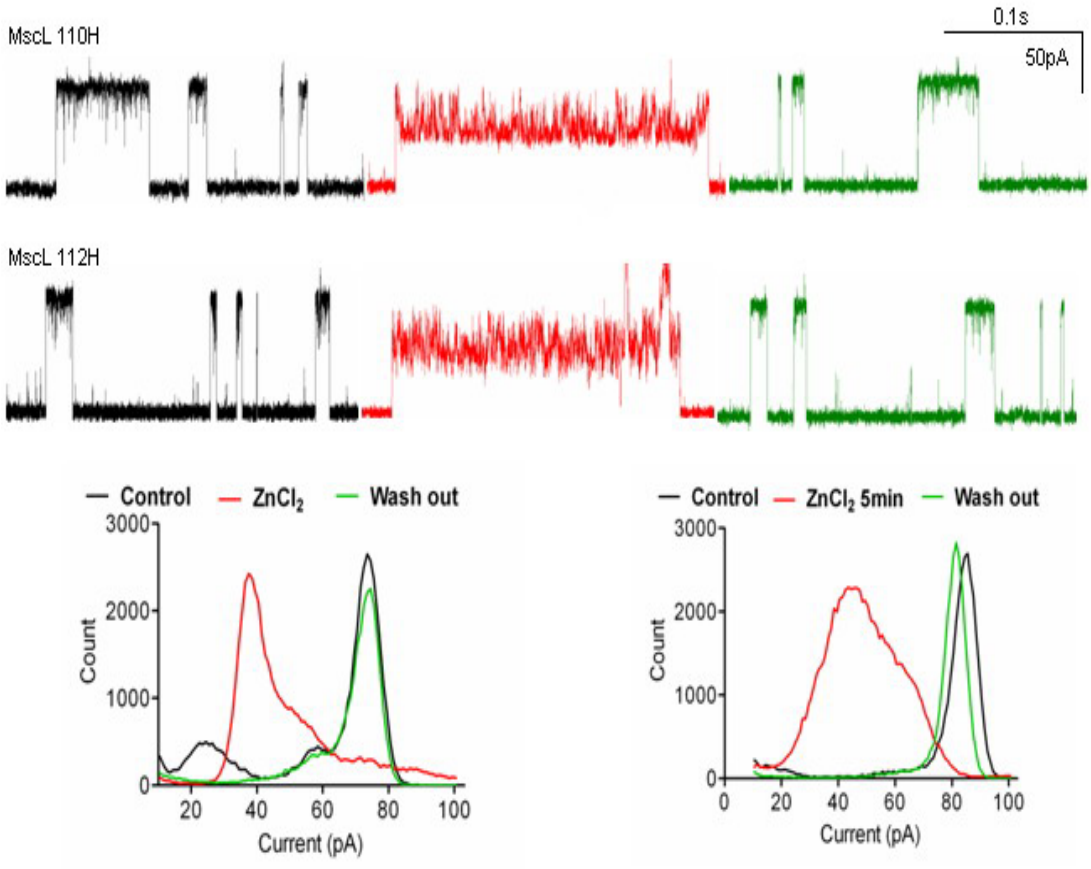

Figure 3-12. Single channel traces of A110H and A112H when exposed to regular patch clamping buffer, and a patch solution of $ZnCl_2$. Point amplitude histograms of the single channel activity of A110H and A112H displaying an average current of roughly 80 pA with regular patch clamp buffer and a decrease to 40 pA when exposed to $ZnCl_2$.

The current for both mutants was roughly 80 pA before the exposure to $ZnCl_2$ and a holding voltage of -20 mV. Once they were exposed to the heavy metal, the conductance decreased by half from ~4 nS to ~ 2 nS and the channels stayed open longer. Once the $ZnCl_2$ solution was rinsed out, the conductance as well as the activity resumed normal activity. Hence, we have developed an MscL channel in which the conductance can be reversibly decreased by heavy metals.

Discussion

Despite the fact that the C-terminal region of MscL was resolved from the crystal structure, its physiological role is unclear. Molecular Dynamic stimulations and electron paramagnetic resonance, EPR studies have both supported the notion that part of the C-terminal region does form a α-helical bundle at physiological pH (7.0), but the predicted structure is quite different from that shown in the crystal structure. The state of the bundle during the gating process is also controversial, some evidence suggests it remains as a bundle and plays the role of a molecular size filter allowing certain osmolytes to transverse the channel's pore (*51, 53*). On the other hand, each of the previous studies have had their flaws, and some studies have demonstrated that quite large solutes pass through MscL. This leads us to question the importance of the C-terminal. Does any conformational change occur in this region? Does it affect the overall function of the channel, and if so, mutations to which area (linker or S3-bundle) will enable a decrease in conductance?

Here, in an attempt to better understand the dynamics of the C-terminal region, we probed the proximity of residues A110-A112, A114, E119-L122, L128, and L129 located in the C-terminal region. The results from this study indicate first, that none of the mutations affect strong phenotypes. This is consistent with the observation that most GOF phenotypes are found along the pore of the channel. For instance, two well known GOF mutation sites are in positions G22 and G26 located are near the constriction point of the closed channel (*3*). Substitutions with hydrophilic residues to position G22 yields severe GOF mutants, as in the same manner a substitution with Histidine to residue G26 also yields an extreme GOF mutant (*3*).

The only mutant that did not significantly complement the LOF phenotype was the double mutant L121C/L122C. This mutant, according to Molecular Simulation modeling, spin-labeling, and cysteine substitution, is located in the S3-bundle (*51, 53*). The reasons why this mutant is a

LOF mutant are not clear. However, its location in the upper part of the 3-bundle (refer to Figure 3-4) may affect the stretching of the linker region during opening of the pore if the S3-bundle remains together. If the S3-bundle opens and folds into the membrane as shown in early molecular modeling studies, then the crosslinking that occurs during osmotic downshock at position L121C/L122C may affect the mobility of the cytoplasmic region. One might anticipate that this will cause MscL to respond to higher tension, creating a loss of function mutant. Mutations at E119C/V120C, which are also expected to exist at the opening of the bundle region but not expected to face each other, would not create such a LOF mutant because, as expected, they were not as efficient at forming disulfide bridges and multimers, so presumably had more functional channels. In fact, in most of the experiments, dimers rarely formed with this double mutant.

Results from this study secondly supported the concept that the S3-bundle remains in the cytoplasm during gating as shown in Figure 3-13, right. Mutants L121C/L122C and L128C/L129C were previously generated and their ability to form disulfide bridges was observed in a previous study by Sukharev *in vitro* using biochemical assays and patch-clamping. In his study the biochemical assays were conducted in ambient, reduced, and oxidative conditions, while all of the electrophysiology was only performed in ambient conditions (*51*). He assumed that because crosslinking was observed in both of the oxidative and ambient conditions biochemically, then the bundle remained close during gating and the activity would be the same. In our study, the electrophysiology was taken one step farther using saturation experiments. During these experiments the change in channel activity and conductance are examined when exposing the cystiene mutations to oxidized and reduced conditions (results not shown). A tetra-mutant of L121C/L122C and L128C/L129C was generated and inside-out patch

clamping was formed. Results from this study illustrated there was not a change in the number of active channels or their conductance when the tetra-mutant was placed in either oxidative or reduced conditions, suggesting that these residues are buried inside the S3-bundle and that they are unlikely to move upon gating. With this knowledge, we predicted that we would be able to generate a lesser-conducting channel by constraining the linker between the second transmembrane domain and the S3 bundle.

Residues A110, A111, A112, and A114, which are farther up the C-terminal region, were characterized for the first time in this study. Dimerization also occurred with these residues. The highest percentage of dimerization occurred with A110C and A112C under osmotic shock conditions. These residues are predicted to reside just above the S3-bundle in the linker region as shown in Figure 3-13. As they are likely dynamic, cytoplasic, and as we predicted they would come in close enough proximity to crosslink. We also predict that disulfide bridging would occur due to the dynamics of the region. This supposition was supported by the generation and study of a triple mutant consisting of residues A110C/A111C/A112C, (AAA). The disulfide bridging studies of this mutant also resulted in dimers, trimers, tetramers, and pentamers, and the electrophysiological studies of this mutant under ambient conditions showed a decrease in the conductance of the channel (results not shown). When exposed to a reducing environment with 5% of βME, the conductance returned back to a normal full-conducting state, implying the disulfide bridging links two or more of the subunits together and changes the characteristics of the protein by decreasing the conductance. These findings lead us to generate additional mutations within this region: site specific single Histidine mutations at residues A110 and A112.

We coordinated heavy metals with the histidines and observed a decrease in conductance by 50% (refer to results in Figure 3-12). Reversibility was also demonstrated; when the heavy

metals were removed from the system, the conductance normalized. Future research should definitely include adding this molecularly engineered Histidine channel to the tethered lipid bilayer device. If in the future the sensitivity of the channel could be increased to the femtomolar range of detection, this would be the first generation of modulated MscL biosensors for the detection of heavy metals.

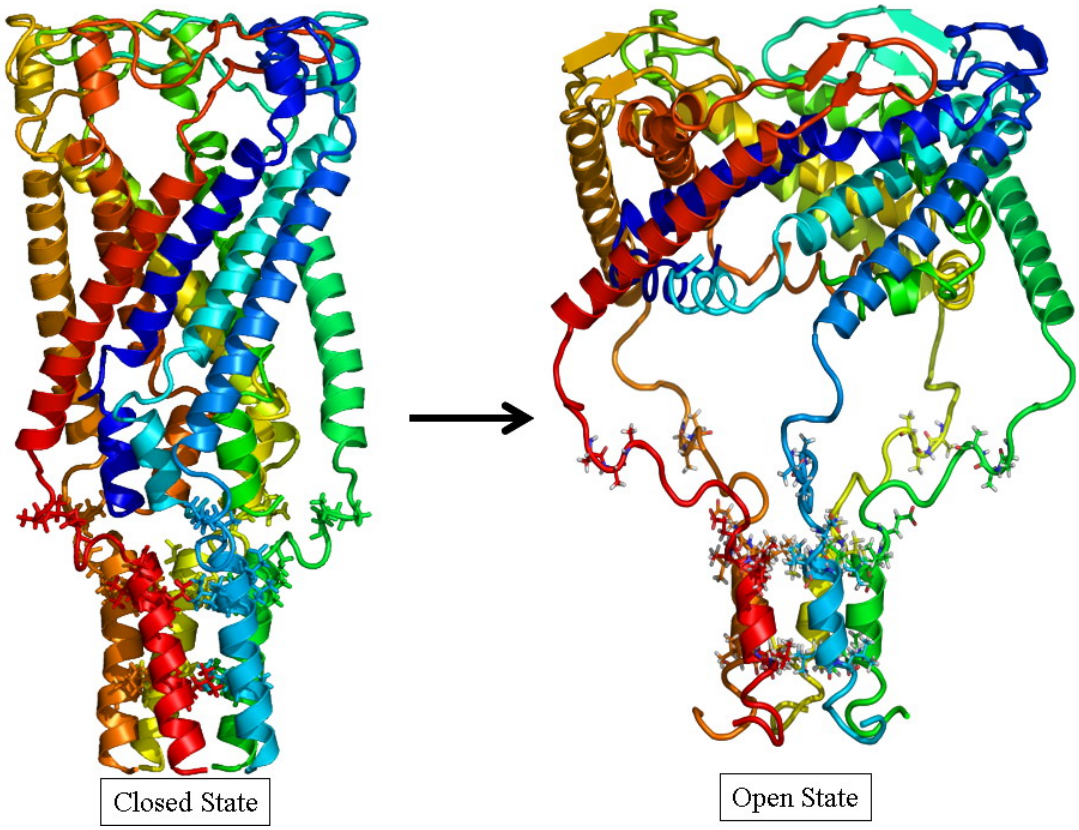

Figure 3-13. Closed and opened state of MscL with mutations generated in this study highlighted.

Conclusion

The aims of this study were 2 fold. First, the objective was to determine if the pentameric α-helical bundle within the C-terminal of MscL changes conformation from a closed state to an open state during osmotic shock. The second goal was to determine what area of the C-terminal region would enable manipulation of single channel activity and decrease channel conductance

with information obtained from the 1st objective. This was done *in vivo* using a classical scanning biochemical assay. Results from this study supported the newer molecular model of MscL in the protein data base (pdb), which depicts the hydrophobic residues buried in the bundle and the hydrophilic residues exposed on the outside. Our studies strongly suggest that the S3-bundle remains closed during gating. An even more exciting discovery obtained from this study was the generation of two new mutants that coordinate heavy metals and decrease the conductance of the protein. Moreover, this reaction is reversible when the heavy metals are removed the channel activity returns to normal.

Future experiments will include ways of isolating and purifying these mutants in order to study them *in vitro* within liposomes and in a tethered lipid bilayer membrane. Currently, purification of MscL is done using a nickel affinity column that binds to a 6-His-tag placed on the C-terminal of MscL. Possible cleavage of the His-tag could be done once the protein is eluted during purification to ensure the metals are interacting specifically with Histidine mutation and not the His-tag. With an increase in sensitive for the heavy metals, a future experiment could investigate the Histidine mutant as an actual biosensor within the device. Short-term projects will include looking for reversible decreases in conductance of the Histidines mutants when incorporated in the tethered lipid bilayer.

CHAPTER 4
TESTING THE ELECTRICAL STABLITY OF DIFFERENT LIPID BILAYER COMPOSITIONS OF DPhPC/DPhPE

Introduction

Planar lipid bilayer systems were first introduced in 1966 as an electrochemical transducer for detecting antigen-antibody and enzyme-substrate reactions (*119*). These systems are experimentally engineered over small apertures, between 1 μm-1mm in diameter, creating a thin barrier separating two aqueous solutions. Since then, these artificial bilayer lipid membranes have been used as novel biological sensing systems incorporating isolated protein receptors that bind specific analytes. Some recent studies have examined the membrane permeability, while others have exclusively introduced active transporter proteins, allowing for control over ion permeability (*8, 70, 120*).

Planar systems offered the advantage of isolation, over traditional studies of ion channels in their native environment. Scientists are able to select the bilayer's composition, control the thickness of the membrane, examine the effects of different lipid architectures, and vary the surrounding solutions of ion channels within planar BLMs (*6, 8*). One disadvantage of using planar systems is the lack of stability associated with establishing the bilayer within either a pore or a hole. For this reason, researchers turned to integrating planar BLMs with solid supports (*7, 11, 62, 65, 72, 73, 102, 121*). Despite this disadvantage and the frustrating nature of the freely suspended planar system, it is still used to examine different lipid compositions, and they provide enough stability to study small ion channels like Gramicidin (*77, 97, 122, 123*).

In this study the tip-dip planar bilayer method (explained in chapter 2) was used to determine the best lipid ratio between DPhPC and DPhPE. This planar linear method establishes the bilayer at the tip of the microelectrode and measures the isolated channel activity, once the proper resistance is obtained, using an Ag/Cl electrode. The lipid ratio that displayed the longest

lifetimes, low current leakage, and remained stable under high applied potentials served as the lipid environment to test Gramicidin as a model channel.

An important aspect of forming a stable bilayer is to reduce current leakage and hole formation which relates to random transitions in current amplitude. If a change in current occurs without the presence of an ion channel, the bilayer is said to suffer from current leakage. Mechanical stress, thermal stress, and electrical stress can all cause conformational changes in the bilayer producing these meta-stable pores. Holes formed from electrical stress or electroporation are of particular interest in this research.

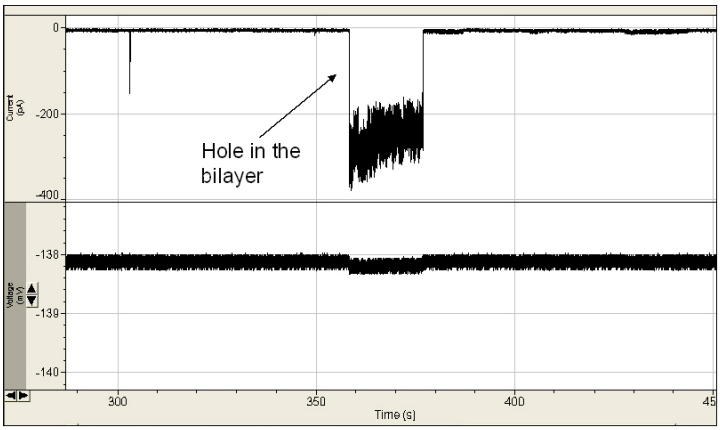

Figure 4-1. A reversible hole in the bilayer formed from electroporation with an applied potential of -138 mV, and a current transition of more then -200 pA.

These hydrophilic e-pores are formed from an applied electric field and they maintain lifetimes on the order of several milliseconds. This affects the stability of the bilayer and can lead to both reversible and irreversible breakdown if the pore is of extreme magnitude as shown in the Figure 4-1.

In addition to irreversible breakdown, electroporation can pose a problem to this research. Small pores with smaller conductance can also form in the bilayer when low potentials are applied to the system. This response can be mistaken for single ion channel activity if the

current leakage is uniform as shown the Figure 4-2 when 80 mV are applied to a bilayer composed of 100% DPhPC.

Figure 4-2. Mini-electroporation of a 100% DPhPC bilayer at 80 mV. Pores have a uniform current flow of 10 pA.

Other artifacts that contributed to experimental noise include current jumps, background current ramps, and some electrical noise. The sensitivity of the recording system allows it to detect all current changes regardless of the source. When possible, quality data from trials with current artifacts are included after background filtering, while other runs are disregarded. Therefore, forming a stable bilayer with a high electrical resistance is vital to the tip-dip method. Two variables that could decrease electroporation, electrical, and background noise in the system are the tip diameter and the gigaseal's stability.

Methods and Materials

DPhPC and DPhPE lipids were mixed in the following molar percentages: 50PC/50PE, 100PC, 100PE, 70PC/30PE and 30PC/70PE. The powdered form of each lipid was dissolved in Chloroform and stored at -20°C.

This method was explained in detail in Chapter 2. Briefly, when performing a tip-dip recording, a silver wire was coated in a commercial bleach solution for 30 minutes to create a silver/silver chloride Ag/Ag/Cl electrode. Excess bleach on the surface of the wire was rinsed

away with distilled water followed by washes with the buffer solution KCl 250mM, $CaCl_2$ 1mM, and Morpholinopropanesulfonic acid, MOPS 5 mM. A Teflon well plate was cleaned using distilled water (pH 7.4) and with ethanol. After the well plate dried, we used disposable pipettes to add the MOPS buffer solution and inserted the ground electrode into one of the wells within the Teflon well plate We then added the lipid mixture to the surface of the solution. The lipids formed a monolayer on the surface of the buffer within 10 mins. The micropipette tip was prepared by a Micropipette Puller with a heated filament. Borosilicate capillaries were used to create the microelectrode tip and were purchased from Warner Instruments Inc., were 7.5 cm long and 1.5 mm wide. One capillary created two tips because the filament heated the glass vertically in the center resulting in two 3.25 cm long micropipette tips. The tip's diameter should be in the range of 0.50-5.00 μm (*78*). This diameter range enables the tip to produce an effective gigaseal with the bilayer support. The gigaseal in-turn ensures adequate electrical resistance for the patch, which theoretically prevents current leakage. For these experiments, the Micropipette Puller is set to produce tips with a diameter of 1 μm to ensure sensitivity. Over many trials, the following anecdotal observations are made:

- Freshly pulled tips (within 5 minutes) effectively formed bilayers
- Tips covered for days, not exposed to dust in the air, could produce stable bilayers
- Used tips did not reliably yield gigaseals
- If the tip touched any solid surface before the experiment, a gigaseal could not be established
- If air bubbles near the tip resulted from filling the microelectrode, gigaseals are difficult to establish

Scanning Electron Microscopy, SEM images of the microelectrode's tip in Figure 4-3 enabled visualization of the observations stated above. The first image of the tip indicates the inner diameter is less then 1.00 μm across while the second and third images show the outer diameter as roughly 1.50 μm across.

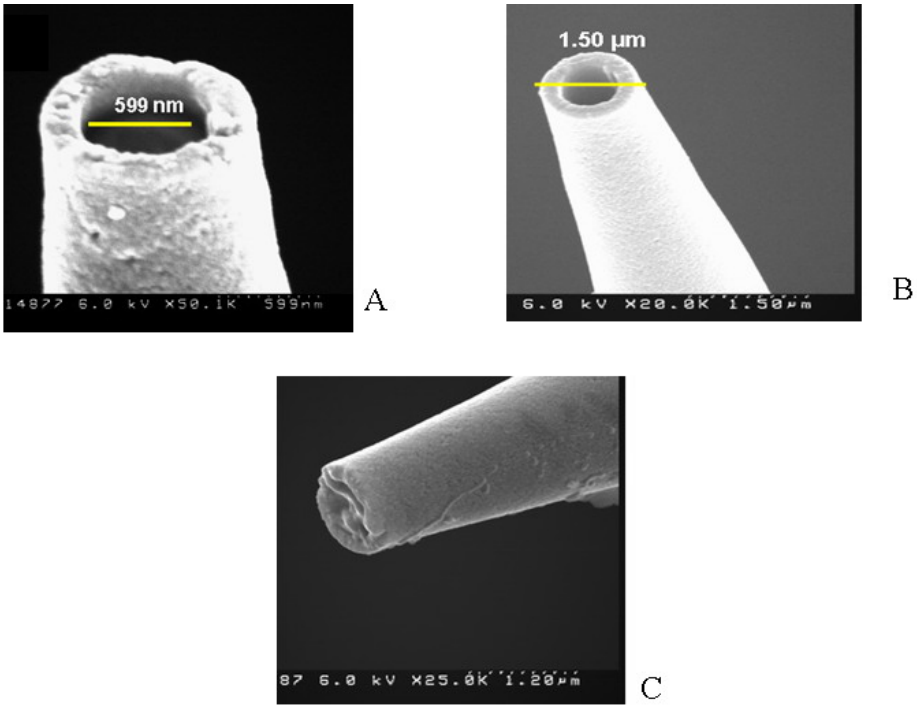

Figure 4-3. SEM images of the borosilicate pipette tips. A) Freshly pulled tip with an inner diameter is less then 1.10 µm across. B) A tip that was covered for three days the diameter is still less then 1.50 µm range. C) A tip after it has been dipped in a bilayer solution of DPhPC prior to SEM analysis.

Depending on the patch clamp technique of choice, the isolated patch can be between 1-10,000 μm^2 and the unitary conductance of ion channels is in the order of several picosiemens (pS). Therefore, the resistance of the bilayer is vital to all patch clamp experiments, especially the tip-dip method. It ensures adequate electrical isolation of the membrane patch, a reduction in the current noise recording, and theoretically prevents current leakage. For single ion channel studies, the tip diameter should ideally be between 1-5 μm^2 which allows the resistance within the Giga-ohm range. This is known as a gigaseal. The experimental setup, the amount of electrical noise in the environment, the morphology of the microelectrode tip, and the bilayer support, all affect the establishment of a gigaseal. A vibration absorbing base and a copper mesh Faraday cage were utilized to limit electrical noise, while a plastic cover protected the experimental-setup from dust and debris. The tip diameter as discussed above was kept between

1-1.5 μm which helped optimize obtaining the proper resistance. Compared with other planar bilayer methods, the tip-dip method provides a greater probability of obtaining gigaseals ranging from 1.2- 10 GΩ (*124*). We observed gigaseals from 1.20 GΩ to 20 GΩ which are comparable with literature (*124*).

Results of Lipid Ratios

The stability of five different lipid ratios of DPhPC and DPhPE (which will be addressed as either PC or PE for the duration of this chapter) were studied to determine which one would be integrated on the device. The ratios are as followed: 100% PC, 100% PE, 50PC/50PE, 70PC/30PE, and 30PC/70PE. A typical experiment begins with obtaining a gigaseal and applying potentials between ± 150 mV.

Pure PC Planar Bilayers

PC planar lipid bilayers were analyzed first. Gigaseal formation with this lipid composition occurred 56% (n=22) of the time and the bilayer remained stable between potentials 20-80 mV. Pore formation, however occurred at threshold potentials of 80 mV or greater. The pore formation was heterogeneous as shown in Figure 4-4 where it opened and closed for 1.5 seconds.

Lifetimes of the bilayers were usually between 2-10 minutes and once electroporation occurred, it continued at potentials as high as 125 mV and as low as 40 mV. In addition, the baseline was unstable and would drift between 1-3 pA during experiments. Quantitatively short spiky events also appeared lasting less than 2 seconds throughout the lifetime of the bilayer. We concluded pores produced were independent of the applied potential, randomly forming large and small pores with conductance of 0.4 nS to 10 pS.

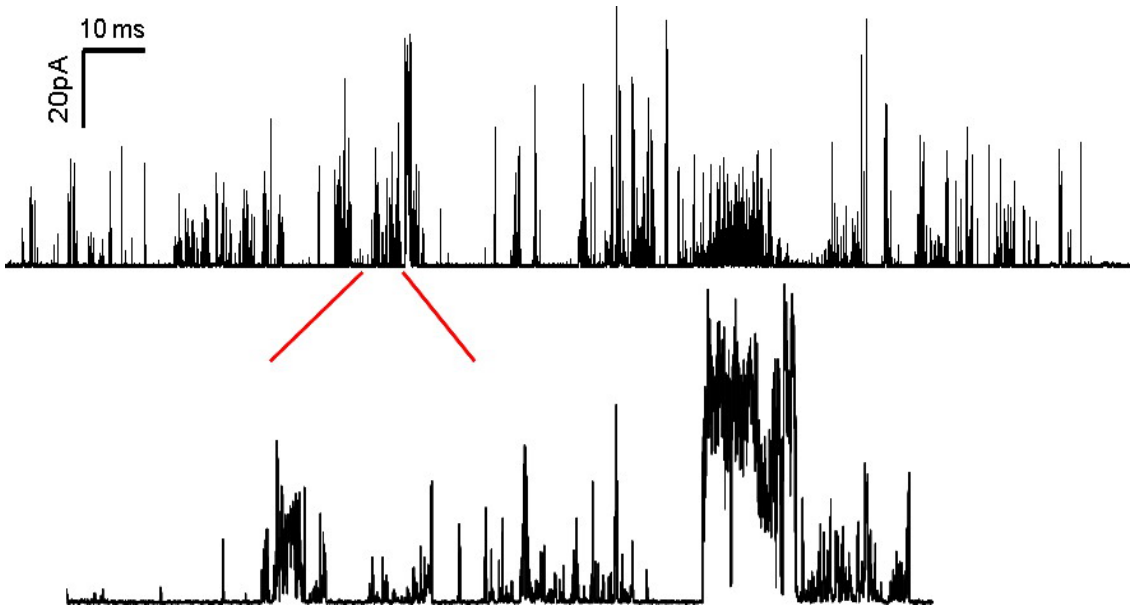

Figure 4-4. Electroporation of 100% PC at 120mV with a bilayer lifetime of 56 minutes. The time spent at120mV was 2mins. The current changes range between 10-80pA.

Pure PE Planar Bilayers

The smaller PE head group in 100% PE planar lipid bilayers easily formed strong gigaseals ranging from 5-10 GΩ 75% of the time (n=15). Threshold potentials were higher than that of 100% PC at 200 mV with electroporation observed 36% of the time (n=6). After 1-2 minutes of applying potentials, pore formation was consistent and more uniformed than pores formed with 100% PC planar bilayers.

The bilayer's baseline remained stable having a high recovery rate, with the uniformed pores conducting in the range of 20-40 pS. There was also more electroporation activity at negative potentials for this lipid composition although the buffer is symmetrical. Bilayer lifetimes were as long as 30 minutes to 1 hour before electrical breakdown occurred whereby the seal strength decreased from the giga-ohm to either mega or kilo-ohm range.

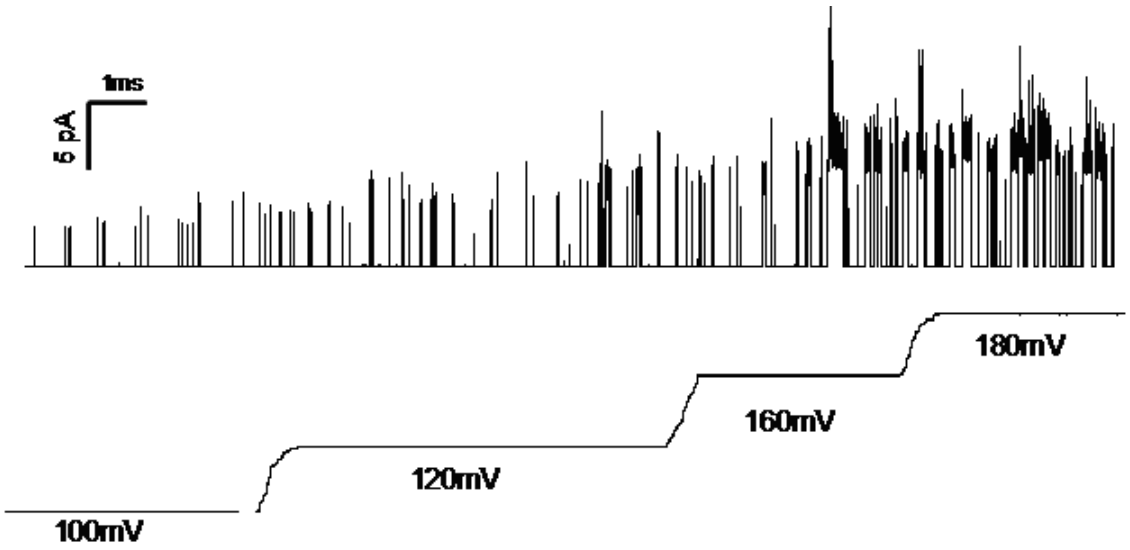

Figure 4-5. Electroporation of 100% PE planar lipid bilayer with potentials applied from 100mV-180 mV.

50PC/50PE Planar Bilayers

Planar bilayers composed of 50PC/50PE were exceptionally unstable. Forming a gigaseal with this ratio was rare and the baseline was unstable with very low applied potential (3-10 mV). Electroporation that did occur was closely followed by a disruption of the bilayer. Threshold potentials for electroporation were as low as 40 mV. The bilayers were short lived, with lifetimes less then a minute. Figure 4-6 shows instability of the bilayer at 40 mV with current fluctuations between 5 pA and zero.

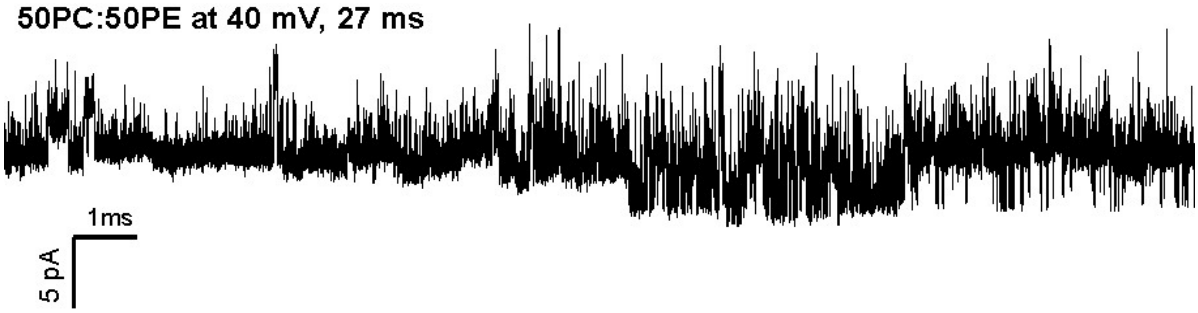

Figure 4-6. Electroporation occurring with a 50PC/50PE bilayer within the 1st 25 sec.

Admittedly, the instability with this lipid ratio is very unclear. We do however; believe both the high hydration state of PC and possible raft formation within this system could contribute to the instability of the 50/50 lipid composition. This theory will be examined in detail during the discussion.

70PC/30PE and 30PC/70PE Planar Bilayers

Results from both 70PC/30PE and 30PC/70PE showed many similarities. Gigaseals between 2-10 GΩ formed 75% of the time for both ratios (n=19). Threshold potentials for electroporation were above 120 mV for both of the mixtures. When electroporation occurred the activity took on the characteristics of the majority lipid present in the mixture. For instance, e-pores formed in 70/30 PC/PE were random with current changes ranging from 0 pA-5 pA, and they possessed a drifting baseline. E-pores formed with the 30PC/70PE lipid composition remained uniformed and the current decreased with decreasing applied potentials giving the pores very stable unitary conductance. Bilayer lifetimes were also long for both of the lipid mixtures, lasting on the order of several minutes to an hour.

The lipid mixture 70PC/30PE was a bit more stable and suitable for our studies in comparison to the lipid composition 30PC/70PE. If the stock solution of 30PE/70PC was left at room temperature, a white film would precipitate out of this solution and electroporation occurring with this mixture was very characteristic of single channel activity. Therefore we investigated the 70PC/30PE lipid mixture further. We exposed this lipid system to ramp voltages and the "episodic" protocol. Ramp voltages as shown in Figure 4-7; automatically applied potentials from zero to 200 mV, then from 200 mV to -200 mV within 3 seconds, and we studied Gramicidin in this lipid composition.

Results from these experiments indicated that 70PC/30PE lipid bilayers could survive rapid potential changes applied to the system. Similar to the ramp voltages, the episodic protocol

was used to determine the conductance of the bilayer. During these experiments, automated potentials from negative 200mV to positive 200 mV were applied to the system for several seconds as shown in Figure 4-8.

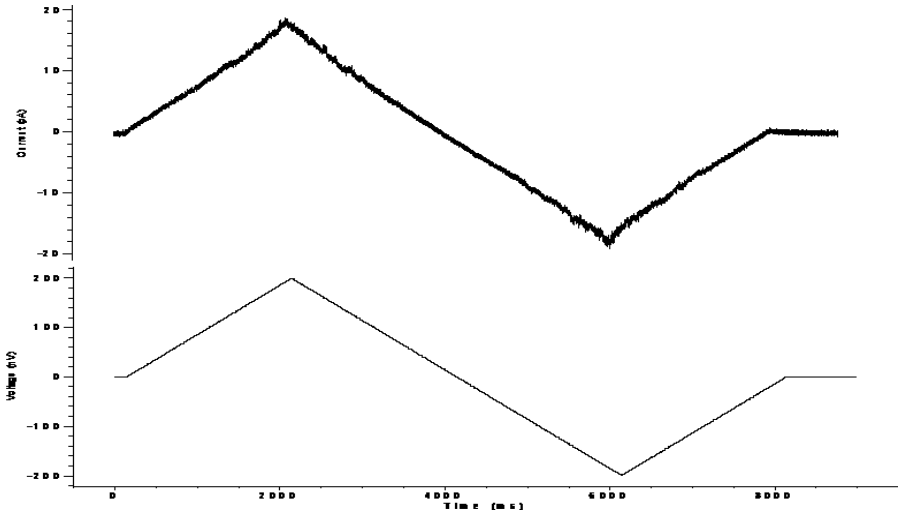

Figure 4-7. Ramp voltages applied to the 70PC/30PE lipid mixture. Potentials from zero to 200 mV, then from 200 mV to -200 mV were applied the lipid system within 3 seconds.

The bilayer followed Ohms law and the current did increase when increased potentials were applied; and decreased when lower potentials were applied. Both of the ramp and episodic protocol apply various voltages within seconds.

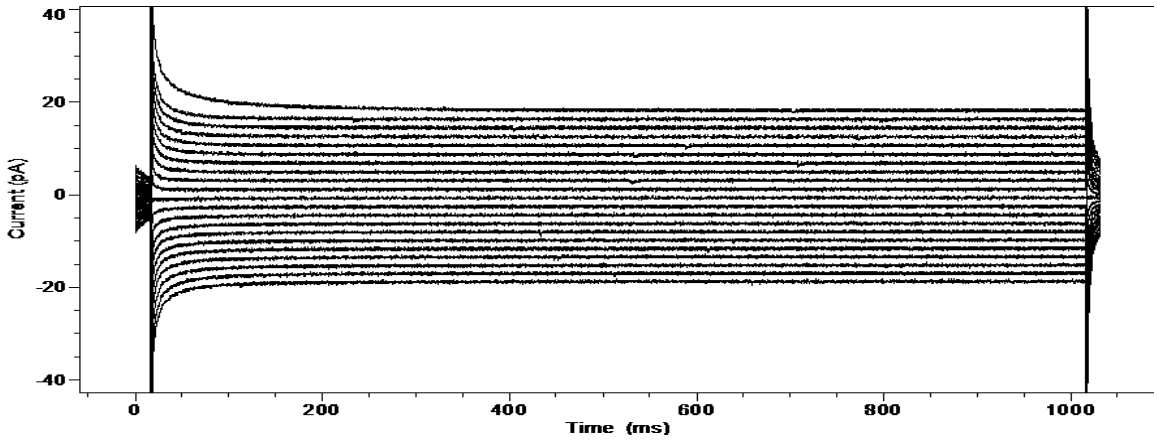

Figure 4-8. Episodic trace of the current in pA obtained lipid bilayer composed of 70PC/30PE when 0 to both +200 mV and -200 mV were applied simultaneously.

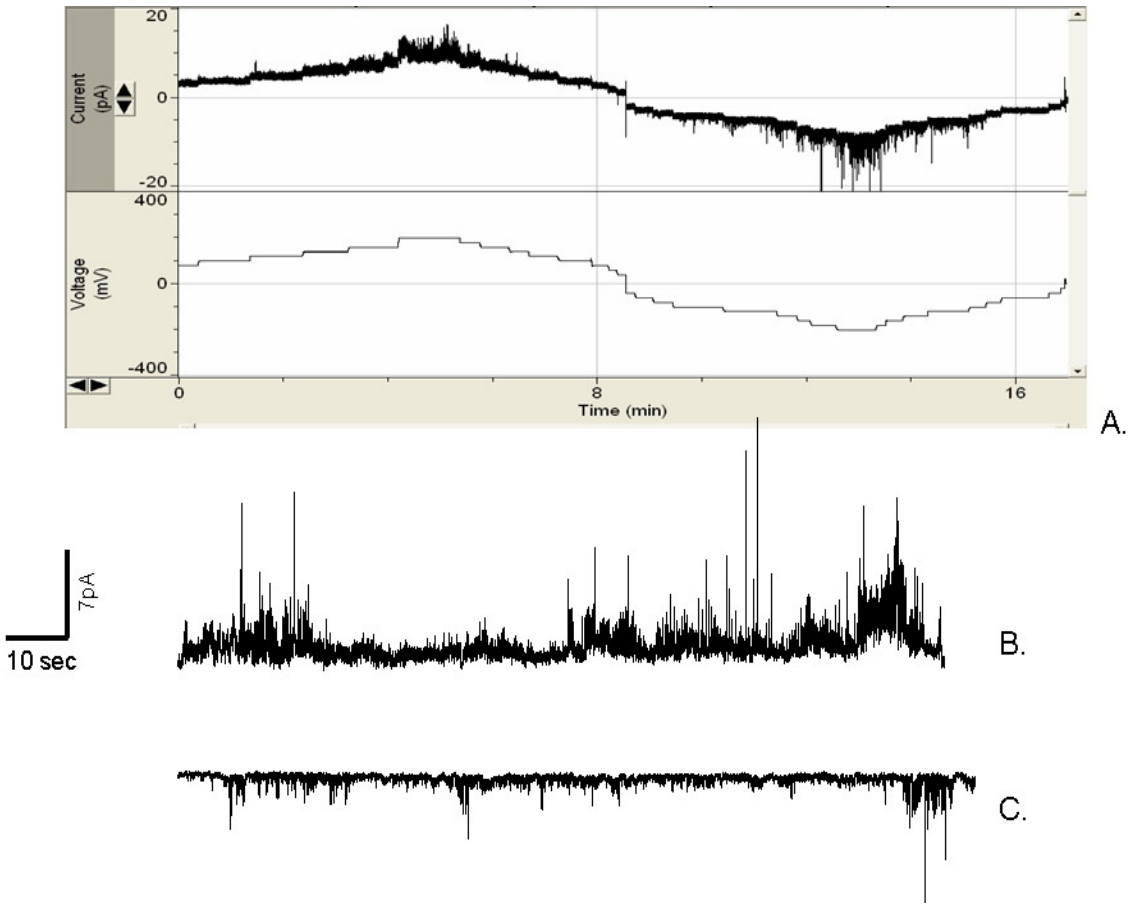

Figure 4-9. An 18 minute trace of 70PC/30PE lipid mixture. A) Raw-data of the current to voltage relationship over time when 50-200 mV was applied for 10 minutes followed by -10 mV to -200 mV and back to zero. B) A trace of the sample obtained at 200 mV C) A portion of the sample at -20 mV.

Using the gap-free protocol enabled the study of the stability of the bilayer over long periods of time. Bilayers with this lipid composition were long-lived with electroporation occurring after minutes of the bilayer existing without any change in currents. As shown in Figure 4-9, this lipid ratio did however experience some reversible bilayer breakdown within a 16 minute trace.

Single Channel Results of Gramicidin in 70PC/30PE bilayer

Incorporating Gramicidin A as a model channel in the 70PC/30PE lipid composition resulted in single channel activity comparable to literature. As shown in Figure 4-10 the single

channel conductance of Gramicidin is 67 pS which is in agreement with literature values of 60-70 pS (n=19) (*19, 123*).

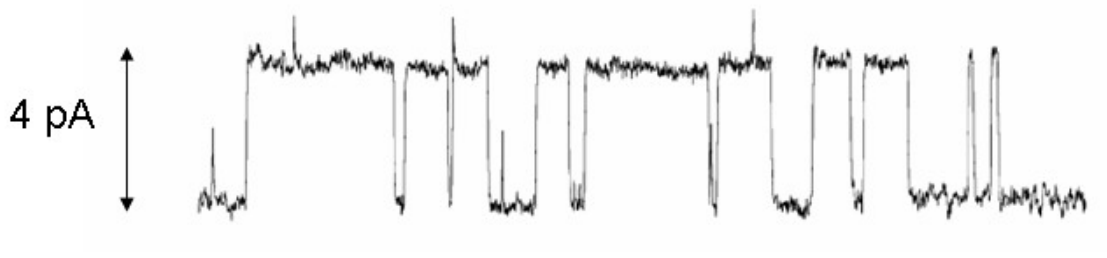

Figure 4-10: Single channel conductance of Gramicidin A is around 67 pS when 60 mV is applied.

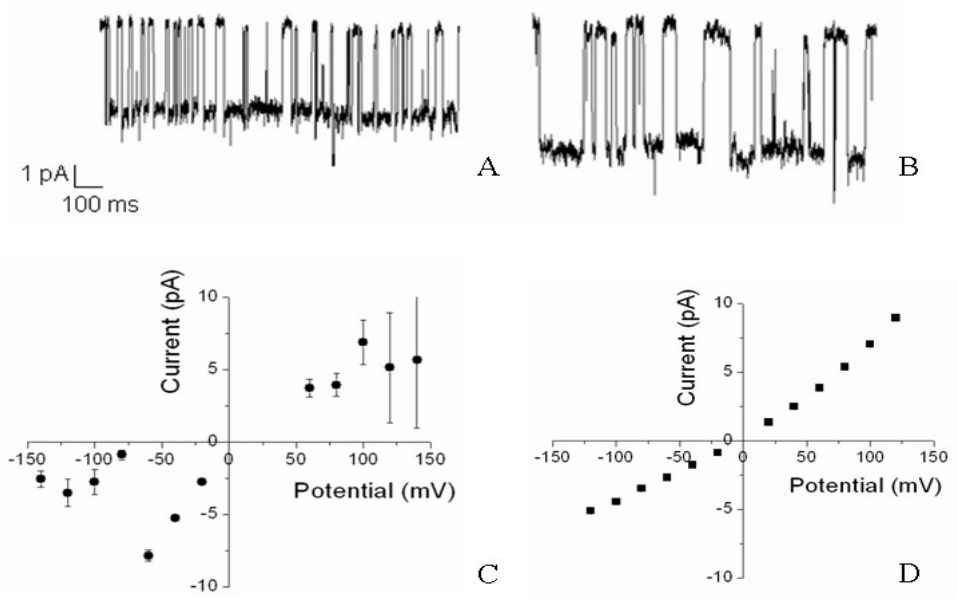

Figure 4-11. Plots of a 1.5 second run at negative 100 mV with and without Gramicidin. A) 70PC/30PE pure lipids B) 70PC/30PE with Gramicidin. Plots of the change in current between the opened and closed states (I), against applied potential (V). All points on the IV curve were the average of n ≥ 3 different experiments. Standard error bars were plotted; if bars are not readily visible, then the SE was approximately the height of the dot. C) 7PC/30PE lipid mixture. D) 70PC/30PE with Gramicidin A.

The single channel kinetics was slow with channel activity occurring for at least one minute continuously. Open dwell times ranged from 1 μs- 10 ms. I-V curves as shown in Figure 4-11 did allow us to distinguish between electroporation and single channel activity of

Gramicidin. The linear fit and the low error bars proved that current fluctuations were linked to Gramicidin opening and closing.

We also examined the best buffer concentration for Gramicidin in the 70/30 lipid ratio. Gramicidin is known to be selective to small monovalent cations like potassium. Determining an ideal potassium chloride concentration will allow for enough ions to create a measurable current, yet avoid dehydration of the device. We studied 3 different KCl concentrations: 125 mM, 250 mM, and 350 mM.

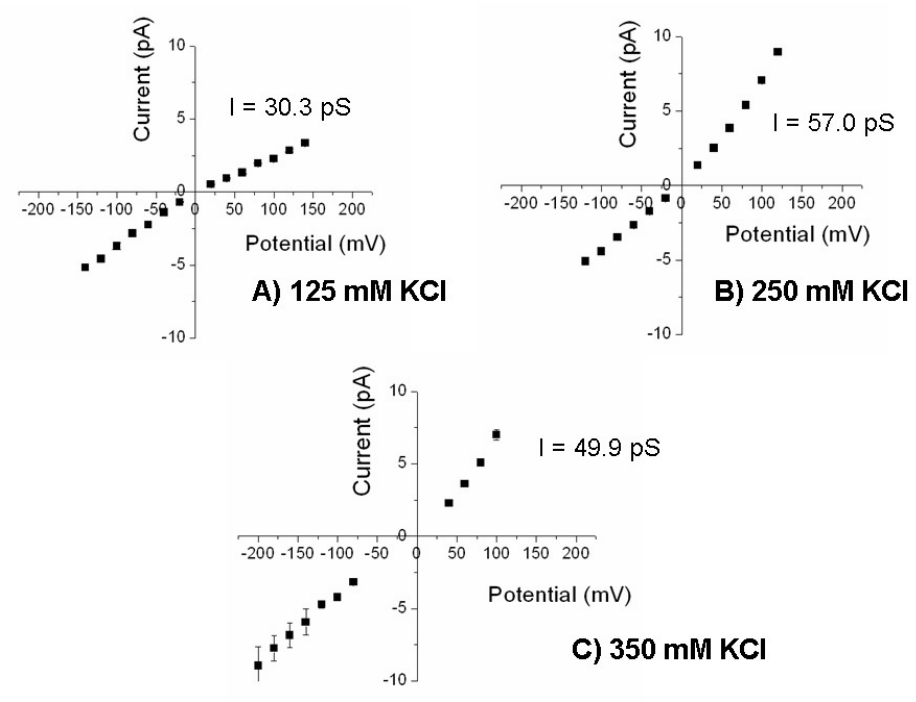

Figure 4-12. Plots IV curves for Gramicidin A for various KCl concentrations. All points on the IV curve were the average of n ≥ 3 different experiments. Standard error bars were plotted; if bars are not readily visible, then the SE was approximately the height of the dot. A.) IV curve displaying a conductance of 30 pS when 125 mM KCl is present in the buffer. B.) IV curve displaying a conductance of 57.0 pS with 250 mM of KCl. C.) IV curve displaying a conductance of 49.9 pS when 350 mM of KCl is present in the buffer solution.

The concentration of Morpholinopropanesulfonic acid (MOPs), $CaCl_2$, at pH of 7.4 was kept constant. Results showed that 125 mM gave rise to a low conductance. There was little

difference between results from both 250 mM and 350 mM, therefore we decided to use 250 mM KCl as shown in Figure 4-12.

Discussion

When considering the above results, it is important to understand the current theories surrounding the development of electroporation. First, one must understand how the hydration state affects the stability of the bilayer and the behavior of water molecules under an applied electric field. Second, the technique and the lipid composition when analyzing the results must also be considered. In addition one must also consider the system at hand. This is the first time diphytanoyl lipids have been studied using the tip-dip method therefore electroporation could possibly be a characteristic of this combined system.

The Effect of Hydration State on the Stability of Bilayers and Electroporation

The stability of the bilayer is greatly affected by the hydration state of the membrane. In 2004, Dr. Peter Tieleman used molecular modeling to investigate the process in which electroporation occurs and how its dependence on the hydration state of the bilayer membrane (*125*). He found that water molecules surround three parts of the lipid bilayer: the carbonyl chains, the phosphate back bone, and the lipid headgroup. The amount of water molecules surrounding each region is separated into three different water layers adding to the fluidity of the bilayer. Each water layer is depended on the charge and hydrophobicity of each region of the bilayer. The first water layer has the least amount of water molecules and is localized around the carbonyls from the fatty acid chains in the hydrophobic part of the membrane (*125-127*). Depending on the conformation or structure of the bilayer (cis or trans) roughly five to six water molecules exist in this first layer adding to the hydration of the bilayer. The second water layer exists around the phosphate backbone of the lipid at the water/lipid interface (*127*). The amount

of water molecules in this region changes, depending on the properties of the headgroup which forms the third water layer of the bilayer (*127*).

The size, polarity, charge, and hydrophobicity of the headgroup determine the existence of the 3rd water layer and controls the exposure of the phosphate groups to the bulk water phase surrounding the bilayer (*127, 128*). For example, the choline group of Phosphatidylcholine PC headgroup is extremely hydrophobic due to the three methylene groups bonded to the nitrogen (*127, 129*). The PC headgroup is therefore pulled inwards towards the membrane. This exposes the phosphate group and its charges to the aqueous phase allowing 18-20 water molecules to bind per lipid (*127*). The hydrophilic amine group present on Phosphatidylethanolamine (PE) forms a compact layer above the carbonyl hindering mobility of the phosphate backbone and its exposure to water (*127*). They link via H-bonding to adjacent phosphates producing a compact, rigid head group network at the bilayer surface with roughly 4-6 water molecules bonded per lipid (*127, 130*).

The water molecules along with the natural dielectric potential of the bilayer creates an overall bilayer dipole potential that becomes polarized when an external potential is applied (*127, 131*). The two parts contributing to the bilayer dipole potential are the surface potential and the membrane potential. When an external electric field is applied to the bilayer in a time dependent manner charged groups and dipoles re-orientate (*127*). Using molecular dynamic simulations to atomically map this process Tieleman *et. al.* found that pore formation during electroporation is driven by local electric field gradients at the water/lipid interface when an external potential is applied (*125*).

Water molecules move into the field gradient increasing the probability of water defects penetrating into the bilayer (*125, 128*). These defects are the molecular basis of electroporation

which occurs in the pico-nanosecond time range. Water molecules once inside the bilayer, H-bond with water molecules already present forming what is now termed "water fingers" that span the bilayer forming "water pipes" (*125, 126, 128*). At this point a deformation of the headgroup occurs whereby it curves into the bilayer to accommodate the water fingers. Both the lipid chains and the headgroups are now exposed to water. Water pipes become fully hydrophilic pores when the headgroups completely align the surface of the pores which results in a change in capacitance or conductance that is observed as a current peak (*125, 128*).

When applying these theories to the results obtained in this study, certain characteristics of the different lipid mixtures can be better understood. For instance, because of its high hydration states, bilayers where PC is the most abundant lipid present could theoretically be comprised of an unstable baseline and random pore formation. Gauger *et al.* compared hydration states of both PC and PE with diphytanoyl-tail, to palmitoyl chains groups using FTIR and Karl-Fischer water titration (*90*). Results suggested that DPhPC has the highest water uptake in comparison to other phosphocholine (DOPC, POPC, OPPC, DPPC). The ability of this lipid to retain water molecules could explain the instability and frequent occurrence of electroporation at low potentials. The study also found that the hydration state of DPhPE was higher in comparison to DOPE, and POPE (*90*). Methyl groups within the diphytanoyl-tail add to the random disordering and water uptake during the lamellar bilayer phase (*90*). This could lead to an increase in water fingers when a high electric field is applied.

The uniformity and potential thresholds over 120 mV for bilayers where DPhPE is the most abundant lipid could be explained by considering the lower hydration state and the size and hydrophobicity of the headgroup. Because the amines present on the headgroup H-bond with neighboring phosphates forming a tight compact headgroup orientation, more energy i.e. higher

potential thresholds would be require to move more water in the bilayer. In addition, the dipole alignment by H-bonding of the water molecules in the bilayer is going to be stronger because of the higher energy and the hydrophobic environment of the inner bilayer.

Experiments from lipid composition 50/50 PC/PE faced both a high hydration state, and possible raft formation or phase domains. This formation occurs when different lipids do not fully integrate; instead, they form isolated islands leading to the instability of the bilayer under an applied electric field. They are ideally tightly packed and separated. In biological membranes these domains usually consist of high concentrations of sphingolipids and cholesterol. Computational simulations including Monte' Carlo and Coarse-grained Marink-models have been employed in modeling these lipid raft or coexisting phases formed by mixed bilayers. Wong *et al.* used the coarse-gained Marrink-model to study the mixtures of dipalmitoyl phosphatidylcholine and ethanolamine DPPC and DPPE and found that DPPE lipids tend to move to the center of the bilayer (*132*). They also found that areas enriched with DPPC bilayers were slightly thicker but could not fully explain this phenomenon (*132*). This theory has not fully been proven and is currently under debate. It is however, a possible explanation for the unstable bilayers that were formed with 50DPhPC/50DPhPE in this research. To date, we have no indication of lipid raft formation or phase separation occurring with the 70PC/30PE lipid mixture.

Tip-dip and Diphytanoyl Lipid System

The tip-dip method may not be the best technique for studying diphytanoyl lipid mixtures due to their large hydration states which may make them more quantifiable to electroporation due to the bilayer forming horizontality at the tip of the pipette. In other planar bilayer methods the bilayer is either painted on a small hole separating two buffers filled compartments or formed on a moveable aperture at the air/water interface. Diphytanoyl lipids have been studied using the

painting method where the electroporation threshold potentials were around 250 mV(*6*). The tip-dip method which is both inexpensive, and user friendly may have lower electroporation thresholds. The details of this phenomenon are not fully understood. However to test the effect of adding a membrane protein, which has been proven to increase the stability of bilayers, Gramicidin A was incorporated into the lipid bilayer.

70/30 DPhPC/DPhPE was chosen as the lipid environment because it is one of the most common lipid ratios used in literature, and stable bilayers were formed with high threshold potentials. The electroporation events were not uniform and they did not follow Ohm's law which makes them easy to distinguish from single ion channel activity. In addition, since we will be using vesicle fusion to create a bilayer on the device, 70PE/30PC would not form stable vesicles due to the high negative spontaneous curvature of the PE group. Spontaneous curvature (SC) relates the cross-sectional areas of the headgroup to the acryl chain moiety. Negative SC can occur if the lipid has long fatty acid chains and a small headgroup. PE is smaller than PC; therefore it has a higher negative SC value which might have caused it to precipitate out of solution at room temperature. Lastly, 70PC/30PE was chosen because a small amount of PE does increase the stability of the PC bilayer.

Conclusion

In an attempt to establish the ideal diphytanoyl lipid environment for studying single ion channels in a tethered device, different lipid ratios were compared using the tip-dip method. Diphytanoyl lipids are a vital component of this research due to their increased durability and stability when tethering to solid supports such as the gold surface on the device. In this novel combined system of incorporating diphytanoyl lipids of PC and PE with the tip-dip method, electroporation was unfortunately observed and characterized. Results indicated all of the lipid-ratios suffered from e-pore formation due to electrical breakdown. This was the first time that

electroporation was reported at such low potentials as 125 mV and 40 mV which may be characteristic of using the tip-dip method with diphtanoyl lipids. The phenomenal pore formation was random; however we were able to distinguish it from single ion channel conductance by plotting I-V curves.

The lipid ratio of 70PC/30PE was chosen as the most stable lipid ratio and will be used as the synthetic lipid environment to study both Gramicidin and MscL on the device. Even-though the threshold potentials were around 125 mV, studying Gramicidin in this lipid ratio provided positive results with the conductance and dwell times of the channel being comparable to results from literature. This suggests that diphytanoyl lipids in a ratio of 70PC/30PE can form stable bilayers suitable for single channel measurements.

CHAPTER 5
FUNCTIONAL STUDIES OF GRAMICIDIN AND MSCL WITHIN A TETHERED LIPID BILAYER MEMBRANE

Introduction

Mechanosensitive (MS) ion channels sense tension in the cell membrane causing a change in structural conformation that opens the channel's pore. They are proposed to be of essential importance in physiological processes such as touch, hearing, balance and osmoregulation (*21, 38, 133, 134*). *Escherichia coil's* mechanosensitive channel of large conductance (MscL) is one of the most studied MS proteins. It has a conductance of ~3 nS with several known intermediate states, and appears to play a crucial role in protecting bacterial cells from osmotic downshock (*135*). MscL is a homopentamer with two subunits that span the membrane twice connected by a perplasmic loop and the N- and C-termini reside in the cytoplasm. The first transmembrane domain forms the constriction point of the closed channel; the second transmembrane domain interacts with the lipid matrix. MscL was first purified and cloned by Kung *et al*. who were also able to retain its functionality *in vitro* (*115, 136*).

E. coli's MscL robust properties make it an attractive candidate for nanosensory applications. This protein has been isolated, purified, and reconstituted into several different liposomes, and remained functional (*4, 10, 53, 111, 137-141*). *In vitro* studies were done on mutants of this protein to study its conductance, lipid-protein interactions, structure, and single channel functionality (*46, 51, 53, 130, 139, 142, 143*). A number of mutants for *E. coli's* MscL were generated that add sensory adaptations for pH, heavy metals, light, and redox reactions. For instance, Kloda *et al.* studied the pH sensitivity of a cluster of residues located within the cytoplasmic region of MscL (*4*). They found that the RKKEE cluster of charged residues inherently affected the tension required to gate MscL. If substitutions where made with the opposite charged residue, this proton sensor would have an altered sensitivity to membrane

tension (*4*). Iscla *et al.* designed metal binding sites using histidine substitution to the pore lining of MscL, changing the channel's sensitivity in the presence of heavy metals (*110*). Yoshimura *et al.* created a cysteine substitution with residue G22 and generated a channel with a greatly enhanced sensitivity to membrane stretching by adding charged sulfhydryl reagents within the channel's pore (*3*). Iscla *et al.* recently utilized cysteine trapping of single-cysteine mutations within the N-terminal region; these mutations created a redox-dependent alteration of gating of MscL. Light-sensitive mutants of MscL were achieved with photo-sensitive chemicals tethered to the pore of the protein; Kocer *et al.* attached synthetic compounds that underwent light-induced charge separation to reversibly open and close MscL's pore (*111*). Incorporating any of the above mutants within the tethered lipid environment would have potential as a nanoscaled electrical sensor. As a first step, the single channel characterization of the wild type (WT) MscL must be demonstrated and characterized within the tethered bilayer system before incorporating any of the "sensory-designer channels".

Here we present results from a technique that utilized tethered bilayer lipid membranes (tBLM) to measure single channel activity of the MscL. The tBLM is part of an engineered microelectronic array chip, illustrated in Figure 5-1, which can ultimately serve as a stabilizing environment for nanosensor-ion channels. The tethers work as stable anchors and serve as spacers to the underlying gold surface which forms an ionic reservoir and allows an ionic flow through the channel. The presence of the tethers increases the viscosity which results in lowered ion mobility in the reservoir when compared to the bulk solution.

Incorporating MscL into the tBLM offers many advantages over traditional proteoliposome formation for *in vitro* functional analysis. tBLM provide mechanical mobility, functional stability, and a non-denaturing environment for membrane protein (*57*). These bio-

mimetic supports enable the functional characterization of single ion channel activity on a solid substrate. It also enables protein-protein and lipid-protein interactions by providing a membrane environment with minimal irreversible bilayer breakdown. Both analytical and physical techniques that require a solid support, such as surface plasmon resonance and Atomic Force Microscopy (AFM), can now be employed for characterization with the tBLM.

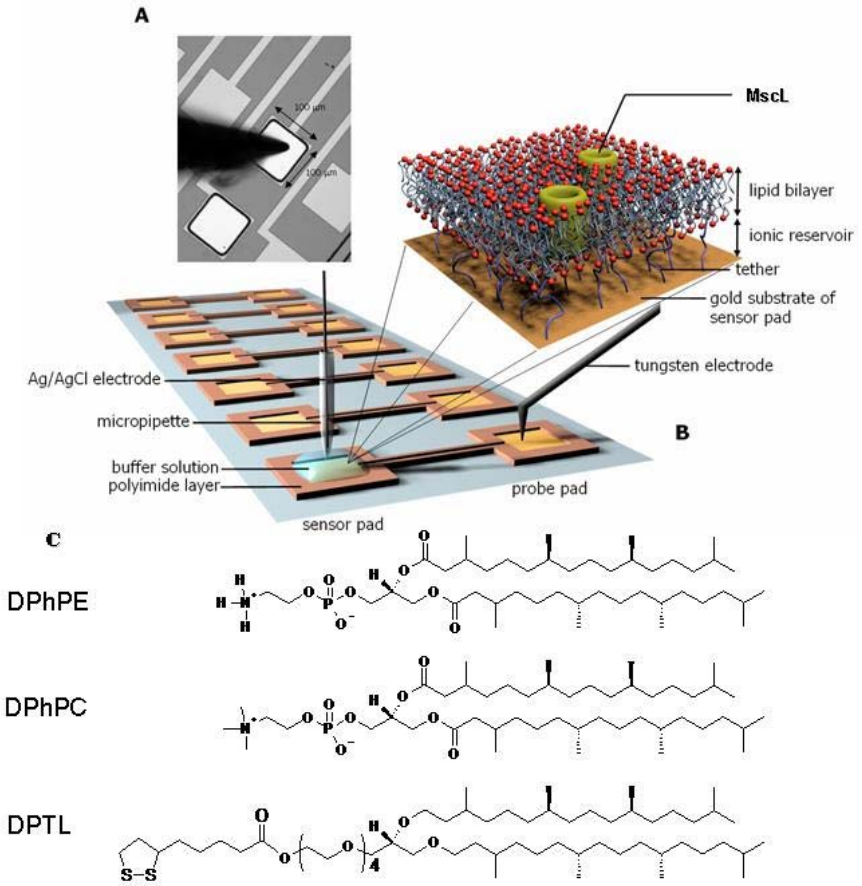

Figure 5-1. Tethered bilayer membrane array. A) Optical microscope image of the probe pad and the tungsten electrode. B) Graphical representation of the engineered tethered bilayer membrane array. The lower left corner shows the gold sensor pad covered by a tethered bilayer lipid membrane (tBLM) incorporating MscL ion channels. C) The molecular structures of the species used in the tBLM. Image designed by Dr. Henk Keizer and borrowed with permission.

This approach is new and promises an exciting base of fundamental knowledge that can be associated with single ion channel studies. Most importantly, this technique does not require the

tedious patching of blisters for *in vitro* analysis that is associated with patching reconstructed mechanosensitive channels in proteoliposomes (*31, 38*).

Before reconstituting MscL into this system, we studied the single channel activity of Gramicidin as a model channel within the tBLM. Gramicidin forms a transmembrane pore when the two 26Å long segments connect at their N-termini. Six H-bonds at the dimer junction stabilizes the pore in this conformation. This channel has a simple structure and has been well characterized in its natural environment, planar lipid bilayers, liposomes, tethered-bilayers and polymer cushion-lipid bilayers (*17, 58, 76, 122*).

To characterize an ion channel in this new system, specific single channel parameters were examined including the conductance, the stability of the bilayer on the microchip, and in the case of MscL, a method of providing enough tension to the system to cause the channel to open.

Materials and methods

Materials

The materials and methods are explained in-detail in Chapter 2, and are briefly discussed as follows: a 7:3 molar ratio of the archaea phospholipids, 1,2-diphytanoyl-sn-glycero-3-phosphocholine (DPhPC) and 1,2- diphytanoyl-sn-glycero-3-phosphoethanolamine (DPhPE), were used to form the bilayer; 2,3-di-O-phytanoyl-sn-glucero-1-tetraethylene glycerol-D, and L-α-lipoic acid ester lipid (DPTL) were used as tethers (synthesized according to a literature procedure (*81*)). Morpholinopropanesulfonic acid (MOPS), Potassium chloride, calcium chloride, and potassium hydroxide used to make the buffer solutions.

Proteins

Gramicidin A was commercially produced. This protein did not require an isolation or purification; it was stored in methanol at -20°C.

MscL containing a C- terminal 6His-tag was expressed in the mscL-null strain PB104 using the pB10b expression vector. First, cells were grown to an OD of about 0.6 and induced with 1mM IPTG for 30 min at 37°C. Membrane fractions were separated and resuspended in extraction buffer (50 mM Na_2HPO_4/Nah2PO_4, pH 8.0, 300 mM NaCl, 20 mM imidazole plus 2% (v/v) Triton X-100) (*96*). Then the suspension was incubated with 500 ul of Ni-NTA agrose (Qiagen) for 30 min at room temperature. The matrix was loaded on a 10 cm column and washed with 10 ml extraction buffer with 50 mM imidazole and 1% Triton X-100. The protein was eluted in 1.5 ml extraction buffer with 200 mM imidazole and 0.2% Triton X-100. Lastly, the protein was analyzed by SDS-Page gel for purity.

Device

The gold device was fabricated in the Microelectronics Research Center at the University of Texas, Austin, in Dr. Ananth Dodabalapur's laboratory by Dr. Daniel Fine. The microelectrode arrays used contained 66 pixels per wafer. Each sensor pad formed by evaporation of 3 nm of Ti followed by 500 nm of a 60% Au / 40% Pd alloy on the silicon substrate. A 200 nm gold layer was deposited on top of the alloy; a polyimide resist was photolithographically applied to define the pad size and electrically isolate the pads from each other. The device was cleaned with a rinse of hexane, acetone, ethanol, and water, and then treated with UV/ozone for 10 minutes.

Preparation of the Tethered Bilayer

First, the device was submersed into a 0.3 mg/ml DPTL-ethanol solution and left overnight. The wafer was rinsed with ethanol and water. The lipid composition of 70PC/30PE (2 mg/ml) was mixed and the chloroform solvent was evaporated under vacuum and the lipids were hydrated in 1 ml of MOPs buffer (5.0 mM MOPS, 250.0 mM KCl and 0.1 mM $CaCl_2$, titrated to pH=7.4 using KOH). The lipids were heated at 50 ^{o}C until we obtained a clear solution

(ca 1 hour). After cooling to room temperature, the suspension was sonicated for 5 minutes, followed by filtration through a 0.45 μm filter. The vesicle size was determined with a Dynamic Light scattering (DLS) detector from Brookhaven Instruments. Vesicle diameters of 150-500 nm were typically found. Finally, a drop of the vesicle solution was deposited on the gold DPTL treated sensor pad and left for >8 hours at 4°C, or at room temperature for 2 hours. This initiated vesicle fusion, i.e. formed the tethered bilayer. Prior to the electrophysiology examinations, a drop (5 μl) of MOPs buffer solution was applied to the treated sensor pads.

Protein Reconstitution

Since Gramicidin (0.2 mg/ml) was made synthetically the protein was directly mixed with the lipids to create proteioliposomes. The lipid solution (2 mg/ml in chloroform) containing the 70PC/30PE lipid ratio was mixed with Gramicidin (0.2 mg/ml in methanol) to obtain a final lipid-to-protein ratio of 1000:1. The vesicle preparation and tethered bilayer formation is explained above.

MscL was obtained after purification and the product was concentrated to 0.9 mg/ml and gel filtration was used to remove the excess imidazole. MscL was reconstituted into the tethered bilayer with a protocol similar to that of Gramicidin or by the development of proteoliposomes in which detergent was extracted with biobeads. The details of this procedure are explained in Chapter 2; briefly, after the lipid vesicle are formed via sonication, 1% Triton X was added to loosen the bilayer. Purified MscL was slowly added in a 1:120 protein to lipid ratio. The protein-lipid-detergent matrix was then heated in the water bath at 60°C for 30 minutes. While the sample was heating, Biobeads (Bio-Rad) were washed 3X with the MOPs buffer used to create the vesicles. The proteoliposome solution was added to the bio-beads and incubated with light rotation for either 4 hours at room temperature or overnight at 4°C. The proteoliposome solution was lastly removed from the bio-beads and stored at 4°C.

Electrophysiology

Recordings of single channel activity were obtained with two electrodes. The active electrode was a conventional patch pipette containing an Ag/AgCl electrode and filled with buffer solution. The reference electrode consisted of a gold coated tungsten electrode that was positioned onto the probe pad. Both electrodes were connected by the headstage to an Axon Patch-Clamp amplifier (Axopatch 200B. Molecular Devices Corporation, Union City CA). The signal was passed through a low-pass 5 kHz and digitized at a sampling rate of 20 kHz using a Digidata 1322A from Molecular Devices Corporation. Afterward, a giga-seal was obtained and 2 µl of the protein (Gramicidin 0.2 mg/ml or MscL 900 ug/ml) solution was added. Gramicidin channels formed sporadically as monomers within each portion of the bilayer dimerized.

In order to gate MscL, we had to create tension in the bilayer. As given by the Maxwell stress tensor, an electric field applied over a lipid bilayer induces a perpendicular stress in the membrane. This stress can be viewed as an increase in the membrane area and can cause changes in the curvature, i.e. flexoelectricity. This phenomenon has been demonstrated in both lipid bilayers (*144*) and cell membranes (*145*). Because we have no way of monitoring pressure on the device, a voltage was applied to induce tension in the membrane. According to Needham and Hochmuth, the membrane stress (σ), as a function of the transmembrane potential (V), may be expressed as: $\sigma = \varepsilon\varepsilon_0(d(2/d_e^2)V^2$ where ε is the dielectric constant of the surrounding medium (ca 60), ε_0 is the permittivity of free space constant, d is the bilayer thickness (~ 4 nm), and d_e is the dielectric thickness (~ 3) (*146*).

Proteioliposomes of MscL are known to sense tension around 12 dynes/cm (*10*). This tension corresponds with an electric field of 300 mV according to Needham and Hochmuth's equation. This threshold voltage was applied using a patch-clamp amplifier; and used to create enough stress in the membrane. The single channel signals were passed through a low-pass 1

kHz filter and digitized at a sampling rate of 50 kHz. Single channel analysis was conducted in the same manner as with traditional patch clamping techniques.

Results

In this present work, the functional characterization of Gramicidin and MscL were studied using a tethered bilayer system. This system is one of seven different methods recently adapted to study membrane proteins on solid supports. The first steps in developing the tBLM, were to establish a monolayer on the gold's surface, tether the bilayer via vesicle fusion, and test the resistance of the bilayer.

The stable thiolipid system, DPTL, served as the monolayer component which tethered the bilayer to the gold's surface. Previous experiments were performed in our laboratory utilizing Atomic Force Microscopy (AFM) to characterize monolayer formation and vesicle fusion. This technique uses a semiconductor tip attached to a cantilever that traces the surface of a material (*147*). The tip's deflection along the surface is measured by a laser and plotted as a function of tip position. These experiments were conducted in tapping mode with the semiconductor's tip tapping across the sample surface. Results from this investigation are shown in Figure 5-2. It was proposed that the monolayer deposition occurred within a 24 hour period wherein DPTL vesicles first rupture and then form islands (*147*). The islands eventually swell through solvent diffusion to form the final ~4.7 nm monolayer system (*147*).

Unilamellar vesicles of 70DPhPC/30DPhPE, with or without proteins, were added to the monolayer system. The small vesicle size enabled the bilayers to rupture rapidly as they fused with the DPTL monolayer in a six hour time span at room temperature (*147*). Dynamic light scattering, as explained in Chapter 2, provided insight on the size distribution of the vesicles. The sizes of the LUV ranged between 100-200 nm as shown in the appendix.

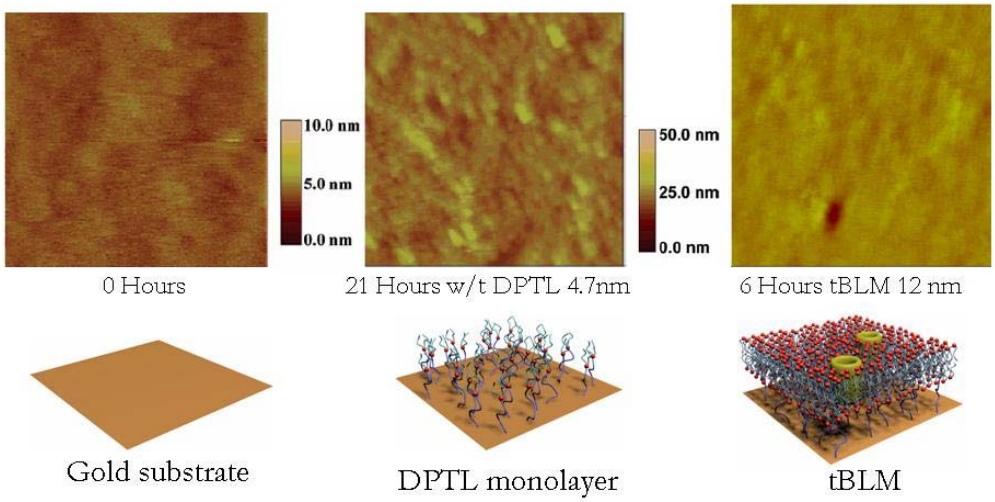

Figure 5-2. AFM images of the monolayer deposition and vesicle fusion process. The first image is of the gold substrate. The second image is of the gold substrate with the monolayer self assembled on the surface and spanning roughly 4.7 nm long. The third image has both the tBlM and the monolayer deposited on the gold's surface. Together the DPTL and the bilayer is roughly 12 nm high. DPTL. Images adopted from reference (*147*) with permission from Henk Kasier and Brain Dorvel.

After vesicles fused with the monolayer, we took precautions to avoid electroporation in the membrane since high voltages were applied. A stable giga-seal was always obtained before adding the protein; and no signals were detected before the addition of either one of the ion channels. The bilayer was considerably more stable when tethered to the gold surface in comparison to freely suspending it as in the tip-dip method. Out of 47 bilayers analyzed, 25 exhibited electroporation, while 22 of the bilayers were free of electroporation and were very stable over long periods of time when exposed to high voltages as shown in Figure 5-4. The electroporation threshold potential varied from 100-300 mV with the most electroporation observed at 300 mV. These findings are more comparable with the literature (threshold potentials 200-400 mV) than the membrane rupture threshold potentials (120-200 mV) concluded in Chapter 4 where the tip-dip method was utilized with this lipid mol compositions (*148, 149*). The electroporation is seemingly induced by the application of high potentials

applied to a weakly formed bilayer. The pores formed ranged from extremely small to large stable pores that inhibit the bilayers ability to maintain the giga-ohm resistance necessary to observe single channel conductance. The e-pores that did form displayed variable conductance and none of the traces displayed consistence electroporation. Most of the time when it did occur, irreversible breakdown of the bilayer followed. Small current transitions in the range of 0.1-5.0 pA conducting 30-70pS were observed with this system. On the other hand, we also observed bilayers that were extremely stable for over 10 minutes at 300 mV (data in the appendix) and several I-V curves were generated enabling the calculation of the resistance of the bilayers (data in appendix).

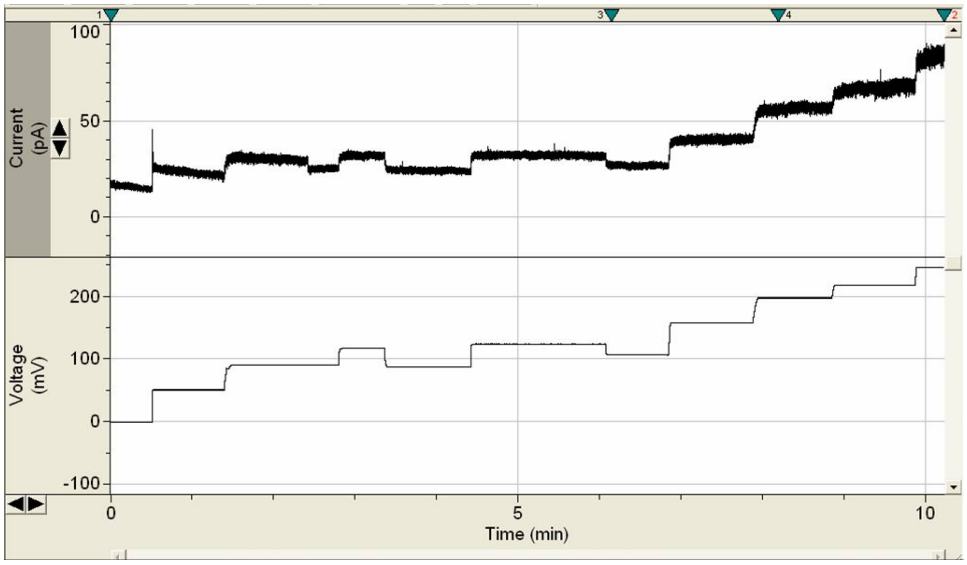

Figure 5-4. A stable tethered bilayer form from vesicle fusion of 70PC/30PE LUVs. The bilayer was stable for ten minutes while being exposed to voltages ranging from 50-250 mV with a resistance of 2.1 GΩ (calculated using Ohms Law)

Results of Gramicidin Reconstituted into the tBLM

The simple helical structure of Gramicidin allowed the protein to sustain high temperatures and dehydration overnight when reconstituting the protein into lipid vesicles of 70PC/30PE. The signals obtained from gramicidin were similar to those found in the literature as seen in Figure 5-5. They also correspond with the signals obtained from the tip-dip recordings (Ref. to Figure 5-

5). Experiments and results in Figure 5-5 were published in a collaborative effort with Chenyu Zhu and Dr. Martin Andersson (*77*). In Figure 5-6, an I-V curve was plotted of the current to voltage relationship for Gramicidin within the tip-dip system and the tBLM device. When negative potentials were applied to the tBLM on the device there were decreases and a small plateau of the current demonstrating rectification of the protein (see appendix). Rectification occurs when there is any form of limitation that allows ions to flow through the channel in one direction better than another. Known mechanisms include Mg block and blocking the pore with part of the protein, whether it be a "ball and chain" at one end of the protein or allosteric constraints in the pore. In this case, we hypothesize; it is due to the small ionic reservoir and the slowed mobility, due to high viscosity, of the ions in the reservoir of the tethered region relative to the large buffer reservoir above the bilayer.

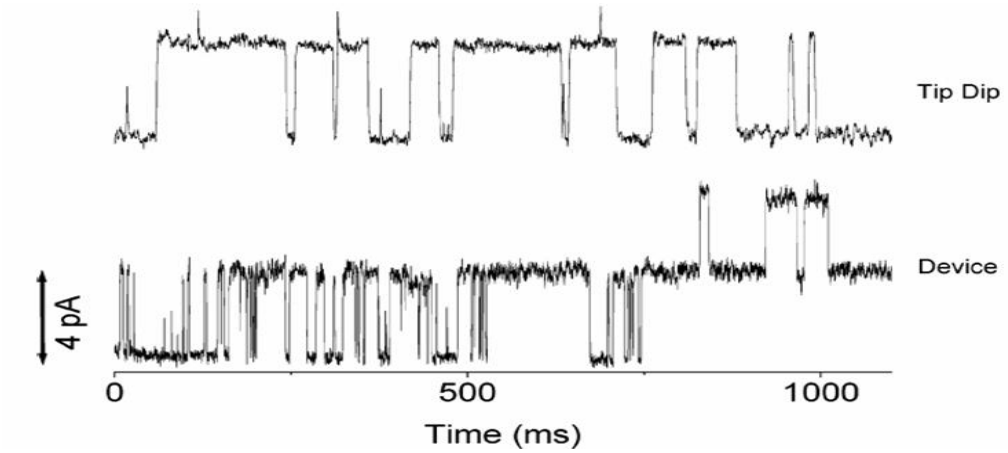

Figure 5-5. Single channel activity of Gramicidin at an applied voltage of 60 mV with a conductance of 60 pS. The upper trance was recorded using the tip-dip method, and the lower trace was obtained on the device. In both traces, one open channel corresponding to a current of roughly 4 pA was observed. Two channels were open within the tethered bilayer as indicated by the 2nd current change of roughly 4 pA.

When negative voltages are applied the positive K^+ ions try to rush from the limited ionic reservoir were the tethers and small size of this region alters the conductance observed in the system (see figure and discussion in appendix). Krishna *et al.* studied the interfacial capacitance

of the reservoir region using the Stern model of ionic distribution, and concluded that this region has properties similar to a dense hydrated gel with restricted ionic mobility (*76, 83*).

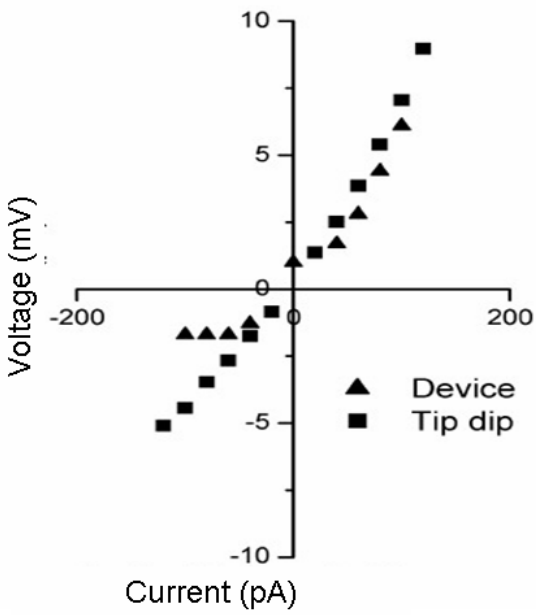

Figure 5-6. I-V curves of Gramicidin in the tBLM on the device and within the tip-dip system. Negative potentials were applied to the tBLM on the device and current responded in a small plateau. This we configured was due in part to the ionic reservoir and the slowed mobility of the ions in this region.(*77*).

Gramicidin is known to pass a maximum conductance of 90 pS due to the constricted small size of the pore (*18*). Larger current transitions were observed in some of the experiments (41% n=12) as shown in Figure 5-7. These current transitions ranged from 11 pA to 60 pA. The idea of multiple channels being open is not completely ruled out, nor is the less favorable explanation of electroporation occurring. If more than one channel is open simultaneously, the conductance and the current would ideally increase as shown in Figure 5-5 and Figure 5-7. The bilayer in Figure 5-6 maintained a giga-seal between 2.9-3.1 GΩ for 28 minutes while facing applied voltages ranging from 20 mV-300 mV. Single channel activity of Gramicidin was observed at 155 mV. We also observed single channel activity at voltages as high as 238 mV (data not shown). This activity was comparable to activity reported in literature where Gramicidin's

conductance range is between 20-90 pS and in previous experiments conducted on the device by veteran lab members (*17, 19, 20, 123*). We concluded that the 70PC/30PE bilayer was sufficient; and incorporated WT MscL to the tBLM system after 12 experiments of analyzing the activity and optimizing the conditions for proteoliposome fusion with Gramicidin.

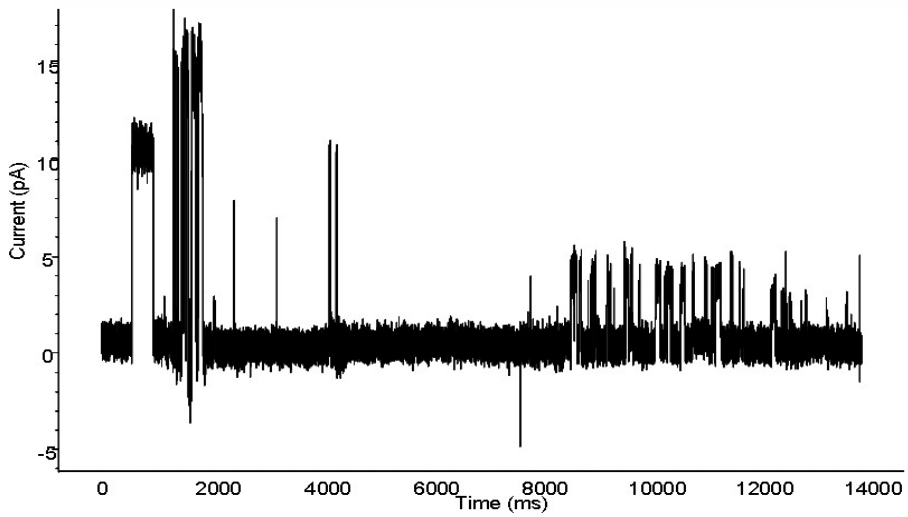

Figure 5-7. Single channel activity of multiple Gramicidin channels opened within the tethered lipid bilayer. Multiple channels open at 155 mV with current transition corresponding between 4-15 pA and the conductance was between 26-90 pS.

Single Channel Analysis of MscL

Single ion channels exhibit stochastic activity. Theoretically, the durations of events and the order in which they occur are random variables (*99, 100*). Parameters representative of single channel activity, and the information contained in each event, are measured from statistical distributions (*78, 100*). Three specific aims exist when analyzing single ion channel activity of MscL reconstituted in this new system: 1) determination of ionic selectivity or preference, 2) the duration of open and shut times for lifetime studies (*100*), and 3) amplitude studies to understand ion permeation (conductance) through open channels at different ionic compositions.

Ionic Selectivity

MscL is not selective to specific ions because of its large pore size, and natural response to elute cytoplasmic solutes before cell lyses. Therefore all ions present in the buffer solution within the tBLM permeated the channel.

Lifetime Studies

Lifetime distributions of MscL in the tethered system, determined from probability density functions, displayed fast kinetics with the channel open in the range of several ms. These are smaller, and comparable to those found in literature with spheroplast (*34, 64, 150*).

Conductance

Analysis of amplitude histograms assisted in the identification of fully open and sub-states during continuous traces. Sub-states are conducting states where the channel is neither fully open nor closed. All digitized current can be plotted as a histogram with a peak for each shut and open level.

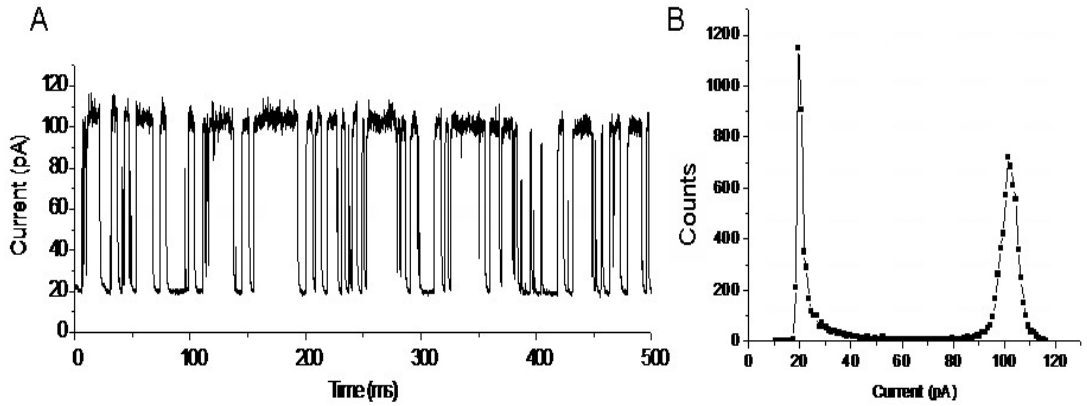

Figure 5-8. Single channel activity of WT MscL in the tLBM system: When 300 mV was applied to the membrane MscL opened conducting 266 pS. A) The channel is closed at 20 pA and the change in current to the open state is 80 pA B) The unitary conductance of ~300 pS is obtained by dividing the change in current by the voltage applied (*64*).

The area under the peak is proportional to the time spent at that level. Unitary conductance is calculated by dividing the mean amplitude calculated from the amplitude histograms by the applied potential.

In order to create tension in the bilayer and cause MscL to open, an electrical field induced membrane stress (σ) strong enough to trigger an opening of the MscL channel was applied. According to Needham and Hochmuth (*146*), the tension as a function of the transmembrane potential (V) can be expressed as: $\sigma = \varepsilon\varepsilon_0(d(2/d_e^2)V^2$ (*151*). This tension corresponds to a transmembrane potential of ~300 mV, which is in very good agreement with our findings. Figures 5-8 and5-9 display single ion channel activity of WT MscL within a 70 DPhPC/30 DPhPE tethered lipid bilayer matrix. The closed state of the channel is at 20 pA before normalization, while the open state is around 100 pA; this gives a unitary conductance of 266 pS when 300 mV is applied according to Ohms law. The conductance of WT MscL obtained from using spheroplast and *in vitro* using liposome is 3 nS. The lower conductance observed with the tBLM is not completely understood.

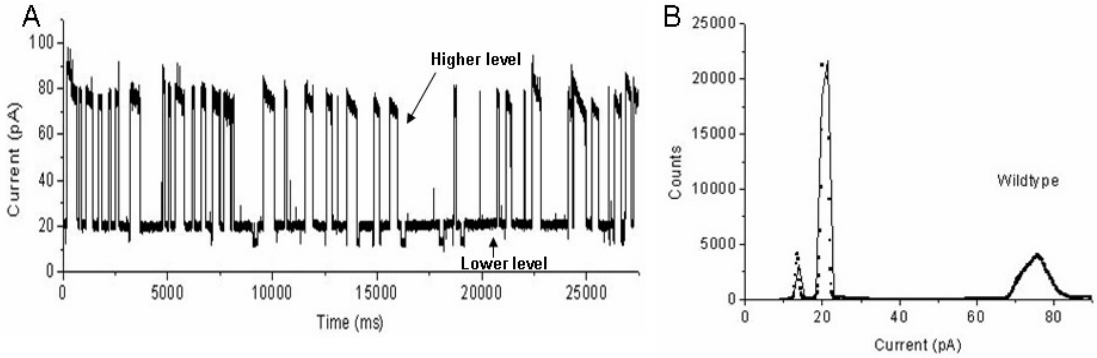

Figure 5-9: MscL displaying two conducting-states: A.) Single channel trace with the lowest sub-state conducting ~ 3 pS and the large sub-state conducting at 255 pS. B.) Point amplitude histogram displaying the multiple levels including a small substrate around 15 pA (*64*).

Possible explanations could include, but are not limited to, the diphytanoyl lipid environment, the lack of an external applied pressure, and the presence of the limited ionic

reservoir between the Au surface and the bilayer. In this reservoir the ion mobility is decreased because of the lack of free space that results from the tethers.

The high applied voltage of 300 mV required to gate WT MscL, was a challenge to obtain. Most of the bilayers would rupture and loss their giga-seal resistance before 300 mV was applied or the channel did not always respond at 300 mV. Therefore, channel activity was analyzed from a small sample pool. In order to obtain a greater sample size and decrease the voltage required to gate MscL, Dr. Blount suggested we incorporate a voltage sensitive mutant, K31E. This mutant inhibited the growth of *E. coli* by creating leaky MscL channels that responded to lower tension thresholds in the cellular membrane and to negative applied voltages (*28*). This was configured from both whole cell physiology and electrophysiology experiments which examined K31E's response to -20 to -100 mV being applied to sphereoplast; K31E showed a dramatic increase in the probability of opening at the higher voltages (*28*). Blount *et. al.* concluded that this observation was probably due to the charge reversal in this position (see Figure 5-10), which interfaces with the electric field of the membrane (*28*). Thus, we set out to determine if this mutant would be observed at lower voltages when inserted within the microchip device. The K31E mutant was molecularly engineered and reconstituted into the 70PC/30PE lipid mixture in order to create proteoliposomes. Vesicle fusion with K31E proteoliposomes was also researched instead of adding the protein to the tBLM once it formed. This was an attempt to increase the probability of protein reconstitution into the tBLM.

Results from K31E reconstituted into the tBLM are shown in Figure 5-10. Single channel activity was observed at lower potentials, as predicted. The channel became active when 85 mV were applied while conducting at 178.5 pS which is lower then that the conductance of MscL

within the tBLM. However, when 143 mV was applied, we observed conductance as high as 350 pS (refer to Figure 5-11).

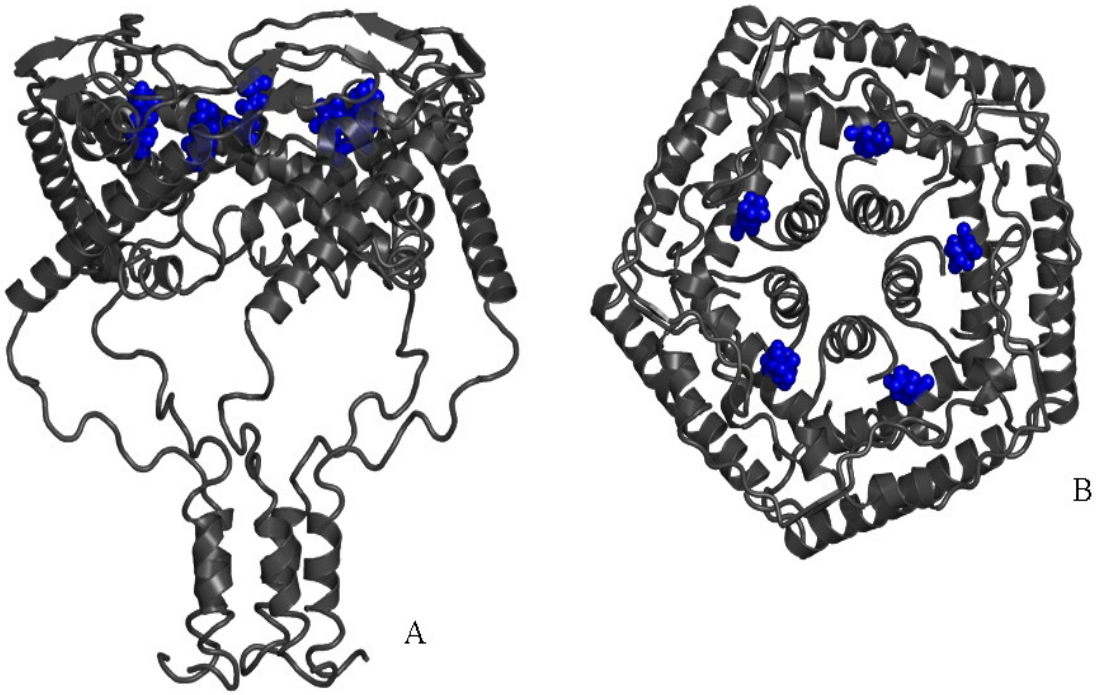

Figure 5-10. MscL with the lysine in the 31 position highlighted. In this study the positively charged lysine was mutated to glutamic acid which has a negative charge. This mutant is voltage sensitive. A) Side view. B) Top view

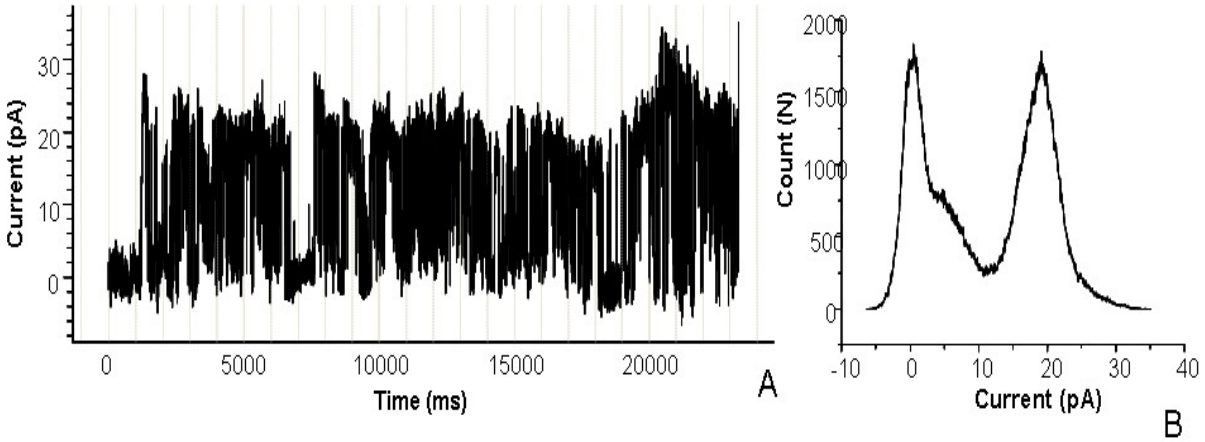

Figure 5-10. Single channel recordings of K31E (voltage sensitive mutant of MscL) within the tBLM. The upper trace displays burst open and closing events at 178.5 pS. The lower trace is a point amplitude or all-points histogram displaying the current levels observed in the above trace. The open current transitions were 20 pA.

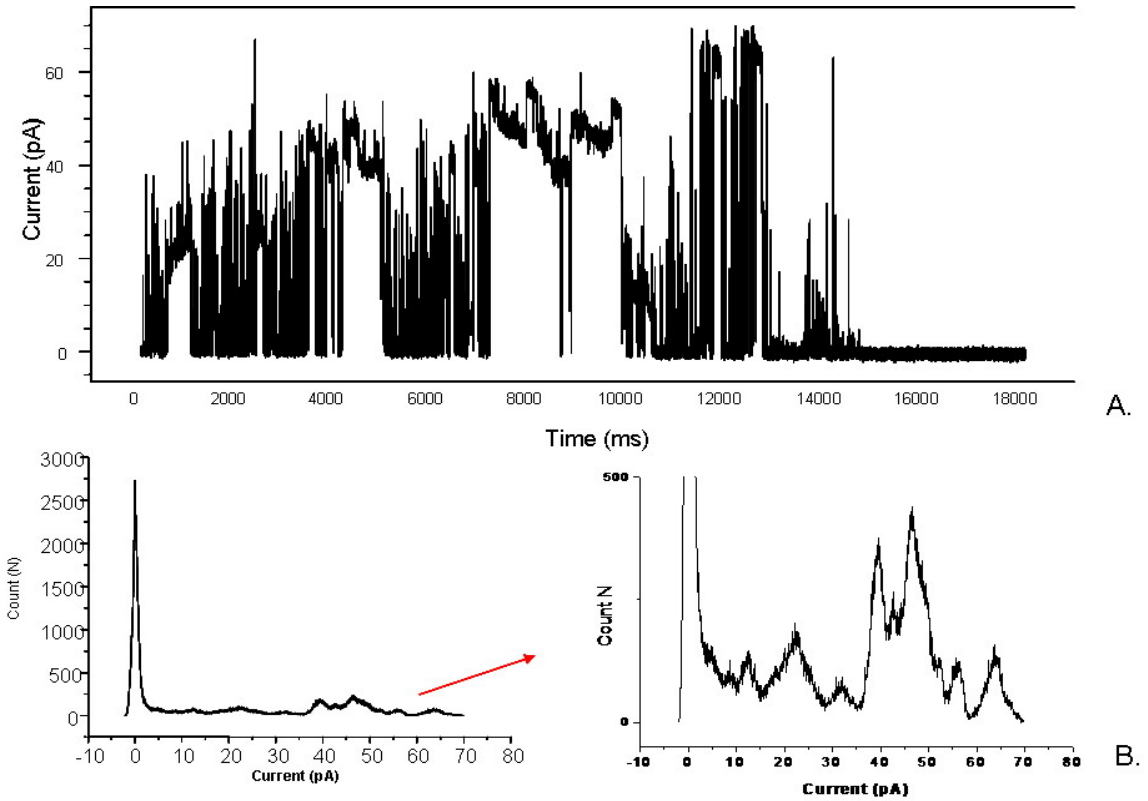

Figure 5-11. Single channel activity of K31E at 143 mV. A.) Displays burst opening and closing events at 143 mV giving way to current transition as large as 60 pA. B.) A point amplitude or all-points histogram displaying the current levels observed in the above trace. The open current transitions was 60 pA providing a conductance of 350 pS

We also observed conductance as low as 50 pS and well above 300 pS as shown in Figure 5-11. MscL is known to have multiple sub-conducting states (*152, 153*). Ghazi *et al.* performed patch-clamp studies on MscL in both proteoliposomes and shereoplast and found that the channel conductance ranged from 100-2,300 pS depending on the applied negative pressure (*153*). Sub-conductance states may be actually forming within the tBLM.

The single channel kinetics of the K31E mutant was fast and the number of events was low. This result was comparable to changes in single channel kinetics observed with this mutant in blisters and sphereoplast (*44*). Most activity transpired at the beginning of the experiments. Although still preliminary, results obtained from this mutant are extremely promising.

Discussion

The tethered lipid environment is a new concept for integrating ion channels onto solid supports. These ion channels, particularly *E. coli's* MscL, can be modified for nanosensory applications within solid supports. In this study, we characterized the single channel activity of Gramicidin, WT MscL, and a voltage sensitive mutant K31E-MscL within the tBLM. In order to create tension in the tBLM, a high voltage was required and then applied to the system. The resulting conductance of MscL was low in comparison to the conductance obtained from single channel studies within sphereoplast and protioliposomes (*10, 26, 36*). This result was characteristic of ion channels reconstituted within the tBLM. So far, our lab has reconstituted four different ion channels independently within the tBLM system and observed lower conductance for all of the channels except for Gramicidin (*64, 77, 112*). Gramicidin's simple structure and small pore(s) may have enabled it to maintain its small conductance between 50-90 pS within the device (*77*). We also were able to observe channel activity at different voltages from Gramicidin because channel gating was independent of the applied voltage.

The observed conductance was lower in tBLM for the other channels than in their natural environment or in liposomes as shown in Table 5-1. The three channels include MscL, Maxi-K, and the synthetic self-assembling protein M2δ (a synthetic ion channel based on the channel-lining domain of the nicotinic acetylcholine receptor (nACHR) from *Torpedo californica*). The Maxi-K channel, which was isolated from mouse brain and muscle, then expressed in *Xenopus laevis* oocytes, is both Ca^{2+} activated and voltage sensitive (*112*). The conductance is greater than 200 pS. Within the tBLM, the conductance obtained was 37±2 pS (*112*). The M2δ channel consists of three or more single peptides that come together in the bilayer and form a pore with a diameter that ranges from 5-15 nm (*14*). The unitary conductance of 15 pS was observed for M2δ within the tBLM (*112*). This conductance is three-times lower than the conductance of

templated-M2δ under normal patch-clamp conditions. Finally, as reported in this study, the conductance of MscL is also 10 times lower within the tBLM than in other environments. This lower apparent conductance (and the large conductance range for all channels) of multiple channels could be caused by the atypical phytanoyl phospholipids environment, the limited reservoir volume, constriction of the ion channel from the isoprenoyl-tail region of the tethers, an interfacial capacitance, or interactions at the gold surface (*112*). A likely trend existing with the results from the four channels studied in this device is the larger the conductance of the channel, the more attenuation of the conductance observed in the tBLM as shown in Table 5-1.

Table 5-1. Conductance comparison between the ion channels reconstituted in the tBLM and reported conductance.

Ion Channels	Reported Conductance (pS)	Conductance within the tBLM (pS)	References
Gramicidin	20-90	50-90	(*77, 122, 123*)
M2	15-45	13-15	(*14, 88, 154-156*)
Maxi-K	90-300	30-50	(*97, 156, 157*)
MscL	100-3000	50-300	(*10, 64, 153*)

While a limited reservoir seems a likely explanation for the attenuation of the conductance of the channels studied, additional artifacts associated with the individual protein could also lead to the lower conductance. For instance, since single transmembrane peptides of M2δ self-assemble within the bilayer into a trimer, tetramer, pentamer, or even a hexamer, the lipid environment within the tBLM might favor the formation of a trimer. The conductance of the trimer as examined by Montal *et al.*, using the painting method and results from our research investigating this channel using the tip-dip method, is 15-20 pS (*14, 86, 155, 158*). The lowered conductance of MscL may in part be due to one of its known sub-conducting states. According

to Sukharev *et al.*, MscL has 3 sub-conducting states: S2, S3 and S4, and a fully open state O5 (*153, 159*). The different conductance states range from 1.03 nS to 3.37 nS when the protein is reconstituted in Azolectin liposomes (*159*). Therefore, when MscL is reconstituted within the tBLM system, the channel may not fully open, which may contribute to the lowered conductance.

To completely understand the underlying dynamics of the tBLM system and its resulting single channel activity, a more sophisticated equivalent circuit model is required. This model will enable a more accurate account for the actual transmembrane potential within the tBLM system, and the possible control of the conductance range. In addition, it should enable the probing of channel fluctuations in a "voltage or current clamp" configuration within a micro-array system.

Another limitation we were able to address was the extreme high voltage requirement used to gate MscL within the tBLM. Many of the bilayers ruptured before withstanding voltages near 300 mV, which seemed to be required to create enough tension in the bilayer to open MscL. By incorporating the voltage sensitive K31E-MscL mutant, as expected we were able to observe single channel activity at much lower voltages. However, there were technical differences between the study of the wild type and K31E channels. First, in order to increase expression levels of the usually poorly-expressed K31E mutant, the C-terminal from residue 110-136 was truncated. While there are no indications in patch clamp that the truncated channel is more sensitive to voltage, one would like to perform the proper control. Thus, a C-terminal truncated MscL was also generated with the anticipation that its activity would be similar to WT MscL on the device. Early results, however, were inclusive due to negative results; the experiments are technically difficult because of the large voltage requirements for opening the channel, which

often disrupts the bilayer. Second, as described in Material and Methods, a slightly different procedure was used to incorporate the channel into the tBLM. Here again, it seems unlikely that this change would lead to the increased sensitivity for the K31E channel. Hence, while the simplest interpretation of the data is that, as expected, the K31E mutant shows increased voltage sensitivity, additional controls should be performed in the future to rule out the possibility that minor technical alterations played some role in the increased sensitivity observed.

Conclusions

In this study, we examined the functional characteristics of Gramicidin, MscL, and a voltage sensitive conjugate of this channel reconstituted on a tethered membrane bilayer. The channel was gated on an applied voltage, which according to our calculations, gives rise to a stress on the lipid bilayer that is similar to pressure induced tensions. This high voltage requirement for WT-MscL increased the amount of irreversible breakdown of the bilayers before channel activity could be observed. Therefore, a voltage sensitive mutant K31E was integrated into the tBLM and it gated at much lower voltages ranging from 85 mV to 150 mV. Conductance from this channel was comparable to MscL in the device and the fast single channel kinetics were similar to results of this mutant in sphereoplast (*44*). Furthermore, these findings show the possibility of using MscL as either a release valve or a "designer sensor" channel for engineered membrane devices. If MscL was to serve as the actual sensor component within a microchip system, the large conductance of the channel may cause some limitations in the device.

Since the conductance of MscL and the voltage sensitive mutant is already 10 times lower within the tBLM then its natural conductance, further extensive studies should examine a range in which these channels conduct in this system. Once this range is determined, and the proper controls are done with both MscL and K31E, then alterations to either channel should be

researched where the conductance can be decreased or increased. The earlier C-terminal mutation studies in Chapter 3 offer many advantages in decreasing the conductance of the channel without affecting the pore of the channel. Cysteine mutations to this region can create sensitivity to redox reagents, as well as decrease the conductance by disulfide-bridging in this area. Histidine mutations to the upper C-terminal region, more specifically A110-A114, can create sensitivity within the channel for heavy metals. The binding events can be interpreted by the decrease in single channel kinetics and conductance. The beauty of incorporating the Histidines mutants to this region is the reversibility back to MscL's normal activity once the heavy metals are removed. All in all the ability to incorporate MscL into the tBLM system was the first step, and has opened the door to limitless possibilities of bettering this micro-bio-electronic construct.

CHAPTER 6
CONCLUSION

When creating a biosensor based on single ion channel activity, there exist several components at the bio-molecular level that must be fully understood. For instance, conformational changes within the protein must be understood in order to incorporate sensory components to key regions. The protein's ability to reconstitute successfully into non-native lipid environments and remain active should also be investigated. An electrically stable lipid environment must also be studied. In this body of research we have analyzed the proximity and mobility of vital residues in the C-terminal region of the Mechanosensitive Channel of Large Conductance. The structure of this region during gating of the channel was under debate and our results support the theory of this region remaining closed during gating. Results from this study supported the new molecular model of MscL in the protein data base (pdb-2ORA).

An even more exciting discovery was obtained from the generation of new mutants. The first mutant, AAA (A110C, A111C, and A112C) is able to decrease the conductance of MscL when placed in oxidative conditions, and this reaction is reversible. The second set of mutants are A110H and A112H, which can also decrease both the conductance and single channel activity of MscL in presence of heavy metals. This reaction is also reversible. Future experiments should include ways of isolating and purifying these mutants in order to study them *in vitro* within liposomes and a tethered lipid bilayer membrane. Currently, purification of MscL is done using a nickel affinity column that binds to a 6-His-tag placed on the C-terminal of MscL. Possible cleavage of the His-tag could be done once the protein is eluted during purification to ensure the heavy metals interact with the single Histidine mutations rather than the His tag.

The second part of this project was an attempt to establish the ideal lipid environment for studying single ion channels in a tethered device for biosensor applications. Therefore different diphytanoyl lipid ratios were compared using the tip-dip method. Diphytanoyl lipids were vital components of this research due to their increased durability and stability when tethering to solid supports such as the gold surface on the device. In this novel system of incorporating diphytanoyl lipids of PC and PE with the tip dip method; electroporation was unfortunately observed and characterized. Results indicated all of the lipid-ratios suffered from pore formation due to electrical breakdown, both reversible and irreversible. This was the first time that electroporation was reported at low potentials such as 125 mV and even 40 mV which may be characteristic of using the tip-dip method with diphtanoyl lipids.

The lipid ratio of 70PC/30PE was chosen as the most stable lipid ratio and was integrated as the synthetic lipid environment for both Gramicidin and MscL on the tBLM device. Before we decided to move on to the tBLM, we analyzed single channel activity from Gramicidin using the tip-dip method. This was the first time this channel has been studied in this particular lipid system and analyzed by the tip-dip method. This system offered a number of both advantages and disadvantages. For instance, the ease in preparation was definitely a plus due to the thermodynamically challenging nature of establishing bilayers (*97*) This research also added to the fundamental knowledge of Gramicidin channel. One of the disadvantages was the appearance of electroporation within the bilayers that could be mistaken for single ion channel activity if using a synthetic ion channel or one that is not as characterized as Gramicidin. The e-pore formation was random; and we were able to distinguish it from single ion channel conductance by plotting I-V curves and evaluating the kinetics of the pores formed in comparison to channel activity. Studying Gramicidin in this lipid ratio using this method

provided positive results with the conductance and dwell times of the channel being comparable to results from literature proving that diphytanoyl lipids in a ratio of 70PC/30PE can actually form stable bilayers suitable for single channel measurements. These results brought us one step closer to understanding the mechanisms of different lipid species, especially those that can be integrated on to solid supports which was completed in our next study using first the model channel, Gramicidin, followed by MscL and a voltage sensitive mutant of MscL, K31E which as predicted appears to respond to lower applied voltages.

The single channel response of Gramicidin within the tBLM was a bit different then that of MscL within the system. Gramicidin's activity was comparable with other techniques used to analyze this model pore. MscL on the other hand, displayed a 10 fold decrease in conductance on the device. This characteristic has however been observed with other large channels within the tBLM system. Many reasons including the tethered ionic reservoir, the lipid environment, and the voltage induced gating could have affected the protein's activity within this system. The channel was gated upon an applied voltage, which according to our calculations was due to a stress on the lipid bilayer similar to pressure induced tension required to open MscL. One of the benefits of inducing gating by an applied potential, was the incorporation of a voltage sensitive K31E MscL mutant into the tBLM. This mutant's single channel activity was comparable to MscL within the device were the conductance range was around 300 pS. The kinetics of this channel in the tBLM was also similar to inside-out patch clamping assays. More research with this mutant should be conducted to determine a more in depth conductance range and single channel characterization within the tBLM

Future changes to the overall configuration of the tBLM system should also be considered to qualify control over more parameters on the device. For instance, Wolfgang Knoll *et al.* has

studied the tBLM system, in particular the DTPL molecule, for the last ten years in order to understand its affect on the lipid bilayer and the movement of ions in this region (*61, 65, 66, 68, 79, 81, 104*). In 2005, he worked in collaboration with Lizhong He and Renate Naumann at the Max Planck Institute for Polymer Research incorporating hydrophilic thiols with the goal of increasing the fluidity of the ionic reservoir within the tBLM system (*79*). With the success of these experiments, Knoll *et al.* combined polymer supported bilayer and the tethered bilayer to create the polymer-tethered lipid bilayer system on modified substrates (*104*). This configuration increased the fluidity as well as the distance between the bilayer and substrate surface with the overall distance of the polymer-tether being 11.2 nm in diameter instead of the 1.4 nm-3 nm DPTL linker regions.

An alternative to measuring the activity of single ion channels within the tBLM should also be considered. Since there is a capacitance associated with the membrane, the solution interfaces above and below the membrane, and resistance within the membrane, the electrolyte solution, and the ion channel, a sophisticated equivalent circuit model is required to study the exact ion-channel activity. This model will enable a more accurate account for the actual transmembrane potential within the tBLM system. In addition, it should enable the probing of channel fluctuations in a "voltage or current clamp" configuration within a micro-array system. Impedance Spectroscopy as been used as the modulating detection system for ion channels within tBLMs (*62, 65, 69, 74, 76, 79, 80, 102, 160*). In this technique an ac potential is applied to an interface between 2 electrodes and impedance (resistance of alternating current) is analyzed.

The results, from this study, nonetheless show the possibility of also using MscL as a release valve for engineered membrane devices. The large conductance of the channel within the

tBLM device is 10 fold lower then reported observations in model systems. It is still however, one of the largest conducting channels to date. The fact that it also senses tension in the bilayer can enable this channel to be reconstituted with another biosensor and serve as a release valve whereby: the other channel does the sensing, and opens allowing ions to translocate into the ionic reservoir between the gold surface and lower leaflet of the bilayer. It is theoretically predicted that the smallest of channels conducting at 50 pS can fill the ionic reservoir within 100 secs. MscL could sense the tension in the bilayer and open releasing the constituents in the reservoir, thereby increasing the durability of the overall biosensor device. The earlier C-terminal mutation studies in Chapter 3 offer many advantages in creating designer channels with readable recognition events. Cysteine mutations to this region can create sensitivity to redox reagents, as well as decrease the conductance by disulfide-bridging in this area. Histidine mutations to the upper C-terminal region can create selectivity within the channel for heavy metals. The binding events can be interpreted by the decrease in single channel kinetics. The beauty of incorporating either one of these mutants to this region is the reversibility back to MscL's normal activity once either the redox reagents or heavy metals are removed. Therefore MscL offers two distinct yet important characteristics to future stochastic sensors based on single ion channel activity.

APPENDIX 1
DLS OF THE SIZE DISTRIBUTION OF 70PC/30 PE

The Figures below show the intensity of the vesicles size distributions directly after extrusion (A), a week later (B) and two weeks after storage at 4°C (C).

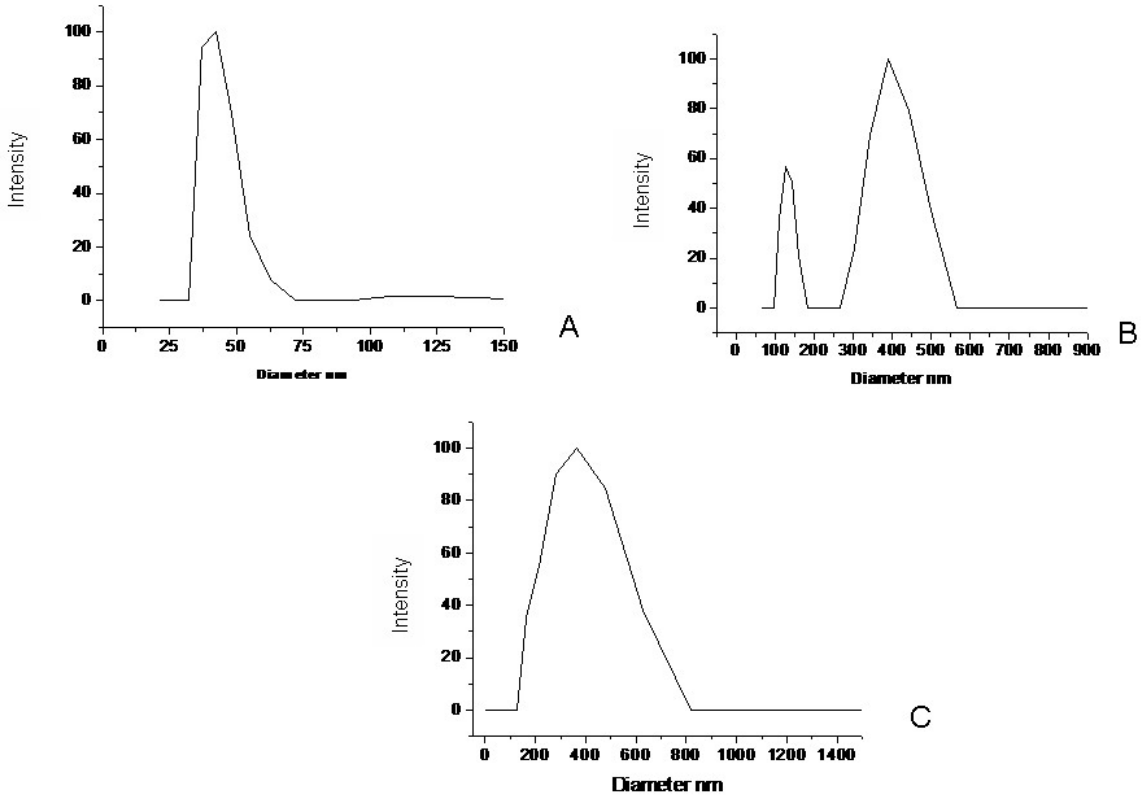

APPENDIX 2
STABLE BILAYER TRACE AND I-V CURVES

This appendix includes supporting data for the stability of the 70PC/30PE lipid bilayer within the tBLM. The 1st Figure below is a trace of a stable bilayer formed by the 70PC/30PE lipid composition within the tBLM. The calculated resistance is 4.08 GΩ, and the applied voltage is 300 mV. The time scale of the trace is 30 minutes.

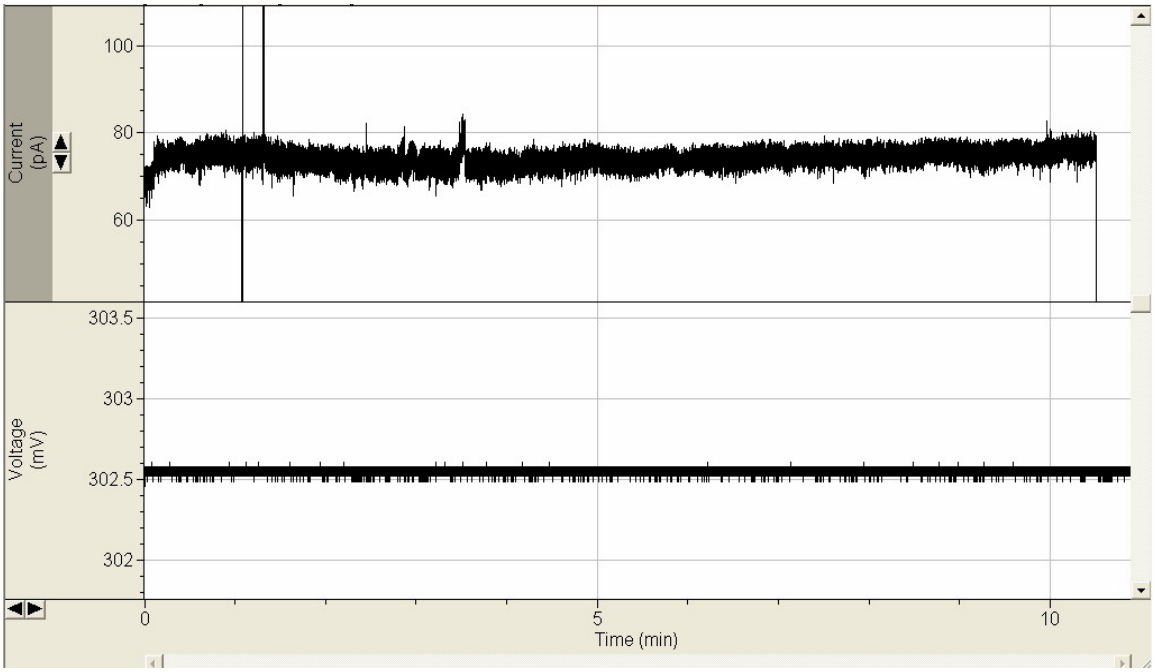

These Figures are I-V curves from three different stable bilayers within the tBLM. The resistance of the I-V curve calculated from Ohms law was 4.5 GΩ for Figure A, 2.1 GΩ for Figure B, and 2.8 for Figure C.

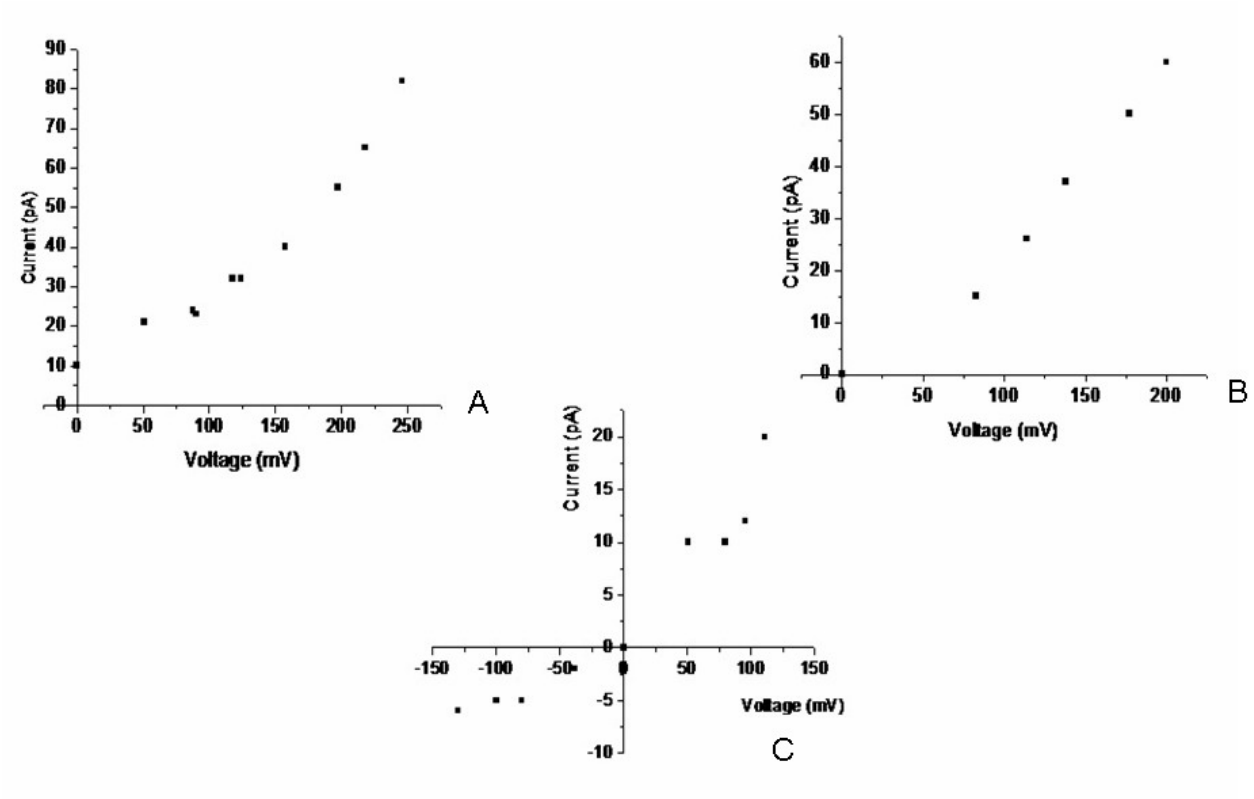

APPENDIX 3
PROTEIN RECTIFICATION WITHIN THE DEVICE

This appendix yields to explain the flow of potassium ions though Gramicidin and how the dynamics of the tBLM creates protein rectification. When a positive voltage is applied to the Ag/AgCl electrode, Cl^- from the buffer solution react with the newly formed Ag^+ and the K^+ from the bulk solution above the bilayer travel through the open pore of ion channel into the tethered region. When a negative voltage is applied to the Ag/AgCl electrode, the Ag/AgCl is reduced to metallic Ag, and Cl^- flows into the solution. This switch in polarity causes the K^+ within the limited-tethered ionic reservoir, between the gold's surface and the bilayer to travel through the pore of the ion channel. The ion mobility within this region is slowed due to the high viscosity and smaller volume of this region causing, a small rectification with Gramicidin.

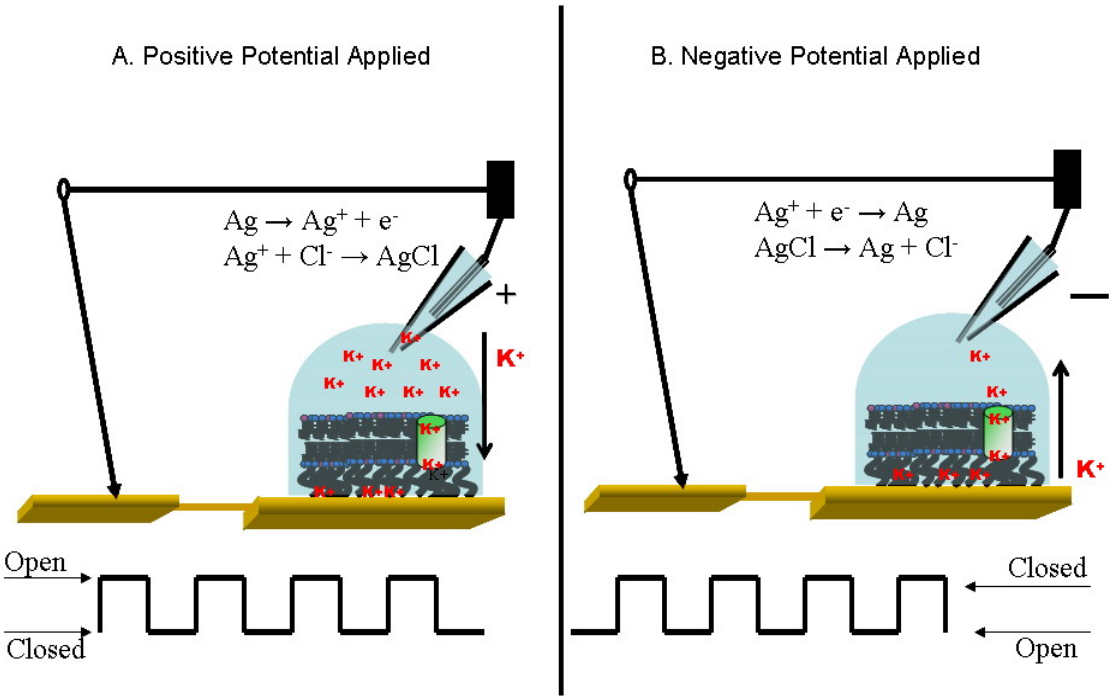

LIST OF REFERENCES

(1) Subrahmanyam, S., Piletsky, S., and Turner, A. (2002) Application natural receptors in sensors and assays. *Anal. Chem. 74*, 3942-3951.

(2) Bayley, H., and Cremer, P. (2001) Stochastic sensors inspired by biology. *Nature 413*, 226-230.

(3) Batiza, A. F., Yoshimura, K., Schroeder, M., Blount, P., and Kung, C. (1999) Glycine 22 is crucial in mechanical gating of the MscL channel. *Biophysical Journal 76*, A138-a138.

(4) Kloda, A., Ghazi, A., and Martinac, B. (2006) C-terminal charged cluster of MscL, RKKEE, functions as a pH sensor. *Biophysical Journal 90*, 1992-1998.

(5) Davidson, M. W. (2004) (1st, Ed.), Florida State University, Tallahassee.

(6) Tien, H. T. (1995) Self-assembled lipid bilayers as a smart material for nanotechnology. *Materials Science and Engineering C3*, 7-12.

(7) Puu, G., and Gustafson, I. (1997) Planar lipid bilayers on solid supports from liposomes - factors of importance for kinetics and stability. *Biochimica et Biophysica Acta (BBA) - Biomembranes 1327*, 149-161.

(8) Winterhalter, M. (2000) Black lipid membranes. *Current Opinion in Colloid & Interface Science 5*, 250-233.

(9) Liu, A. L. (2006) *Advances in Planar Lipid Bilayers and Liposomes*, Vol. 3, 3 ed., Elsevier, London.

(10) Moe, P., and Blount, P. (2005) Assessment of potential stimuli for mechano-dependent gating of MscL: effects of pressure, tension, and lipid headgroups. *Biochemistry 44*, 12239-12244.

(11) Castellana, E., and Cremer, P. (2006) Solid supported lipid bilayers: From biophysical studies to sensor design. *Surface Science Reports 61*, 429-444.

(12) Yeagle, P. (2005) *Structure of Biological Membranes*, Vol. 1, 1 ed., CRC.

(13) L.Nelson, D., and Cox, M. M. (2005) *Lehniger Principles of Biochemistry*, fouth ed., Sara Tenney, New York.

(14) Montal, M. O., Iwamoto, T., Tomich, J., and Montal, M. (1993) Design, synthesis and Functional Characterization of a pentameric Channel Protein that Mimics the Presumed pore structure of the Nicotinic Cholinergic Receptor. *Federation of European Biochemical Societies 320*, 261-266.

(15) Hille, B. (2001) *Ion Channels of Excitable Membranes*, Sinauer Associates, Inc., Sunderland, Massachusetts.

(16) MacKinnon, R. (2004) Potassium channels and atomic basis of selective ion conduction (Nobel Lecture). *Angewandte Chemie 43*, 4265-4277.

(17) Urry, D. W. (1971) The Gramicidin A transmembrane channel: A proposed (L,D) eelix. *Proc Natl Acad Sci U S A 68*, 672-676.

(18) Koeppe, R. E. (1996) Engineering the Gramicidin channel. *Annu. Rev. Biophys. Biomol. Struct. 25*, 231-258.

(19) Cross, T. A., Arseniev, A., Cornell, B. A., Davis, J. H., Killian, J. A., Koeppe, R. E., Nicholson, L. K., Separovic, F., and Wallace, B. A. (1999) Gramicidin channel controversy - revisited. *Nature Structural Biology 6*, 610-611.

(20) Ring, A. (1992) Influence of ion occupancy and membrane deformation on gramicidin A channel stability in lipid membranes. *61*, 1306-1315.

(21) Hamill, O. P., and Martinac, B. (2001) Molecular basis of mechanotransduction in living cells. *Physiological Reviews 81*, 685-740.

(22) Chiang, C.-S. (2005) in *Department of Biology* pp 164, University of Maryland at College Park, Bethesda

(23) Strange, K. (1994) *Cellular and Molecular Physiology of Cell Volume Regulation*, CRC Press.

(24) Blount, P., and Moe, P. C. (1999) Bacterial mechanosensitive channels: integrating physiology, structure and function. *Trends in Microbiology 7*, 420-424.

(25) Sukharev, S., and Anishkin, A. (2004) Mechanosensitive channels: what can we learn from `simple' model systems? *Trends in Neurosciences 27*, 345-351.

(26) Blount, P., Sukharev, S. I., Moe, P. C., Nagle, S. K., and Kung, C. (1996) Towards an understanding of the structural and functional properties of MscL, a mechanosensitive channel in bacteria. *Biology of the Cell 87*, 1-8.

(27) Blount, P., Sukharev, S. I., Schroeder, M. J., Nagle, S. K., and Kung, C. (1996) Single residue substitutions that change the gating properties of a mechanosensitive channel in Escherichia coli. *Proc Natl Acad Sci U S A 93*, 11652-11657.

(28) Blount, P., Schroeder, M. J., and Kung, C. (1997) Mutations in a bacterial mechanosensitive channel change the cellular response to osmotic stress. *Journal of Biological Chemistry 272*, 32150-32157.

(29) Sukharev, S. I., Blount, P., Martinac, B., and Kung, C. (1997) Mechanosensitive channels of Escherichia coli: The MscL gene, protein, and activities. *Annual Review of Physiology 59*, 633-657.

(30) Sokabe, M., Sachs, F., and Jing, Z. Q. (1991) Quantitative video microscopy of patch clamped membranes stress, strain, capacitance, and stretch channel activation. *Biophysical Journal 59*, 722-728.

(31) Delcour, A. H., Martinac, B., Adler, J., and Kung, C. (1989) Modified reconstitution method used in patch-clamp studies of Escherichia-Coli ion channels. *Biophysical Journal 56*, 631-636.

(32) Sukharev, S. I., Blount, P., Nagle, S., Moe, P., and Kung, C. (1995) MscL, a mechanosensitive channel in Escherichia coli. *Journal of General Physiology 106*, 9-9.

(33) Berrier, C., Coulombe, A., Houssin, C., and Ghazi, A. (1989) A patch-clamp study of ion channels of inner and outer membrances and of contact zones of E. coli, fused into giant liposomes. Pressure-activated channels are localizedin the inner membrane. *FEBS Letters 259*, 27-32.

(34) Blount, P., Sukharev, S., Martinac, B., and Kung, C. (1994) Molecular analysis of a gene that encodes a mecanosensitive channel in Escherichia-Coli. *Biophysical Journal 66*, A170-a170.

(35) Hamann, A., Bossemeyer, D., and Baker, E. P. (1987) Physical mapping of the K+ transport trkA gene of Escherichia coli and overproduction of the TrkA protein. *J. Bacteriol 169*, 3138-3145.

(36) Sukharev, S. I., Blount, P., Martinac, B., and Kung, C. (1994) Molecular-Identification of Large-Conductance Mechanosensitive Channel Protein from Escherichia-Coli. *Biophysical Journal 66*, A170-a170.

(37) Blount, P., Sukharev, S., Schroeder, M., Nagle, S., and Kung, C. (1996) Mutations that change gating properties of a mechanosensitive channel in E-coli. *Biophysical Journal 70*, Wamd7-Wamd7.

(38) Martinac, B., Buechner, M., Delcour, A. H., Adler, J., and Kung, C. (1987) Pressure-sensitive ion channel in Escherichia-Coli. *Proc Natl Acad Sci U S A 84*, 2297-2301.

(39) Blount, P., Sukharev, S. I., Moe, P., Martinac, B., and Kung, C. (1999) *Methods in Enzymolgy*, Vol. 294, Academic Press, San Diego.

(40) Kung, C., and Blount, P. (2004) Channels in microbes: so many holes to fill. *Molecular Microbiology 53*, 373-380.

(41) Kloda, A., Petrov, E., Meyer, G. R., Nguyen, T., Hurst, A. C., Hool, L., and Martinac, B. (2008) Mechanosensitive channel of large conductance. *The International Journal of Biochemistry & Cell Biology 40*, 164-169.

(42) Corry, B., and Martinac, B. Bacterial mechanosensitive channels: Experiment and theory. *Biochimica et Biophysica Acta (BBA) - Biomembranes In Press, Corrected Proof.*

(43) Blount, P., Sukharev, S. I., Moe, P. C., Schroeder, M. J., Guy, H. R., and Kung, C. (1996) Membrane topology and multimeric structure of a mechanosensitive channel protein of Escherichia coli. *Embo Journal 15*, 4798-4805.

(44) Blount, P., Shroeder, M. J., and Kung, C. (1998) Mutations in MscL, a bacterial mechanosensitive channel, can change the cellular response to osmotic stress. *Biophysical Journal 74*, A239-a239.

(45) Chang, G., Spencer, R. H., Lee, A. T., Barclay, M. T., and Rees, D. C. (1998) Structure of the MscL homolog from Mycobacterium tuberculosis: A gated mechanosensitive ion channel. *Science 282*, 2220-2226.

(46) Moe, P. C., Levin, G., and Blount, P. (2000) Correlating a protein structure with function of a bacterial mechanosensitive channel. *Journal of Biological Chemistry 275*, 31121-31127.

(47) Poolman, B., Spitzer, J. J., and Wood, J. M. (2004) Bacterial osmosensing: roles of membrane structure and electrostatics in lipid-protein and protein-protein interactions. *Biochimica et Biophysica Acta (BBA) - Biomembranes 1666*, 88-104.

(48) Jeon, J., and Voth, G. A. (2008) Gating of the Mechanosensitive channel protein MscL: the interplay of membrane and protein. *Biophysical. Journal. 94*, 3497-3511.

(49) Cruickshank, C. C., Minchin, R. F., LeDain, A. C., and Martinac, B. (1997) Estimation of the pore size of the large-conductance mechanosensitive ion channel of Escherichia coli. *Biophysical Journal 73*, 1925-1931.

(50) Ou, X. R., Blount, P., Hoffman, R. J., and Kung, C. (1998) One face of a transmembrane helix is crucial in mechanosensitive channel gating. *Proceedings of the National Academy of Sciences of the United States of America 95*, 11471-11475.

(51) Anishkin, A., Gendel, V., Sharifi, N. A., Chiang, C. S., Shirinian, L., Guy, H. R., and Sukharev, S. (2003) On the conformation of the COOH-terminal domain of the large mechanosensitive channel MscL. *Journal of General Physiology 121*, 227-244.

(52) Elmore, D. E., Philipson, K. D., and Dougherty, D. A. (2001) Molecular dynamics simulations of the M-tuberculosis mechanosensitive channel of large conductance. *Biophysical Journal 80*, 110A-111A.

(53) Perozo, E., Kloda, A., Cortes, D. M., and Martinac, B. (2001) Site-directed spin-labeling analysis of reconstituted MscL in the closed state. *Journal of General Physiology 118*, 193-205.

(54) Ajouz, B., Berrier, C., Garrigues, A., Besnard, M., and Ghazi, E. (1998) Release of thioredoxin via the mechanosensitive channel MscL during osmotic downshock of Escherichia coli cells. *Journal of Biological Chemistry 273*, 26670-26674.

(55) Ewis, H. E., and Lu, C. D. (2005) Osmotic shock: A mechanosensitive channel blocker can prevent release of cytoplasmic but not periplasmic proteins. *Fems Microbiology Letters 253*, 295-301.

(56) Kong, Y., Shen, Y., Warth, T. E., and Ma, J. (2002) Conformational pathways in the gating of Escherichia coli mechanosensitive channel. *Proc Natl Acad Sci U S A 99*, 5999-6004.

(57) BraachMaksvytis, V. L. B., Cornell, B. A., King, L. G., Osman, P. D. J., Pace, R. J., Raguse, B., and Wieczorek, L. (1997) Tethered lipid bilayer: formation, ionophore incorporation and physical characterisation. *Biophysical Journal 72*, Th288-Th288.

(58) Matsuno, Y., Osono, C., Hirano, A., and Sugawara, M. (2004) Single-Channel Recordings of Gramicidin at agarose-supported bilayer lipid membranes formed by the tip-dip and painting method. *Analytical sciences 20*, 1217-1221.

(59) Richter, R. P., Berat, R., and Brisson, A. R. (2006) Formation of solid-supported lipid bilayers: an integrated view. *Langmuir 22*, 3497-3505.

(60) Goennenwein, S., Tanaka, M., Hu, B., Moroder, L., and Sackmann, E. (2003) Functional incorporation of integrins into solid supported membranes on ultrathin films of cellulose: impact on adhesion. *Biophysical. Journal. 85*, 646-655.

(61) Nauman, C. A., Prucker, O., Lehmann, T., Ruho, J., Knoll, W., and Frank, C. W. (2002) The polymer-supported phospholipid bilayer: tethering as a new approach to substrate-membrane stabilization. *Biomacromolecules 3*, 27-35.

(62) Terrettaz, S., Mayer, M., and Vogel, H. (2003) Highly electrically insulating tethered lipid bilayers for probing the function of ion channel proteins. *Langmuir 19*, 5567-5569.

(63) Plant, A. L. (1999) Supported hybrid bilayer membranes as rugged cell membrane mimics. *Langmuir 15*, 5128-5135.

(64) Martin, A., Okeyo, G., Wilson, D., Keiqer, H., Moe, P., Blount, P., Fine, D., Dodabalapur, A., and Duran, R. (2008) Voltage induced gating of the Mechanosensitive MscL ion channel reconstituted in a tether lipid bilayer membrane. *Biosensors and Bioelectronics 23,* 919-923.

(65) Knoll, W., Frank, C. W., Heibel, C., Naumann, R., Offenhausser, A., Ruhe, J., Schmidt, E. K., Shen, and Sinner, A. (2000) Functional tethered lipid bilayers. *Reviews in Molecular Biotechnology 74*, 137-158.

(66) Knoll, W., Koper, I., Naumann, R., Schiller, S., and Duran, R. S. (2004) Functional tethered bimolecular lipid membranes. *Abstracts of Papers of the American Chemical Society 227*, U853-U853.

(67) Vockenroth, I., Atanasova, P., Knoll, W., and Koper, I. (2005) Platform: Funtional tethered bilayer membranes as a biosensor

Sensors, 2005 IEEE, 603-606.

(68) Breffa, C. (2005) in *Chemistry* pp 150, Max Planck Institut fur Polymerforschung and Johannes Gutenberg Universitat Mainz, Geboren.

(69) Romer, W., and Steinem, C. (2004) Impedance analysis and single-channel recordings on nano-black lipid membranes based on porous Alumina. *Biophys. J. 86*, 955-965.

(70) Steltenkamp, S., Muller, M. M., Deserno, M., Hennesthal, C., Steinem, C., and Janshoff, A. (2006) Mechanical properties of pore-spanning lipid bilayers probed by Atomic Force Microscopy. *Biophys. J. 91*, 217-226.

(71) Reviakine, I., and Brisson, A. (2000) Formation of supported phospholipid bilayers from unilamellar vesicles investigated by Atomic Force Microscopy. *Langmuir 16*, 1806-1815.

(72) Kim, Y.-H., Rahman, M. M., Zhang, Z.-L., Misawa, N., Tero, R., and Urisu, T. (2006) Supported lipid bilayer formation by the giant vesicle fusion induced by vesicle-surface electrostatic attractive interaction. *Chemical Physics Letters 420*, 569-573.

(73) Tamm, L. K., and McConnell, H. M. (1985) Supported phospholipid bilayers. *47*, 105-113.

(74) Raguse, B., Braach-Maksvytis, V., Cornell, B. A., King, L. G., Osman, P. D. J., Pace, R. J., and Wieczorek, L. (1998) Tethered lipid bilayer membranes: Formation and ionic reservoir characterization. *Langmuir 14*, 648-659.

(75) Cornell, B. A., Krishna, G., Osman, P. D., Pace, R. D., and Wieczorek, L. (2001) Tethered-bilayer lipid membranes as a support for membrane-active peptides. *Biochemical Society Transactions 29*, 613-617.

(76) Krishna, G., Schulte, J., Cornell, B. A., Pace, R., Wieczorek, L., and Osman, P. D. (2001) Tethered bilayer membranes containing ionic reservoirs: The interfacial capacitance. *Langmuir 17*, 4858-4866.

(77) Andersson, M., Keizer, H. M., Zhu, C., Fine, D., Dodabalapur, A., and Duran, R. S. (2007) Detection of single ion channel activity on a chip using tethered bilayer membranes. *Langmuir 23*, 2924-7.

(78) Standen, N. B., Gray, P. T. A., and Whitaker, M. J. (1994) *Microelectrode techniques, The Plymouth workshop handbook*, 2nd ed., Company of Biologist, Cambridge, UK.

(79) He, L., Robertson, J. W. F., Li, J., Karcher, I., Schiller, S. M., Knoll, W., and Naumann, R. (2005) Tethered bilayer lipid membranes based on monolayers of Thiolipids mixed with a complementary dilution molecule. 1. incorporation of channel peptides. *Langmuir 21*, 11666-11672.

(80) Cornell, B. A., BraachMaksvytis, V. L. B., King, L. G., Osman, P. D. J., Raguse, B., Wieczorek, L., and Pace, R. J. (1997) A biosensor that uses ion-channel switches. *Nature 387*, 580-583.

(81) Schiller, S. M., Naumann, R., Lovejoy, K., Kunz, H., and Knoll, W. (2003) Archaea Analogue Thiolipids for Tethered bilayer lipid membranes on ultrasmooth gold surfaces. *Angewandte Chemie International Edition 42*, 208-211.

(82) Schreiber, F. (2000) Structure and growth of self-assembling monolayers. *Progress in Surface Science 65*, 151-257.

(83) Krishna, G., Schulte, J., Cornell, B. A., Pace, R. J., and Osman, P. D. (2003) Tethered bilayer membranes containing ionic reservoirs: Selectivity and conductance. *Langmuir 19*, 2294-2305.

(84) Kunze, J., Leitch, J., Schwan, A. L., Faragher, R. J., Naumann, R., Schiller, S., Knoll, W., Dutcher, J. R., and Lipkowski, J. (2006) New method to measure packing densities of self-assembled Thiolipid monolayers. *Langmuir 22*, 5509-5519.

(85) Mathai, J. C., Sprott, G. D., and Zeidel, M. L. (2001) Molecular mechanisms of water and solute transport across Archaebacterial lipid membranes. *J. Biol. Chem. 276*, 27266-27271.

(86) Montal, M., and Opella, S. J. (2002) The structure of the M2 channel-lining segment from the nicotinic acetylcholine resceptor. *Biochimica et Biophysica Acta 1565*, 287-293.

(87) Montal, M., Montal, M., and Tomich, J. (1990) Synporins-synthetic proteins that emulate the pore structure of biological Ionic channels. *Proc. Natl. Acad. Sci. USA 87*, 6929-6933.

(88) Ferrer-Montiel, A. V., and Montal, M. (1993) A negative charge in the M2 transmembrane segment of the neuronal alpha 7 acetylcholine receptor increases permeability to divalent cations. *Federation of European Biochemical Societies 324*, 185-190.

(89) Opella, S. J., Marassi, F. M., Gesell, J. J., Valente, A. P., Kim, Y., Oblatt-Montal, M., and Montal, M. (1999) Structures of the M2 channel-lining Segments from nicotinic acetylcholine and NMDA receptors by NMR Spectroscopy. *Nature Structural Biology 6*, 374-379.

(90) Gauger, D., Binder, H., Vogel, A., Selle, C., and Pohle, W. (2002) Comparative FTIR-spectroscopic studies of the hydration of diphytanoylphosphatidylcholine and -ethanolamine. *Journal of Molecular Structure 614*, 211-220.

(91) Hogrefe, H. H., Cline, J., Youngblood, G. L., and Allen, R. M. (2002) Creating randomized amino acid libraries with the QuikChange (R) multi site-directed mutagenesis kit. *Biotechniques 33*, 1158-+.

(92) Blount, P., Sukharev, S. I., Moe, P., and Kung, C. (1997) Mechanosensitive channels of E-coli: A genetic and molecular dissection. *Biological Bulletin 192*, 126-127.

(93) Levin, G., and Blount, P. (2004) Cysteine scanning of MscL transmembrane domains reveals residues critical for mechanosensitive channel gating. *Biophysical Journal 86*, 2862-2870.

(94) Iscla, I., Levin, G., Wray, R., and Blount, P. (2007) Disulfide Trapping the Mechanosensitive Channel MscL into a gating-transition state. *Biophysical. Journal. 92*, 1224-1232.

(95) Britten, R. J., and McClure, F. T. (1962) The Amino Acid Pool in Escherichia Coli. *Bacteriol Rev 26*, 292-335.

(96) Blount, P., Sukharev, S. I., Schroeder, M. J., Nagle, S. K., and Kung, C. (1996) Single residue substitutions that change the gating properties of a mechanosensitive channel in Escherichia coli. *Proc Natl Acad Sci U S A 93*, 11652-7.

(97) Miller, C., and White, S. H. (1986) *Ion Channel Reconstitution*, Plenum Press, New York.

(98) Hauser, H., and Gains, N. (1982) Spontaneous vesiculation of phospholipids: simple and quick method of forming unilamellar vesicles. *Proc Natl Acad Sci U S A 79*, 1683-1687.

(99) Hamill, O. P., Marty, A., Neher, E., Sakmann, B., and Sigworth, F. J. (1981) Improved patch-clamp techniques for high-resolution current recording from cells and cell-free membrane patches. *Pflugers Archiv-European Journal of Physiology 391*, 85-100.

(100) Byrne, J. H., and Schults, S. G. (1994) *An introduction of membrane transport and bioelectricity* Raven Press.

(101) Ruthe, H. J., and Adler, J. (1985) Fusion of bacterial spheroplasts by electric-fields. *Biochimica Et Biophysica Acta 819*, 105-113.

(102) Terrettaz, S., Ulrich, W. P., Vogel, H., Hong, Q., Dover, L. G., and Lakey, J. H. (2002) Stable self-assembly of a protein engineering scaffold on gold surfaces. *Protein Science 11*, 1917-1925.

(103) Lei, S. B., Tero, R., Misawa, N., Yamamura, S., Wan, L. J., and Urisu, T. (2006) AFM charaterization of gramicidin-A in tethered lipid membrane on silicon surface. *Chem. Phys. Letters 429*, 244-249.

(104) Hwang, L. Y., GoÌˆtz, H., Knoll, W., Hawker, C. J., and Frank, C. W. (2008) Preparation and characterization of Glycoacrylate-based polymer-tethered lipid bilayers on Benzophenone-modified substrates. *Langmuir 24*, 14088-14098.

(105) Leahmann-Horn, F., and Jurkat-Rott, K. (2003) Nanotechnology for neuronal ion channels. *J. Neruo. NeruoSurg. Psychiratry 74*, 1466-1476.

(106) Hombie, F., Cabiaux, V., and Ruysschaert, J.-M. (1998) Channel or channel like Activity associated with pore forming proteins and peptides *Molecular Microbiology 27*, 1261-1263.

(107) Kessel, A., Shental-Bechor, D., Haliloglu, T., and Ben-Tal, N. (2003) Interactions of hydrophobic peptides with lipid bilayers: Monte Carlo Simulations with M2. *Biophysical Joural 85*, 3431-3444.

(108) Miyazawa, A., Fujiyoshi, Y., and Uwin, N. (2003) Structure and gating mechanism of the Acetylcholine receptor pore. *Nature 423*, 949-955.

(109) Saiz, L., and Klein, M. (2005) The Transmembrane domain of the Acetylcholine receptor: Insights from simulations on synthetic peptide models. *Biophysical Journal 88*, 959.

(110) Iscla, I., Levin, G., Wray, R., Reynolds, R., and Blount, P. (2004) Defining the physical gate of a mechanosensitive channel, MscL, by engineering metal-binding sites. *Biophysical Journal 87*, 3172-3180.

(111) Kocer, A., Walko, M., Meijberg, W., and Feringa, B. L. (2005) A light-actuated nanovalve derived from a channel protein. *Science 309*, 755-758.

(112) Keizer, H., Dorvel, B., Andersson, M., Fine, D., Price, R., Long, J., Dodabalapur, A., Koper, I., Knoll, W., Andeson, P., and Duran, R. (2007) Functional ion channels in tetherd bilayer membranes-implications for biosensors. *ChemBioChem 8*, 1246-1250.

(113) Blount, P., Iscla, I., Moe, P. C., Li, Y., and Owen, P. H. (2007) MscL: The bacterial Mechanosensitive channel of large conductance, in *Current Topics in Membranes* pp 201-233, Academic Press.

(114) Steinbacher, S., Bass, R., Strop, P., Rees, D. C., and Owen, P. H. (2007) Structures of the Prokaryotic mechanosensitive channels MscL and MscS, in *Current Topics in Membranes* pp 1-24, Academic Press.

(115) Sukharev, S. I., Martinac, B., Arshavsky, V. Y., and Kung, C. (1993) 2 Types of Mechanosensitive channels in the Escherichia-Coli cell-envelope - solubilization and functional reconstitution. *Biophysical Journal 65*, 177-183.

(116) Blount, P. (2003) Molecular mechanisms of mechanosensation: Big lessons from small cells. *Neuron 37*, 731-734.

(117) Stewart, E. J., Aslund, F., and Beckwith, J. (1998) Disulfide bond formation in the Escherichia coli cytoplasm: an in vivo role reversal for the thioredoxins. *Embo Journal 17*, 5543-5550.

(118) Kadokura, H., Katzen, F., and Beckwith, J. (2003) Protein disulfide bond formation in prokaryotes. *Annual Review of Biochemistry 72*, 111-135.

(119) Liu, A. L. (2006) *Advances in Planar Lipid Bilayers and Liposomes*, Vol. 1, 3 ed., Elsevier, London.

(120) Tien, H. T., and Ottova, A. L. (2001) The lipid bilayer concept and its experimental realization: from soap bubbles, kitchen sink, to bilayer lipid membranes. *Journal of Membrane Science 189*, 83-117.

(121) Tanaka, M., and Sackmann, E. (2005) Polymer-supported membranes as models of the cell surface. *Nature 437*, 656-663.

(122) Troiano, G. C., Stebe, K. J., Raphael, R. M., and Tung, L. (1999) The effects of Gramicidin on Electroporation of lipid Bilayers. *Biophys. J. 76*, 3150-3157.

(123) Hirano, A., Wakabayashi, M., Matsuno, Y., and Sugawara, M. (2002) A single-channel sensor based on Gramicidin controlled by molecolar recognition at bilayer lipid membranes conyaining receptor. *Biosensors Bioelectronics 18*, 973-983.

(124) Fukasawa, T., Miyamoto, T., Fujiyama, R., Okada, T., and Sato, T. (2001) Reconstituted ion channels of frog fungiform Papilla cell membrane. *Zoological Science 18*, 299-307.

(125) Tieleman, D. P. (2004) The molecular basis of electroporation. *BioMed Central 10*, 1-12.

(126) Chen, C., Smye, S. W., and Robinson, M. P. (2006) Membrane electroporation theories: a review. *Med. Biol Eng Comput 44*, 5-14.

(127) Disalvo, E., Lairion, F., Martini, F., Almaleck, H., Diaz, S., and Gordillo, G. (2004) Water in biological membranes at interfaces: Does it play a functional role? *The Journal of the Argentine Chemical Society 92*, 1-22.

(128) Tarek, M. (2005) Membrane electroporation: A molecular dynamics simulation. *Biophys. J. 88*, 4045-4053.

(129) Gawrisch, K., Ruston, D., Zimmerberg, J., Parsegian, V. A., Rand, R. P., and Fuller, N. (1992) Membrane dipole potentials, hydration forces, and the ordering of water at membrane surfaces. *Biophysical. Jounrnal. 61*, 1213-1223.

(130) Meyer, G. R., Gullingsrud, J., Schulten, K., and Martinac, B. (2006) Molecular dynamics study of MscL interactions with a curved lipid bilayer. *Biophysical Journal 91*, 1630-1637.

(131) Pasenkiewicz-Gierula, M., Murzyn, K., Rog, T., and Cazplewski, C. (2000) Molecular dynamics simulation studies of lipid bilayer systems. *Acta Biochimica Polonica 47*, 601-611.

(132) Wong, B. Y., and Faller, R. (2007) Phase behavior and dynamic heterogeneities in lipids: A coarse-grained simulation study of DPPC-DPPE mixtures. *Biochimica et Biophysica Acta (BBA) - Biomembranes 1768*, 620-627.

(133) Sukharev, S. I., Blount, P., Martinac, B., and Kung, C. (1997) Mechanosensitive channels of Escherichia coli: the MscL gene, protein and activities. *Annu. Rev. Physiol 59*, 633-657.

(134) Booth, I. R., and Louis, P. (1999) Managing hypoosmotic stress: aquaporins and mechanosensitive channels in Escherichia coli. *Curr. Opin. Microbiol. 2*, 166-169.

(135) Levina, N., Totemeyer, S., Stokes, N. R., Louis, P., Jones, M. A., and Booth, I. R. (1999) Protection of Escherichia coli. cells against extreme turgor by activation of MscS and MscL mechnosensitive ion channels: identification of genes required for MscS activity. *EMBO J. 18*, 1730-1737.

(136) Sukharev, S. I., Blount, P., Martinac, B., Blattner, F. R., and Kung, C. (1994) A large-conductance mechanosensitive channel in E. Coli. encoded by MscL alone. *Nature 368*, 265-268.

(137) Sukharev, S. I., Blount, P., Martinac, B., Blattner, F. R., and Kung, C. (1994) A Large-Conductance Mechanosensitive Channel in E. Coli Encoded by Mscl Alone. *Nature 368*, 265-268.

(138) Arkin, I. T., Sukharev, S. I., Blount, P., Kung, C., and Brunger, A. T. (1998) Helicity, membrane incorporation, orientation and thermal stability of the large conductance mechanosensitive ion channel from E-coli. *Biochimica Et Biophysica Acta-Biomembranes 1369*, 131-140.

(139) Blount, P., Ou, X., Hoffman, R. J., and Kung, C. (1998) Characterization of randomly generated mutants of MscL, a mechanosensitive channel in bacteria, identifies a functional region of the protein. *Biophysical Journal 74*, A324-a324.

(140) Bartlett, J. L., Levin, G., and Blount, P. (2004) An in vivo assay identifies changes in residue accessibility on mechanosensitive channel gating. *Proceedings of the National Academy of Sciences of the United States of America 101*, 10161-10165.

(141) Corry, B., Rigby, P., Liu, Z. W., and Martinac, B. (2005) Conformational changes involved in MscL channel gating measured using FRET spectroscopy. *Biophysical Journal 89*, L49-L51.

(142) Okada, K., Moe, P. C., and Blount, P. (2002) Functional design of bacterial mechanosensitive channels - Comparisons and contrasts illuminated by random mutagenesis. *Journal of Biological Chemistry 277*, 27682-27688.

(143) Liu, Z. W., and Martinac, B. (2006) MscL adaptation to sustained membrane stretch in liposomes under different amphipaths. *Acta Pharmacologica Sinica 27*, 196-197.

(144) Exerowa, D., Todorov, R., and Nikolov, L. (2004) Amphiphile bilayer films from DPPC: bilayer lipid membranes and Newton black films. *Colloids and Surfaces 250*, 195-201.

(145) Zhang, P. C., Keleshian, A. M., and Sachs, F. (2001) Voltage-induced membrane movement. *Nature 413*, 428-432.

(146) Needham, D., and Hochmuth, R. M. (1989) Electro-mechanical permeabilization of lipid vesicles - role of membrane tension and compressibility. B*iophysical Journal 55*, 1001-1009.

(147) Dorvel, B. R., Keizer, H. M., Fine, D., Vuorinen, J., Dodabalapur, A., and Duran, R. S. (2007) Formation of tethered bilayer lipid membranes on gold surfaces: QCM-Z and AFM Study. *Langmuir 23*, 7344-7355.

(148) Baba, T., Toshima, Y., Minamikawa, H., Hato, M., Suzuki, K., and Kamo, N. (1999) Formation and characterization of planar lipid bilayer membranes from synthetic phytanyl-chained glycolipids. *Biochimica et Biophysica Acta (BBA) - Biomembranes 1421*, 91-102.

(149) Baba, T., Minamikawa, H., Hato, M., and Handa, T. (2001) Hydration and Molecular Motions in Synthetic Phytanyl-Chained Glycolipid Vesicle Membranes. *Biophysical Journal 81*, 3377-3386.

(150) Blount, P., Sukharev, S. I., Moe, P. C., Nagle, S. K., and Kung, C. (1996) Towards an understanding of the structural and functional properties of MscL, a mechanosensitive channel in bacteria. *Biology of the Cell 87*, 1-8.

(151) Simon, S. A., and McIntosh, T. J. (1986) Depth of water penetration into bilayers. *Methods Enzymol. 127*, 511-521.

(152) Sukharev, S., Durell, S. R., and Guy, H. R. (2001) Structural models of the MscL gating mechanism. *Biophysical Journal 81*, 917-936.

(153) Berrier, C., Besnard, M., Ajouz, B., Coulombe, A., and Ghazi, A. (1996) Multiple mechanosensitive ion channels from Escherichia coli, activated at different thresholds of applied pressure. *Journal of Membrane Biology 151*, 175-187.

(154) Raucci, F. J. (2004) in *Molecular Biology* pp 64, University of Florida, Gainesville

(155) Wilson, D. (2006) in *Chemistry* pp 81, University of Florida, Gainesville.

(156) Keizer, H. M., Andersson, M., Chase, C., Laratta, W. P., Proemsey, J. B., Tabb, J., Long, J. R., and Duran, R. S. (2008) Prolonged stochastic single ion channel recordings in S-layer protein stabilized lipid bilayer membranes. *Colloids and Surfaces B: Biointerfaces 65*, 178-185.

(157) Latorre, R., Coronado, R., and Vergara, C. (1984) K+ channels gated by voltage and ions. *Annual Review of Physiology 46*, 485-495.

(158) Oiki, S., Danho, W., Madison, V., and Montal, M. (1988) M2 dealta, a candidate for the structure lining the ionic channel of the nicotinic cholinergic receptor. *Proc. Natl. Acad. Sci. USA 85*, 8703-8707.

(159) Sukharev, S. I., Sigurdson, W. J., Kung, C., and Sachs, F. (1999) Energetic and spatial parameters for gating of the bacterial large conductance mechanosensitive channel, MscL. *J. Gen. Physiol. 113*, 525-540.

(160) Yin, P., Burns, C. J., Osman, P. D. J., and Cornell, B. A. (2003) A tethered bilayer sensor containing alamethicin channels and its detection of amiloride based inhibitors. *Biosensors & Bioelectronics 18*, 389-397.

BIOGRAPHICAL SKETCH

Danyell Wilson was born in Norfolk Virginia in 1981. She attended Booker T. Washington High School where she graduated in the top 15% of her class in 1999. Upon entering Lincoln University, she earned a full scholarship by completing the Lincoln's Advance Science and Engineering Reinforcement (LASER) summer program with a GPA above 3.00 out of 4.00. She participated in several research internships throughout her undergraduate career and received the Minority Assess to Research Careers (MARC) National Institute of Health (NIH) fellowship her junior year. In 2003, she graduated cum laude from Lincoln University with her Bachelor of Science in Chemistry and a minor in Anthropology. Ms. Wilson then received the Alliances for Graduate Education and the Professoriate (AGEP) fellowship, and the Grinter fellowship from the University of Florida's Chemistry department where she began this project. In 2006, Ms. Wilson received her Masters of Science degree from the University of Florida with a focus in analytical chemistry. She changed research division and joined the biochemistry division and continued her research on single ion channel studies. In 2009 Ms. Wilson, received her PhD in Chemistry from the University of Florida with a focus in Biochemistry. Ms. Wilson's long term career goals are to become involved in science education policy.